Flow-induced Transverse Vibration Characteristic of Cantilevered Rectangular and D-section prisms

メタデータ	言語: eng 出版者: 公開日: 2020-10-30 キーワード (Ja): キーワード (En): 作成者: メールアドレス: 所属:
URL	http://hdl.handle.net/2297/00059749

This work is licensed under a Creative Commons Attribution-NonCommercial-ShareAlike 3.0 International License.

Dissertation

学位論文

Flow-induced Transverse Vibration Characteristic of Cantilevered Rectangular and D-section prisms

片持ち弾性支持角柱とD形柱の流れ直角方向の流力振動特性

金沢大学大学院自然科学研究科
Graduate School of Natural Science and Technology,
Kanazawa University

専攻（Division）: Mechanical Science and Engineering

学籍番号(Student ID Number）：1624032017
氏名（Name）　La Ode Ahmad Barata
Chief Supervisor　Dr. Takahiro KIWATA, Professor
Date of Submission　January, 2020

Abstract

Flow-induced vibration of the structure has been widely paid attention in recent years due to their effect on many engineering structures as well as gaining energy harvesting for low power systems such as sensors, electric probe in the confined access or space. By considering the effect of three-dimensional vortex behavior on response amplitude characteristics, elastically mounted bluff bodies, i.e. rectangular and D-section with different aspect ratios L/H (10,7.5,5.0, and 2.5) and side ratios D/H (0.5,0.2, and 0.23) was investigated in a water tunnel (where L is the span length of a prism, H is the height of a prism normal to the flow direction, and D is the depth of a prism). This study is intended to enhance research filed on developing energy harvesting from flow flow-induced vibration as well as physical insight concerning flow-induced vibration in the low flow regime.

All the experimental processes were carried out using a water tunnel facility equipped by measurement instruments and data processors (CPU unit). Meanwhile, the test sections were constructed from stainless steel and mounted elastically to a plate spring attached to the ceiling wall with a jig in the test section of the water tunnel. The results of the experiment showed that all the prisms with different aspect ratios oscillated below reduced resonant velocity (V_{rcr}). The prism with aspect ratios $L/H \geq 5$ had reasonably identic on vibration characteristics. However, the distinctly different on vibration characteristic appeared on a prism below the critical aspect ratio $L/H = 2.5$. The prism with the aspect ratio of 10 and side ratio of 0.2 had a stable and large response amplitude with onset galloping at a low reduced velocity ($V_r \geq 1.5$).

In order to improve dynamic response characteristics, added structure with different lengths (l) was mounted to the rectangular prism with a side ratio of 10.

Moreover, a splitter plate or endplate was also attached to both rectangular and D-section in each of the separated experiment sequences.

The effects of splitter plate on the flow-induced vibration characteristics of cantilevered rectangular and D-section prisms enhanced response amplitude, stable response, and diminished wake interferences effect on the prisms with critical side ratio, D/H=0.5. Meanwhile, attaching endplate at the tip end of a prism with critical aspect ratios ($L/H \leq 5$) suppressed dynamic response, increased wake interferences, and promoted unstable amplitude. Shifting vibration onset was also observed on the prism with an aspect ratio of 10 without any alteration on response amplitude characteristics.

In the case of attaching additional structure on the frontward and backward of the rectangular prism with D/H=0.2 to prevent bending due to the friction, it shifted vibration onset by prolonging the range of reduced velocity with small amplitude then response amplitude achieved meaningful response at the specified V_r. Further, the response amplitude characteristics were similar to that of the plain prism. However, discernible stability of response amplitude was found at the prism with attaching added structure for all three kinds of different aspect ratios L/l even if the side ratio of a stepped prism of 0.45 (nearly close to critical side ratio of 0.5).

Acknowledgments

This Ph.D. fellowship is the agreement between Kanazawa University Japan and Directorate General of Higher Education of Indonesia through *KU-DIKTI* program which is granted by Indonesia Endowment Fund for Education (*LPDP*) under the Agreement document and financial support: **RJ-3612/LPDP.3/2016, S-1095/LPDP.4/2019** (extended grant).

The author would like to gratefully thanks to Chief Supervisor: Dr. Takahiro Kiwata, Professor; and co-supervisors/Associate professor: Dr. Komatsu Nobuyushi; Dr. Takaaki Kono; Dr. Enomoto Hiroshi, and the Fluid dynamic Laboratory staff and research group: Mr. Tomohiro Kuratani, and Mr. S. Mizukami, Mr. R. Nagase, Mr. K. Kawakami, and all the research group member.

Also, the author would like to thank all home university staff, Engineering Faculty staffs and members of Halu Oleo University, Indonesia for administration supports.

Dedicated to my Mother (Monde, Wa), father (Barata, La Ode), and my beloved family wife (Fatimah) and my great children (Wa Ode Nasywah Mufidah Barata), the boys (La Ode Nabhan Husaini Barata and La Ode NAOKI Ishikawa Barata). Gratefully thanks for your dua*'s' and supports.*

Contents

Nomenclature

C_D	drag coefficient
C_L	lift coefficient
C_n	reduced mass-damping parameter of the system, $2m\delta/\rho DH$
Cp	pressure coefficient
Cpb	base pressure coefficient
D	depth of a prism in the flow direction, *mm*
d	depth of added plat/fin, *mm*
f_c	characteristic frequency of the prism, *Hz*
f_n	natural frequency for vortex shedding from a stationary prism, *Hz*
FFT	Fast Fourier Transformation
H	height of a prism normal to the flow direction, *mm*
h	height of added plate/fin normal to the flow direction, *mm*
I	second-moment area, mm^4
L	span length of a prism, *mm*
LES	Large Eddy Simulation
L'	length of a plat spring, *mm*
l	length of added plat/fin, *mm*
m	mass per unit length of the system, *kg*
N	number of data
P_{ave}	average peak amplitude
P_i	peak amplitude
P_{rms}	root-mean-square of the peak amplitude
Re	Reynolds number, UH/v
St	Strouhal Number
U	uniform flow velocity, *m/s*
u	x-component velocity
VIV	Vortex-Induced Vibration
V_r	reduced velocity, U/f_cH
V_{rcr}	reduced resonance velocity, U/f_nH
v	y-component velocity

w	z-component velocity
y	peak displacement of the prism tip
y_{rms}	root mean square of displacement amplitude of the prism tip
δ	logarithmic decrement of the structure damping parameter of a prism
θ_{rms}	root mean square of amplitude angle of the prism tip, °
η_{rms}	non-dimensional amplitude of displacement, y_{rms}/H
υ	kinematic viscosity of water, m^2/s
ω	vorticity magnitude, s^{-1}

Chapter 1
Introduction

1.1. Background

Flow-induced vibration of a structure has been paid attention due to widely happen in many engineering structures such as bridge, pipelines, transmission lines, sea platform, chimney stack, storage tanks, instrument probe, vibrated aircraft, and many other elevated structures. One of the famous phenomena on failure structure due to aeroelastic flutter is Tacoma's narrow bridge which had been collapse just a few months in operation. This structure is a long-span bridge had ever that can be treated as a slender body according to the depth to width ratio. After the incident, several investigations generated to investigate deeply on such structure failure, and shortly, aerodynamic force instability induced by fluid-structure interaction was the dominant description to explain this case. Moreover, aeroacoustics noise due to flow-induced vibration is commonly found in many situations such as transmission lines, raiser structure

In the literature, the aerodynamic force that induced a structure to gallop are commonly found in three types such as low-speed galloping, vortex-induced oscillation, and high-speed galloping with various types of them. Galloping can occur typically for all range flow velocity which depends on the system damping, mass, and aerodynamic shape of the structure. A classical model of wakes structure around the bluff body of the cylinder and rectangular section are defined Kawamura et al. (1984) and Wang, Zhou & Chan (2009) respectively as shown in figure 1.1. In this case, it can be seen that the flow structure of the finite height bluff body is three-dimensional. This flow structure can be found in the engineering structures mentioned in the preceding paragraph.

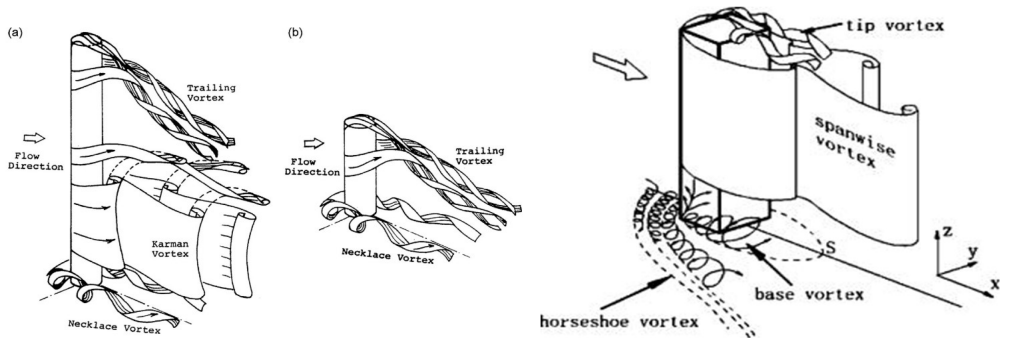

(a) Flow structure around the cylinder (Kawamura et.al., 1984)

(b) Flow structure around the square prism (Wang, Zhou, and Chan., 2005)

Figure 1.1. Flow structure around bluff bodies with the free end

The aerodynamic shape of a bluff body takes an important role in forming the wake structure after body such a prism with a sharp or rounded surface. The separation point influences the interaction of the separated shear layer in the afterbody of the structure. For instance, the structure-separated shear layer interaction of a circular cylinder is different from a sharp corner one such as rectangular prism in terms of the afterbody flow structure. This characteristic also can influence the types of galloping as mentioned above. In a rectangular prism, separation flow inherently takes places at the leading edge and after body flow behavior is determined by the depth to height ratio (side ratio) as found many research article such as Okajima (1990), Nakamura and Hirata (1989), Matsumoto (1999), etc. Therefore, flow characteristics such as Strouhal Number, and fluid forces instead of Reynold number may differ among those cases. Most of the works on flow-induced vibration characteristics including flow wake behaviors were focused on the infinite bluff body which was viewed as a two-dimensional case. Hence, a recent trend on flow characteristics of three-dimensional as found in many engineering structures as the *infinite* bluff bodies are a peculiar work.

In the physical sense, more complexity of those flow wake behavior around the bluff body shall be found in oscillating bluff bodies due to flow instability either

galloping or vortex-induced excitation. This type of excitation can be independent of each other or it is combined excitation. In certain situations, galloping is controlled or suppressed in different ways by means of modifying the damping system, hydrodynamics shape, etc. A few works in controlling galloping can be found in many investigations such as Feng (1968), Kawamura et al. (1984), Williamson & Govardan (2004), Bearman (2011). Those works must also modify flow wake behavior around the bluff body.

Considering three-dimensional wake characteristics around bluff bodies as stipulated in figure 1, wake recovery due to flow separation at the leading edge (for the rectangular case with sharp corner) is pertinent to spanwise length variation. In addition, afterbody shape was also investigated their effects on vibration characteristics in this work.

Finally, one of the recent trends in flow-induced vibration research is harvesting energy from the oscillation motion of the bluff body using the *magnetostrictive* effect of certain metal such as *galfenol.* The independency of such harvester energy becomes interested in a certain area such as remote area or inaccessible space. This study is supposed to support physical insight related to flow-induced vibration over a bluff body rectangular and D-section under low-speed galloping fashion. Moreover, investigation on controlling dynamic response behavior over the bluff bodies was conducted with various modes such as added plat, endplate, and splitter plate.

1.2. Objectives

This work is intended to investigate the dynamic response of elastically mounted rectangular and D-section prism with different aspect ratios in the unsteady water flow. To investigate the effect of span length to depth ratio (aspect ratio) on the response amplitude characteristics, four different aspect ratios of the model were employed in this

research. Meanwhile, in order to maintain a two-dimensional flow field, trailing edge-mounted splitter plate and attached endplate on the prisms model were also investigated to control dynamic response in each of the separated experiment sequences. Moreover, a rectangular bluff body with a stepped model constructed by different added plate length (l) was also investigated in case of their effects on vibration characteristics. All prism models are solely allowed to vibrate in the transverse direction perpendicular to the flow stream.

1.3. Scope of Works

To meet research objectives, some works had been completed as follow

1. Searching relevant academic literature dealing with flow-induced vibration on cantilevered rectangular and D-section prism. A primary concern is a research article, technical report or book references concerning the dynamic response of elastically mounted of cantilevered rectangular prisms, the stability of dynamic responses, Strouhal number, the effect of mounting splitter plate, endplate, and added structure.
2. The experiments were conducted in a water tunnel which was designed to investigate the dynamic response of cantilevered rectangular and D-section bluff bodies with different span length to depth ratio (aspect ratio). In this case, two different aspect ratios for each sample of prism were used and employed in this study. As a result, there were sixteen main specimen condition in total were investigated in term of aspect and side ratio effect.
3. The dynamic response characteristics due to controlling wake flow were also observed by mounting a splitter plate at trailing edge, attaching endplate, and staggered added structure. For rectangular, all aspects and side ratios were employed by splitter plate and stepped structure was selected only for side ratio (D/H) of 0.2

and aspect ratio of 10. Meanwhile, the D-section model was selected based on distinct behavior on dynamic response characteristics that was, the aspect ratio of 2.5; 5.0; and 10 for both side ratios of 0.23 and 0.5. A detailed experiment condition can be seen in chart 1.

1.4. Experimental Design

To achieve the objectives, the experimental process had been conducted which are detailed in the following chart. All the experimental design in this study is intended to study about flow-induced transverse vibration characteristics of cantilevered rectangular and D-section prims with some different parameters as outlined in chart 1.

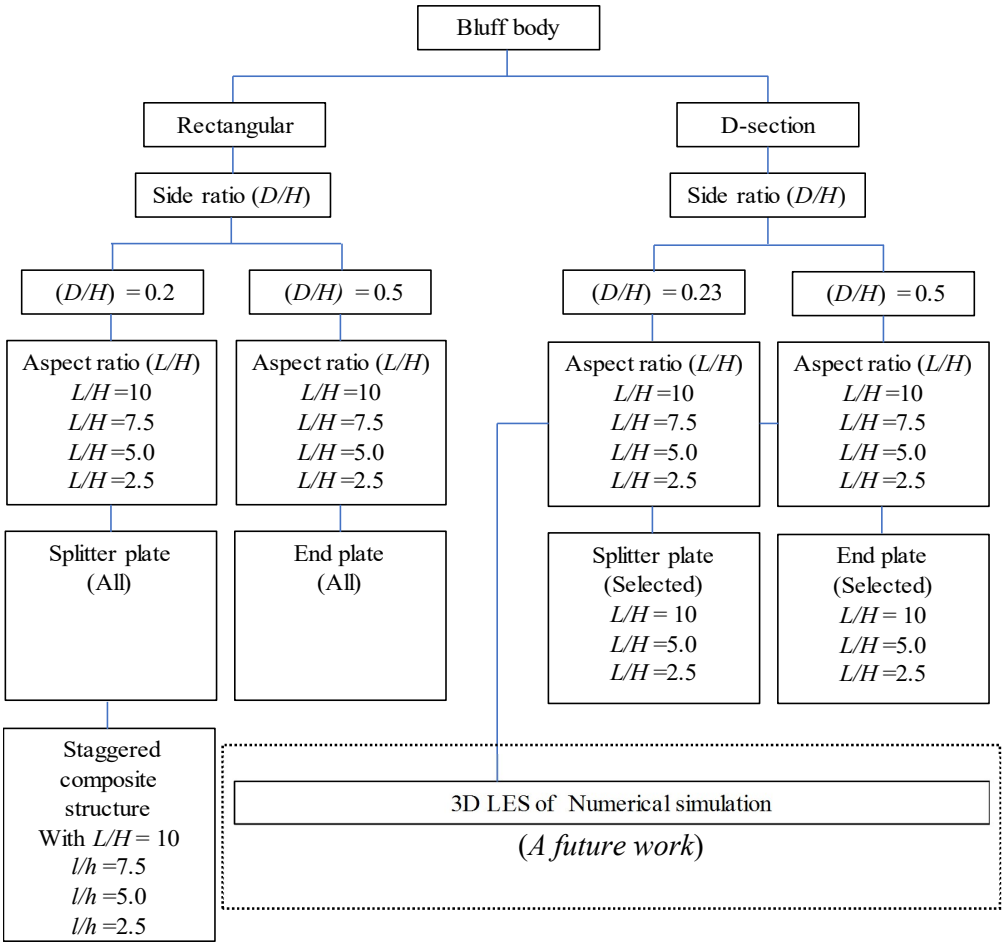

Chart 1. Experimental design

Intentionally left blank

Chapter 2
Literature Review: Flow-Induced Vibration of Rectangular and D-section Prisms

Overview

The remarkable research topics on flow-induced vibration recently are commonly found in the case of the effect of the aerodynamic/hydrodynamic shape of bluff bodies on dynamic responses as well as flow wake behavior around that structure which is correlated to galloping or aeroacoustics. Some bluff bodies shape such circular cylinder, rectangular shape, triangular, and D-shape are commonly found in the case of flow-induced vibration on such those structure. In the field of research point of view, a structure can be exposed to vibration in some situations which is its characteristics depend on mass, system damping, or aerodynamic shape. Controlling flow behaviors are a primary concern of many researchers to investigate flow features and it is widely found in the case of depth to width ratio, span-length ratio, and tandem arrangement effect on the flow field. Meanwhile, after body shape models of bluff body structure such as appended structures such as fin, endplate, and splitter plate are also commonly found on some literature both stationary and elastically mounted structure. Various types of flow-induced vibration on real engineering structures can be found in Naudascher and Rockwell (2005). Some of the considerable investigations on flow-induced vibration related to rectangular structures such as Blevins (1974), Naudascher and Wang (1993), Nakamura and Matsukawa (1986), and Manini et al., (2016) has been found in many research articles. The investigations of flow-induced vibration on semi-circular or D-section bluff bodies have been also demonstrated by Feng (1968), Nakamura and Hirata (1989), Kiwata et al., (2014), Wang (2015), Yamagata et al., (2016).

2.1. Flow-Induced Vibration

Flow over a bluff body can generate an instability of vortex behavior interaction of the structure after the separation occurs. Simply, a bluff body can be defined as the antithesis of hydrodynamic which is hydrodynamic forces that are considered high. Typically, the structure which has a sharp corner normal to the flow stream, separated shear layer takes place at the leading edge, rolled up and interacts with the main part behind/side surface of the structure. A characteristic of afterbody shape influences vortex shedding and reattachment of vortex behavior in the trailing edge.

When the bluff body is elastically mounted structure, an interaction of separated shear layer shedding periodically around the structure. This fluid interaction initiates the bluff body to vibrate with the growth of amplitude depend on the intensity of the shedding frequency of vortex. If the frequency of amplitude continues to grow until reaching to the natural frequency of the structure, strong interaction between shedding and structure takes place, and vortex shedding is controlled by body motion at the natural frequency of the system. In this situation, the shedding frequency of the vortex may couple to the natural frequency of the structure and generate harmonic oscillation while amplitude magnitude may reach one diameter (Feng, 1968). This phenomenon commonly found in elevated structures such as stack, cable line, sea platform, urban building, towers, and bridge structure.

If the shedding frequency (f_s) continues to increase greater than the natural frequency of the system (f_n), this frequency will not synch to the structure frequency and vibration increase linearly until non-linearity of the system vibration is achieved. In some cases, galloping can generate two excitation regions as found in Williamson (2004). Meanwhile, the vortex-shedding pattern is shed on the same side as maximum amplitude

with amplitude may reach much larger than its diameter or cross-section height (Zdravkovich, 1982; Corless and Parkinson, 1988).

Besides of synchronous phenomenon, Feng (1968) presented the hysteresis phenomenon of response amplitude in which a non-linear amplitude was found. It is characterized by suddenly jumping of response amplitude, phase angle, and hydrodynamic forces; either reduced velocity is increased or decreased. This hysteresis phenomenon can be described by the non-linearity of the spring or damping system. The outstanding mathematical models on nonlinearity of response amplitude can be described by Van der Pol and Duffing equations (Holmes, 2005). Van der Pol's equation describes a non-linear damping oscillator which adds energy to the system when oscillation motion is low and subtracts energy at higher amplitude motion (relaxation-oscillation). Duffing equation stands for the stiffness of spring behaviors which exhibits chaotic amplitude and does not obey Hooke's law. Iwan and Blevins (1974) developed a wake oscillator model which is employed these phenomena and this experimental model was developed numerically by Poore et al 1986. A mathematical model for this case can be also found in Cveticanin (2011), Nourazar and Mirzabeigy (2013).

Moreover, elastically mounted structure with a small damping parameter, the structure can gallop with lower vortex shedding frequency and does not synch to the natural frequency of the structure. In the slender structure such as a rectangular prism, the vortices are fed by recirculation in the separated shear layer in the side surfaces or trailing edge, and wake interaction between the side vortices establish a regular wake pattern and an alternating pressure field between to side of surfaces. This type of galloping is independent of vortex shedding effect (Nakamura and Hirata, (1989), Bearman (2011). All types of vibration models mentioned in the preceding description

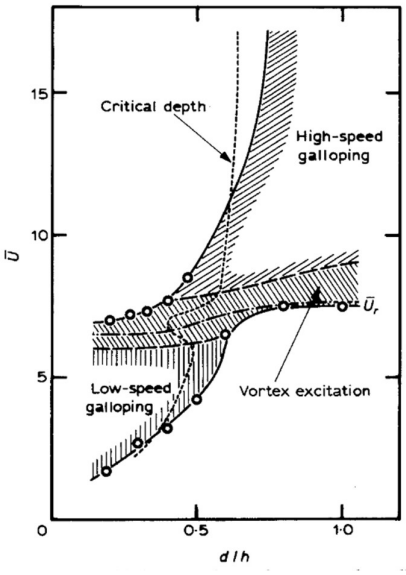

Figure 2.1 Types of galloping based on base suction characteristics over the rectangular bluff bodies (Nakamura and Hirata, 1991)

were figured by Nakamura and Hirata (1991) in the above chart.

The relation of fluctuation of flow velocity component during interaction to the structure can be defined as fluctuating frequency given by the following equation,

$$f_s = \frac{S_t \times U}{H} \tag{2.1}$$

where H is cross-section height perpendicular to flow stream direction, U is flow velocity and f_s is vortex shedding frequency or Strouhal number.

2.2. Rectangular Prism

2.2.1 Side Ratio (*D/H*)

The presence of a sharp corner in the leading edge normal to the flow stream direction of the rectangular prisms brings separation point fixed at the corner of the prism and does not move fore and after on the body as with circular shape. Flow characteristic around rectangular prism change dramatically at certain Reynold number and it causes

unregular developing in hydrodynamic forces and Strouhal number for certain side ratio.

The interaction of separated shear layer with the structure causes the growth of the boundary layer, separates and forms a separation bubble on the side surfaces or behind the prisms. A residual of separation shear layer which is not absorbed by bubble continue to the shear layer in the proportion which is dominated by after body shape (for example width to the height ratio). Hence, the flow feature such as reattachment type and formation of Karman vortex may differ among certain cases. (Okajima, 1982; Laneville and Yong 1983, Yang and Mason, 2019).

Separation point is possible to shift to the trailing edge rather than leading-edge with immediately reattach for extremely low of Reynold number. Once the Reynold number increase, the boundary layer separates from the body. Apart from this develops a separation bubble and the rest (unabsorbed) continue to grow in the trailing edge. The separation bubble in different size can be considered as a buffer layer which grows with fluid and vortices and releasing them when the vortex is shedding (Laneville and Yong, 1983). In the case of the stationary prism, the effect this flow behavior can be seen in the following figure adopted from Okajima,1982; 1990.

The discontinuity of Strouhal number at high Reynold number, Re ($= 4.2\times10^4$) as a function of side ratio (D/H). There were two main points that the abrupt change on the Strouhal number took place at $D/H \geq 2.0$ and after $D/H \geq 6$. After the last side ratio, it was not influenced by the side ratio. Furthermore, the rectangular with $D/H \geq 2.0$ the fluctuation of Strouhal number strongly depends on the range of Reynold number. In this case, there is an evolution of flow interaction to the bluff body which involves some parameters such as reattachment point and widening of wake size due to the growth of vortex shedding. Meanwhile, an abrupt change of hydrodynamic forces which is studied

in the wide range of Reynold Number is found at the prism with side ratio around 0.63. (See also in Nakaguchi 1968, Yu et al 2013).

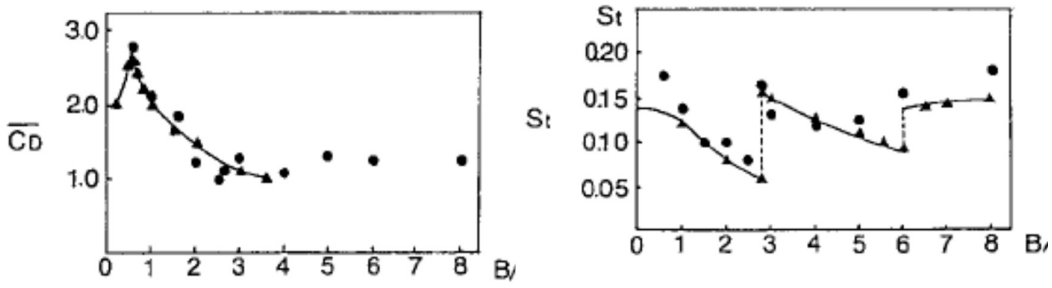

Figure 2.2. Strouhal number and drag coefficient characteristic of flow around rectangular prism both experimental and numeric as presented by Okajima 1990.

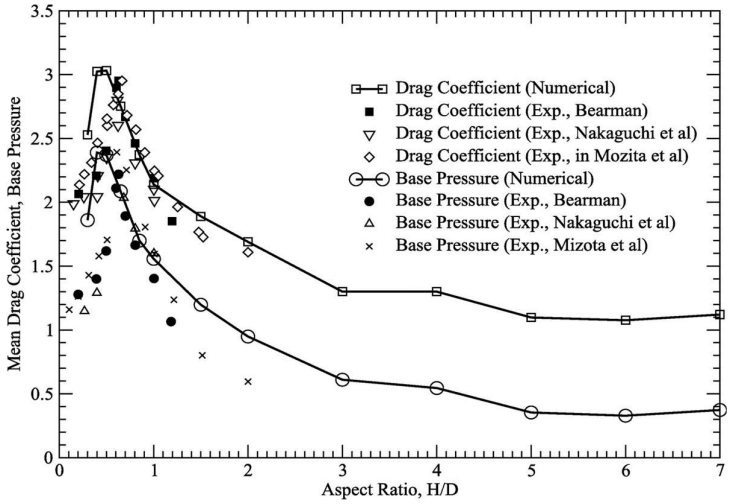

Figure 2.3. Effect of side ratio on hydrodynamic forces reproduced from Yu et al 2013.

Meanwhile, Knisley 1990 confirmed a Strouhal number which was expressed by Okajima that another abrupt on Strouhal number was found in the range of side ratio $8<D/H<10$. He also found that abrupt jump on Strouhal number is $2.5<D/H<3.33$ and another jump took place at $5<D/H<10$. The relationship between Strouhal number and side ratio as presented by Knisley can be seen in figure 2.4 below. Parkinson (1989) attributed the abrupt change on Strouhal number $2.0<D/H<3.0$ due to reattachment of the

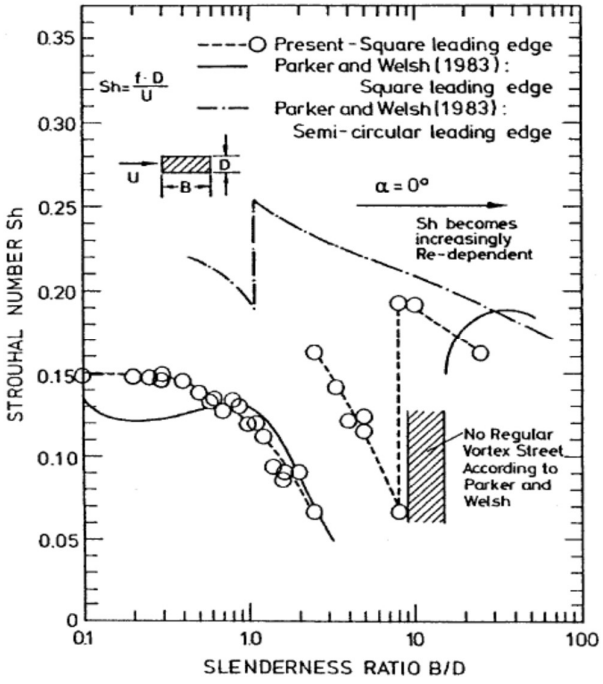

Figure 2.4. Strouhal numbers for rectangular prism with a wide range of side ratios (Knisley 1990)

shear layer on side surfaces with final separation takes place at the corner of the trailing edge.

Nakamura et al (1991) presented a new perspective of Strouhal number in contrast with the previous study. They examine rectangular prism with a side ratio of 3 to 16 in the low-speed wind tunnel with Reynold number range from 10^3 to 3×10^3. The stepwise abrupt jump on Strouhal number was observed with value are approximately equal to an integer multiple of 0.6 which is taken place at $D/H \approx 6$, 9, and 12. Below this side ratio, the Strouhal number equal to 0.6. They observed that there was one dominant spectrum frequency from the fluctuation of velocity on the rectangular prism with side ratio up to 15, and the spectrum of frequency was vast in the prism with a side ratio of 16 with no clear peak is found. However, the clear peak of spectrum frequency gradually decreases

by increasing side ratio and jumps to a higher value at certain side ratios with two dominants peaks at each stage.

The relationship of Strouhal number with the depth of the prism can be written as

$$S_t = \frac{f_s \times D}{U} = 0.6i \tag{2.2}$$

where i = integer $\left(\frac{D}{3}\right)$ for $D/H \geq 3$.

The index of i represents the number of vortices that are formed on the surface.

They argued that vortex shedding from both the sharp corner of the prism whose side ratio of 15 was distinguished by the unstable vortices of the impinging shear layer along the surface of the prism. It was originated around $D/H \approx 3.0$ where the wavelength of vortex shedding was equal to the afterbody depth. The Synchronous between wavelength velocity fluctuation and prism's depth occurs when D/H increased until the limit was approached through a non-linear flow process. When the side ratio was increased, the similar cycles were reversible. Hence, a stepwise of jumping Strouhal number is found.

In the case of an elastically mounted rectangular prism, the flow field, and vibration characteristics are also influenced by side ratio. In the case of rectangular with side ratio less than one, under low-speed range induced vibration, the system typically vibrates with amplitude less than one of cross-section height normal to the flow stream and certain range fluid velocity. This model of vibration only takes place with the ratio of Karman frequency to the natural frequency of the system is less than one. Unlike a circular cylinder that has a limited range of speed and excitation mode, a rectangular bluff body may gallop in a wide range of flow speed either the resonance frequency is less than one or more than one (Corless and Parkinson 1988). Nakamura and Hirata 1991 identified three distinct classes on excitation frequency and vortex shedding frequency ratio, those

were $f_y << f_v$; high-speed range, $f_y \approx f_v$; vortex resonance, $f_y >> f_v$; low-speed range to classify the types of galloping as represented in figure 2.1. Kiwata, et al. (2014) examined the vibration characteristics of an elastically mounted rectangular prism with side ratio from 0.2 to 0.5. He found that all features transverse vibration characteristic typically takes place underneath the resonant frequency.

In the range of after body size below the transition of galloping type, flow features is affected of after-body length in which in the range $D/H < 0.6$, increasing depth size (D) altered wake vortices to form close to the body until reaching $D/H \approx 0.63$ or 0.5 in case of relative-high of turbulent intensity. In this situation, the drag force is maximum. It seems that the interface of the shear layer and afterbody length has a meaningful effect on the pressure loading at the side surface, hence high-speed galloping takes place at D/H equal or around 0.7 and 0.5 for 12% turbulent intensity (Nakamura and Tomonari, 1977).

For mounted elastically the rectangular prism with side ratio $D/H > 1.0$, the following types of excitation from some studies have been provided. The rectangular with side ratio $L/D < 2$ to 3 as leading-edge vortex shedding responsible for body motion and typically vortex resonance is $V_r = 1/St$. This type of excitation is similar to circular cylinder i.e. Karman vortex induce the prism to oscillate (type 1 in figure 2.7). The separation flow at the leading edge creates a wide wake size and combines to von Karman vortex street. However, increase V_r bring the prism to expose to galloping. By increasing side ratio (2 to $3 < L/D < 4$ to 7, the vortices of the shear layer impinge on the side surface and establish a feedback-controlled source of excitation. In this range, Karman vortices are weak due to irregular wake. Transverse vibration induces leading-edge vortices and strengthens impinging vortex excitation (type 2 in figure 2.7). For rectangular with side

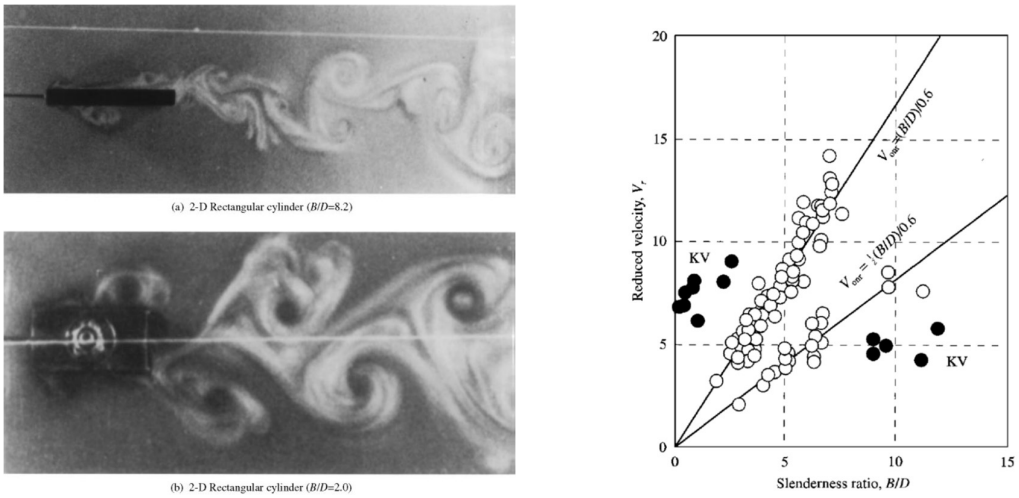

Figure 2.6 (a) flow visualization of vortex shedding over a rectangular prism with long side ratio (b) Onset galloping and Karman vortex (KV) behavior over a wide range of side ratio (Matsumoto, 1999).

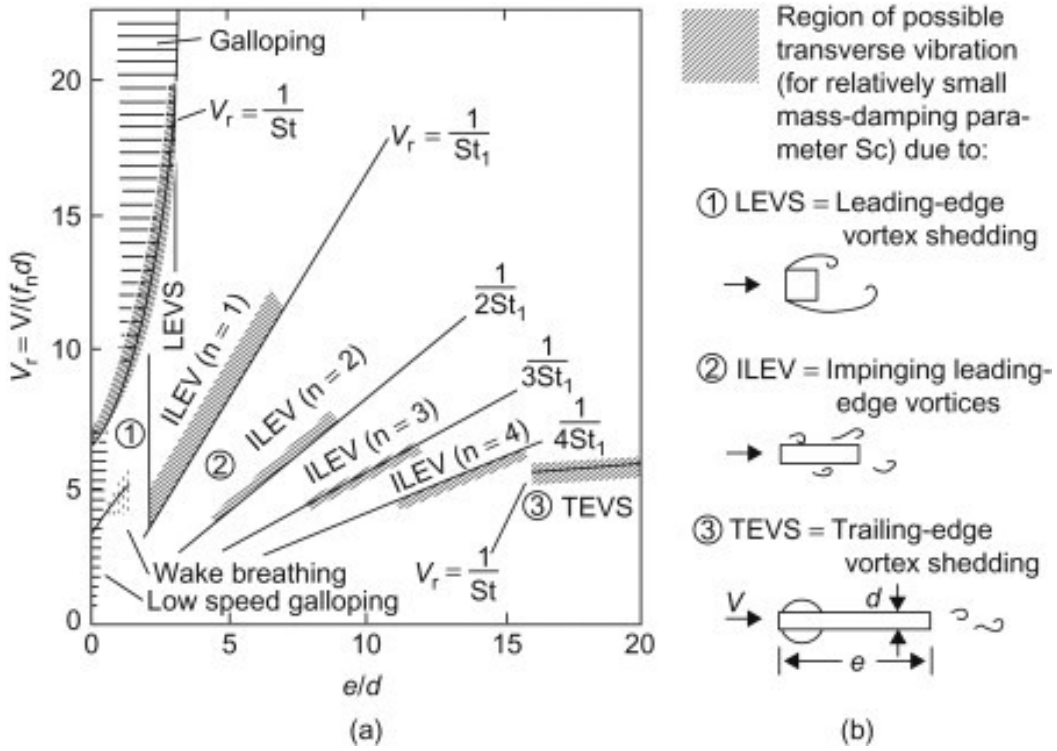

Figure 2.7. (a) The range of flow induces vibration for rectangular prism in crossflow. (b) Models of vortex formation for rectangular with various depth (after Naudascer and Wang, 1993).

ratio $D/H \geq 4$ to 7, the flow remains to reattach on the side surfaces, but Karman vortex street is much narrower and Strouhal number is higher (see figure 2.6). The resonant vibration onset takes place at the low-velocity flow stream. The oscillation mechanism may depend on not only leading-edge vortex behavior but also trailing-edge vortices (type 3 on figure 2.7). Hence, a rectangular prism with a sharp edge within the aspect ratio range below the critical point is less susceptible to vortex-induced vibration than a streamlined surface. This condition is unlike a circular cylinder (Naudascher and Wang, 1983; see also Naudascher and Rockwell 2004, and Matsumoto 1999).

In another perspective in terms of flow characteristics and galloping mechanism over a rectangular prism with a side ratio below the critical point ($D/H \leq 0.6$) has been investigated in some studies both experiment and numeric. Tamura and Dias (2003) studied instability of aerodynamic phenomena of infinite slender rectangular prisms with a side ratio of 0.2 with various damping ratios. They confirmed that response amplitude was independent on vortex induce vibration and has not potential to high-speed galloping range. Above this range, there was no galloping anymore when the reduced velocity increase. (See also Tamura and Itoh 1999).

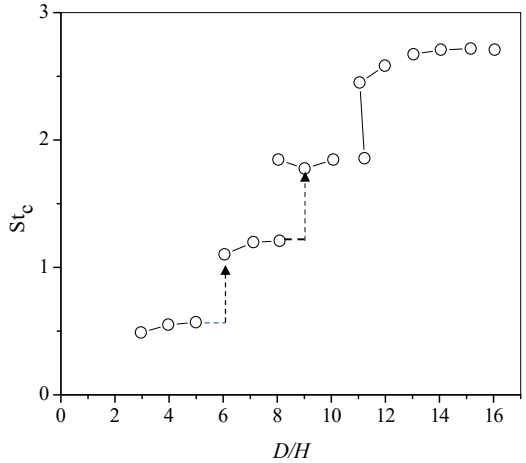

Figure 2.5. Strouhal number evolution under different side ratio (Nakamura, et al, 1991)

The determination of the critical point is also investigated based on the pressure fluctuation under a wide range of reduced velocity. There was a high peak of base pressure found in the prism with a side ratio of 0.4 instead of 0.6 at the prism undergoing oscillation which indicates strong resonance. In addition, no sharp peak of base pressure at the resonance for the prism with a side ratio of 0.6 instead of a weak peak appears near resonance in the square prism. Hence, side ratio D/H = 0.4 was considered as a critical side ratio of an oscillating rectangular prism and 0.67 for stationary prism. Meanwhile, the reduced velocity at resonance was considered to take place at 6.7 (Nakamura and Matsukawa, 1987; Nakamura and Hirata, 1989 and 1990).

2.2.2 Aspect Ratio (*L/H*)

Most of the literature on flow characteristics either stationary or undergoing oscillation of rectangular prism concern in the depth to height cross-section ratio as presented in the previous part. Meanwhile, flow structure around a bluff body is three-dimensional instead of two dimensional that results in the complexity of flow structure behavior is severe. The distinction of flow structure between two and three-dimensional one affects other flow parameters such as aerodynamic forces, pressure distribution, and other flow characteristics. The presence of the end effect of bluff bodies is considered as the main feature on that distinction (see. Kawamura, 1984; Okajima 2004; Rostamy, et al, 2012; Wang and Zhou. 2009; El Hassan, et al. 2015).

The main feature of flow field around the finite length or three-dimensional structure can be constructed as base, spanwise, and trailing vortex as presented by Wang and Zhou 2009 which is essential identic as presented by though it is not identic as the model presented by Kawamura 1984, but essential similar in presenting the three components of vortex mentioned, showing streamwise conical vortices separating from

the tip end. The interaction of the components of the flow field around the structure connects the vortices. Both trailing vortex and base vortex are connected to the spanwise vortex which is linked by downwash and upwash flow respectively. All type of vortices is in the same entity, i.e. arc-type organized model without considering the effect of aspect ratio. The effect of downwash flow on the vortex structure brings upper part of the arc-type structure bends upstream, resulting in the tip vortices. The lower part tilts upstream near the wall forming a base vortex as presented by Wang and Zhou, 2009 in the following figure.

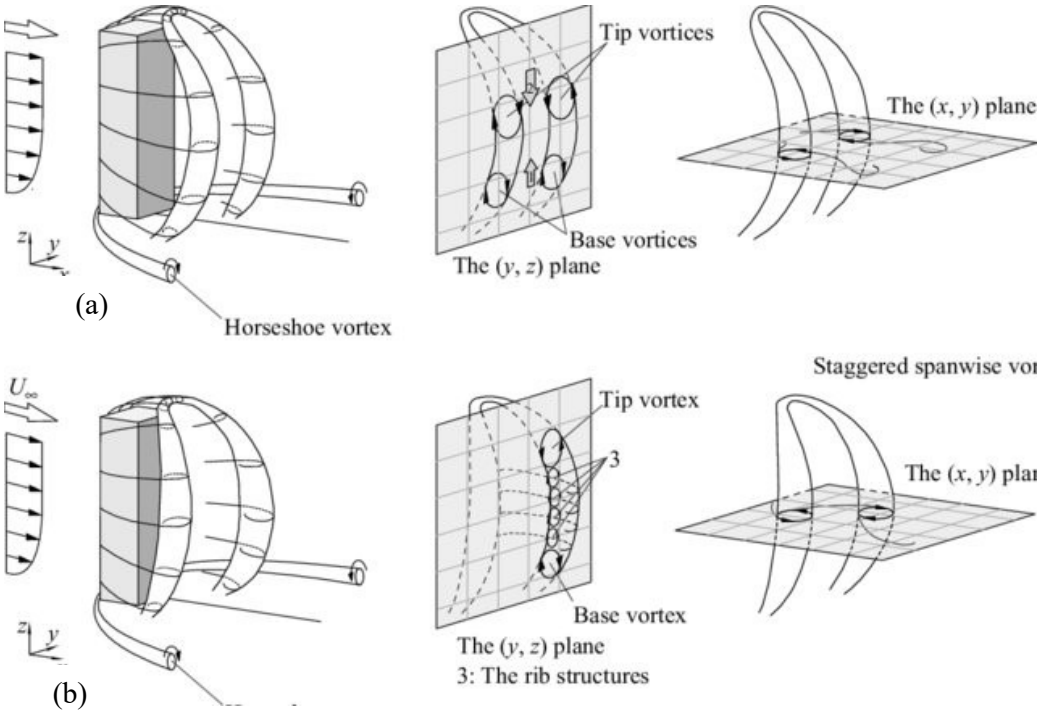

Figures 2.8. Model of the flow structure around a wall-mounted finite-length square cylinder: (a) symmetrically arranged two spanwise vortex roll, (b) staggered arranged spanwise vortex roll (Wang and Zhou, 2009).

The variation of aspect ratio (*L/H*) may change flow field characteristics including the three essentials wake structure mentioned previously. Some studies both cylinder and rectangular (mostly square) such as Kawamura et al., 1984; Matsumoto and Oiwake,

1984, Wang and Zhou, 2009, Okamoto and Sunabashiri 1992, Sumner and Heseltine, 2008 presented that prisms with aspect ratios above critical aspect ratios exhibit distinction on hydrodynamic forces, Strouhal number, base pressure, and flow-field structure. When the aspect ratio of finite prism above critical aspect ratio increases then those flow parameters approach infinite prism characteristics (approaching two-dimensional flow characteristics).

In the case of flow field characteristic, which is responsible for the evolution, those parameters cannot be decoupled from the presence boundary layer effect though its effect is still uncovered well. The presence of anti-symmetrical vortex underneath the boundary layer leads to Karman vortex/spanwise disappear and the vortices waken to be symmetrical type near the base. In addition, near the tip end of prism, it also weakens, hence prism with small aspect ratio interacts with base and tip vortex end due to the control of downwash flow.

The evolution vortex pattern along various aspect ratio with decreasing aspect ratio below critical aspect ratio has diminished base vortex, and Karman vortex suppressed or boarded in the base with symmetrical vortex appear in this range of aspect ratio leading critical aspect ratio take place around 3 (while Donnert, et al, 2007 is $L/H = 2.5$, which supported by Kappler, 2002). Meanwhile, prisms with aspect ratios greater than equal 5 show a similar flow pattern with antisymmetric vortices pattern. This flow pattern descends by decreasing aspect ratio and lead to decreasing mean drag and lift coefficient, base pressure, and Strouhal number. (Taniguchi, et al, 1981; Sumner, et al, 2017; Park and Lee, 2000).

The study about flow characteristics below critical aspect ratio with high Reynold number as mentioned above was also performed by Goncalves, et al 2015. They used

circular prism with an aspect ratio range of $2.0 \leq L/H \leq 0.1$ which the flow features including hydrodynamics forces characteristics are similar to those investigations. Meanwhile, this study was not found alternating forces at the prism with a very small aspect ratio ($L/H \leq 0.2$) due to there are not significant energy forces in the transverse direction. Flow structure formed around the prisms unable to generate alternating forces. The diminished transverse forces including energy are scrutinized as the developing of vortex structure from the end-tip of the prism.

2.3. D-section Prism

Unlike circular cylinder, D-section with the flat surface facing upstream, a separation point remains to take place fixed at the leading edge as commonly found in a rectangular prism. In addition, three-dimensional vortex wake remains exist in this type of cylinder as a circular cylinder for both fixed and oscillating cylinders. As investigated by Feng, 1968, spanwise wake vortex fluctuation was highly correlated to the spanwise length of the cylinder. This correlation is higher than that circular cylinder both stationary and oscillating prism. In the same damping system with a circular prism, the prism oscillation of D-section is much easier to gallop than circular prism with linearly decreasing with increasing the damping system. In contrast, the circular cylinder is only subjected to vortex-induced vibration and does not potential to gallop from the rest below the resonant velocity.

Zhao, et al (2018) studied the flow-induced vibration phenomena over a D-section prism with two conditions of D-section orientations viz. a flat surface facing the upstream and reverse direction with wide range of reduced resonant velocities ($2.3 \leq V_r \leq 20$) and Reynold number $1080 \leq Re \leq 9000$ to catch the possibility of galloping types over this prism. The synchronous region was initiated when the reduced velocity approach 3.0 with

response amplitude was slightly under natural frequency. This investigation is in line with Feng 1968 with a high mass damping ratio as presented in the preceding description that a D-section where the curve section facing downstream shows a similar in response oscillation characteristics and slightly different in peak amplitude compared with circular cylinder (6% less than circular cylinder). According to this investigation, by considering the dynamic response including response amplitude, fluid forces, and phase, three types of galloping were presented, i.e. VIV-dominated response (V_r < 10), transition regime (10<V_r<12.5) galloping-dominated response (V_r >12.5). (See figure 2.9 below). Meanwhile, Parkinson 1963 presented that free vibration of D-section underwent VIV response in the range of reduced velocity of 4.1< V_r <7.9, high speed galloping V_r > 7.9. Meanwhile, they found Strouhal number is 0.140 for fixed prism which good agreement previous investigation such as Brooks 1960 that is 0.135 and Weaver & Veljkovic is 0.150. The occurrence of resonance (V_r=1/S_t ≅ 7.1) was presented lower than that is in Parkinson (1/S_t = 7.4). While Nakamura and Hirata 1989 found the onset of vortex-resonance velocity under stationary D-section (V_r = 1/St) is 6.7 with Strouhal number was 1.149 (see table 1). This value is much higher than the initial synchronous region onset in the classical cylinder that takes place at 5.0 with Strouhal number around 0.12.

In the case of response amplitude of D-section undergoing high-speed galloping as Zhao et al (2018) presented, oscillation frequency ratio (f_y/f_n) around 1.0 for all range of reduced velocity which is much higher than square cylinder reported by Bearman, et al 1987 without hysteresis phenomenon was found in this D-section prism. Unlike the square prism, the insufficient of the afterbody of this D-section does not allow reattachment of the shear layer which is attributed to hysteresis phenomenon in the square prisms (Luo, et al, 2003).

In the reverse position, the response characteristics are like the circular cylinder which is pure to vortex-induce vibration (refer to figure 2.10) with the frequency body oscillation was locked in the natural frequency of the system at $V_r = 3.6$. They also imply that an after body is an independent parameter for vortex-induced vibration in the case of the prism with low mass and damping ratios. The hysteresis phenomenon was also found in this investigation even if the after-body shape which is attributed by other studies is absent (see figure 2.10). In this case, dynamic response characteristics are identic with a classical circular cylinder with the hysteresis occurrences near onset lock-in and desynchronization regions. These findings are in contrast to the review article of Parkinson (1989) and presented by Naudascher and Rockwell 2005. The importance of the afterbody shape was also proposed by Bearman and Davies 1977 in Zhao et al. (2018) that prisms with small after body are not subjected to vortex-induced vibration (VIV) under normal conditions. (See also Tamura, 1999).

Table 2.1. Vortex-resonance velocity (V_r) of bluff bodies at the stationary condition*

Rectangular Prisms							
D/H	0.2	0.3	0.4	0.5	0.6	0.8	1.0
St	0.156	0.156	0.154	0.147	0.143	0.135	0.127
V_r	6.4	6.4	6.5	6.8	7.0	7.4	7.9
D-Section							
D/H	0.5	0.63	0.7	0.77	0.83	0.9	1.0
St	0.149	0.145	0.135	0.132	0.128	0.125	0.123
V_r	6.7	6.9	7.4	7.6	7.8	8.0	8.1

**(Nakamura and Hirata, 1989)*

Even though the D-section (flat surface faces upstream) with a side ratio of 0.5 was categorized a 'soft' galloping as mentioned by Feng 1968, these bluff bodies behave as the vortex-excitation type with the presence of afterbody length. The critical depth with vortex resonance velocity takes place at $D/H = 0.7$ with the resonant reduced velocity takes place at 5.5.

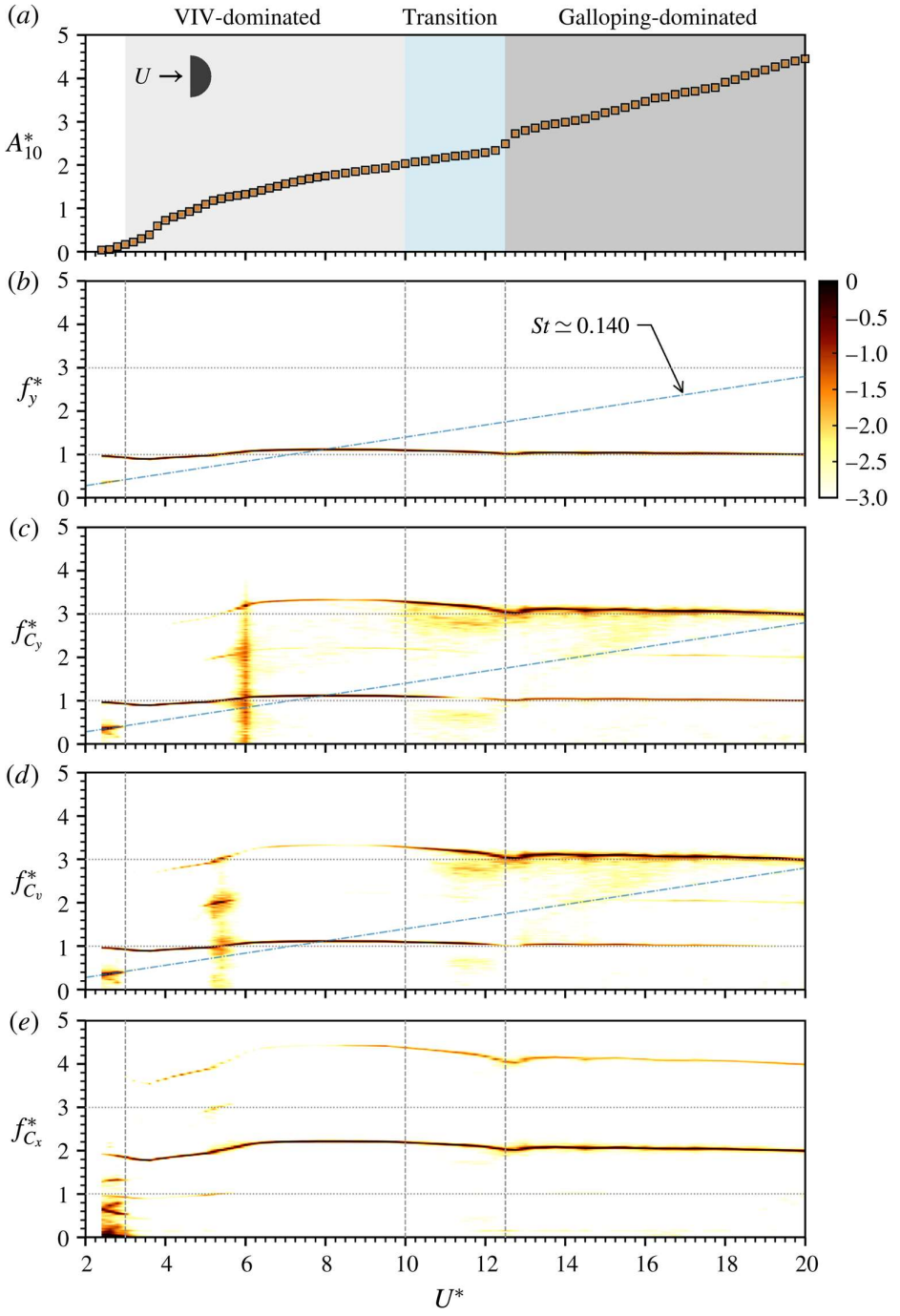

Figure 2.9. The amplitude response and the logarithmic-scale normalized frequency power spectral density (PSD) contours as a function of the reduced velocity. In (*a*): □, measurements with increasing V_r; (■) measurements with decreasing V_r; the VIV-dominated, transition, and galloping-dominated regimes are highlighted in light grey, light blue, and dark grey, respectively. In (*b–e*): the vertical dashed lines represent the boundaries of the response regimes, and the horizontal dotted lines highlight the first and the third harmonics (reproduced from Zhao, et al, 2018).

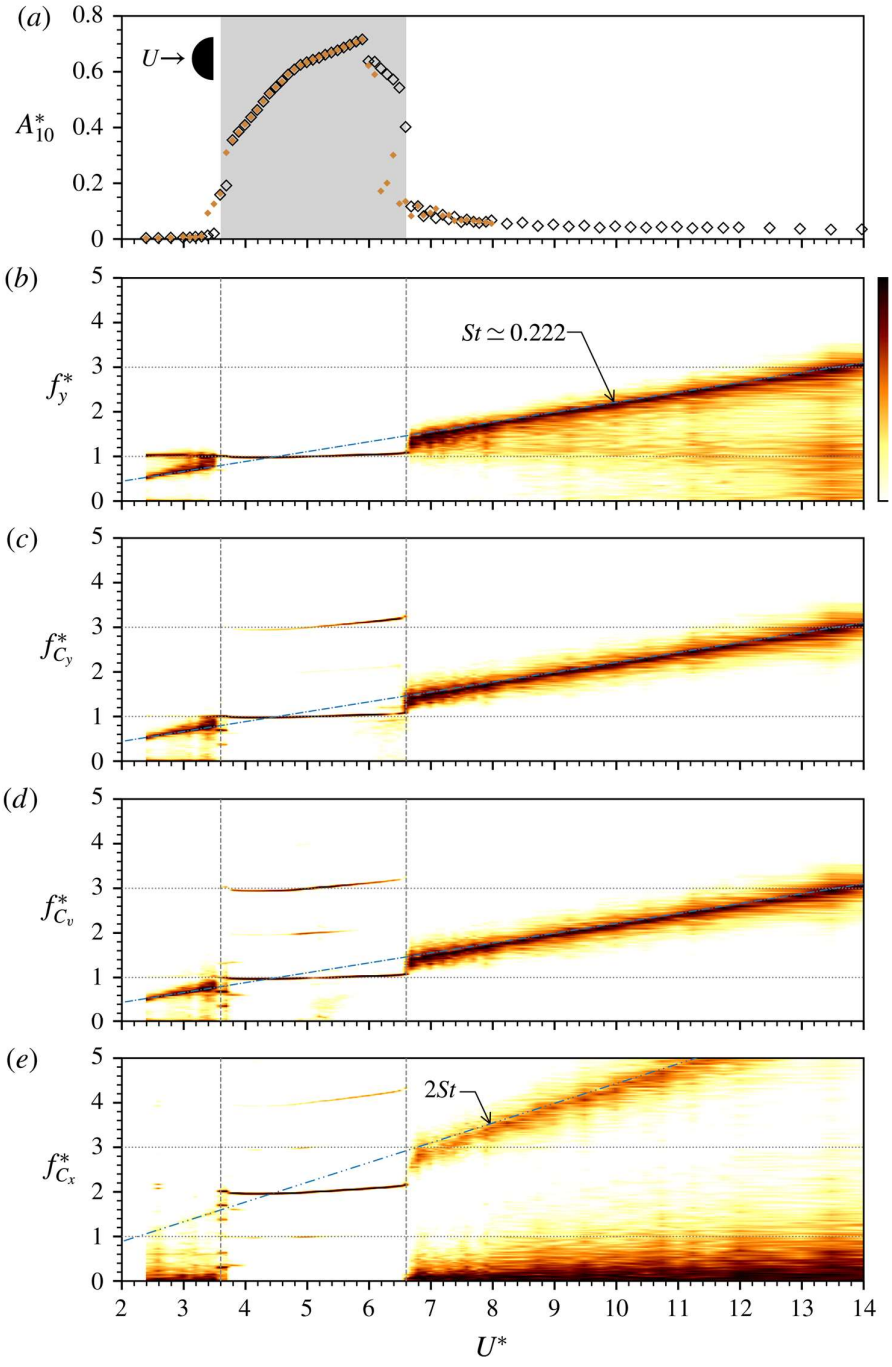

Figure 2.10. The amplitude and the logarithmic-scale normalized frequency PSD contours as a function of the reduced velocity for D-section's curve faces upstream. In (*a*): ◊, measurements with increasing V_r ; ♦, measurements with decreasing V_r . The lock-in region is highlighted by the light grey area in (*a*) and bounded by vertical dashed lines in (*b–e*) (reproduced from Zhao, et al, 2018).

The presence of a sharp peak on-base suction as one indicator of vortex resonance for the prism with short after body length though it does not exactly feature vortex-resonance velocity (Nakamura and Hirata, 1989).

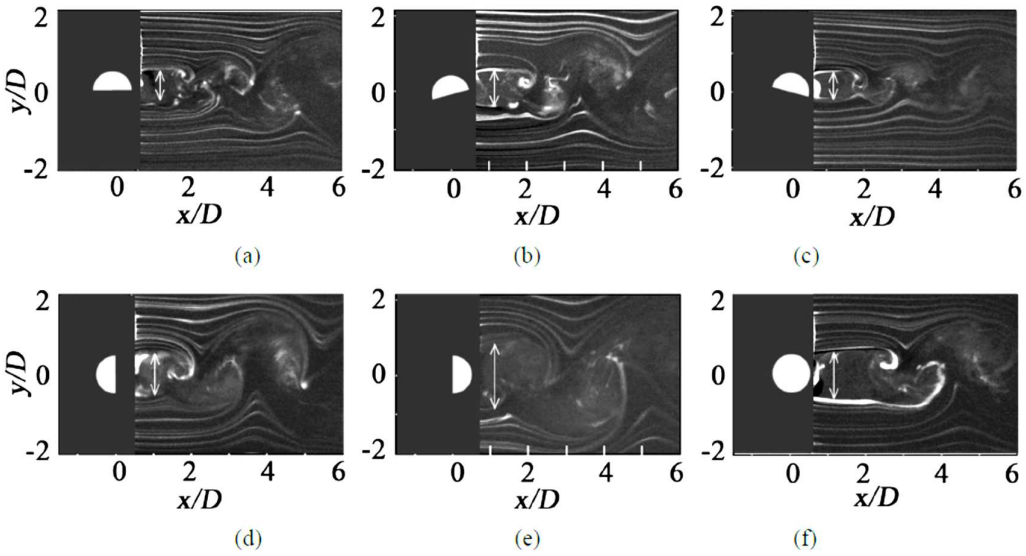

Figure 2.11. Flow visualization around D-section prism with various attack angle: (a) α = 0°; (b) α = -15°; (c) α = 15°; (d) α = -90°; (d) α = 90°; (f) circular cylinder (reproduced from Yamagata, et al, 2016).

In figure 2.11, Yamagata, et al. (2016) visualized the flow field around D-section with various modes of angle attach that D-section with the flat surface facing upstream, bring wide size in vortex area. Aerodynamics forces pressure sound levels are also high relative to their counterparts.

2.4. Fluid-Structure Interaction Parameters

Several parameters used in this study can be consist of flow and structure parameters which influences flow structures- interaction. However, this research only presents some parameters related.

Reynold Number, *Re*

Reynold number is used to classify similarity of flow dynamic which has similar geometrical streamlines and bodies as described by Schilting (1987). The Reynolds number expresses as a ratio of inertial forces to viscous forces. This ratio is an index to classify flow characteristics or phenomena that are expected to occur. The relation between two forces is interchangeable to control force balance i.e. when the ratio is large, inertial force control fluid force balance, when the ratio is small, the viscous forces control the balance.

$$R_e = \frac{\rho U H}{\mu} \tag{2.1}$$

where U is flow velocity, H is characteristic length perpendicular to flow stream, and μ is dynamic viscosity.

Reduced Velocity, V_r

Reduced velocity is a non-dimensional velocity that indexes the magnitude of fluid forces to drive the structure to oscillate with a certain frequency. At the resonance, amplitude-frequency approaches the natural frequency of the system, at the resonance state, the reduced velocity is an inverse of Strouhal number. The frequency characteristic of reduced velocity is measured at stationary water conditions. Hence, at the resonance, it can be written as

$$V_r = \frac{U}{f^* H} \approx \frac{U}{f_n H} = \frac{1}{S_t} \tag{2.2}$$

where f is amplitude-frequency, f_n is the natural frequency of the system at the rest condition. However, in the case of low-speed galloping in which pure instability due to the fluctuation of separated shear layer is applied, this parameter also is still applied to define galloping characteristics (see also in Kiwata, 2014).

Aspect Ratio (*L/H*) and Side Ratio (*D/H*)

Aspect ratio and side ratio represent a geometric shape of the bluff body that a ratio of spanwise length to the height of bluff body normal to the flow while side ratio represents a ratio of depth to the height of the bluff body

$$\frac{L}{H} = \frac{spanwise\ length}{height\ of\ cross\ section} \tag{2.3a}$$

$$\frac{D}{H} = \frac{depth\ in\ line\ flow\ stream}{height\ of\ cross\ section} \tag{2.3b}$$

Mass Ratio, *M*

The mass ratio is defined as prism density times volume of the structure per unit length of prism plus the displaced fluid mass per unit length of prism i.e. water density (ρ') over fluid mass displaced by a prism. Since the volume of a prism is equal to the mass volume displaced by water, then the mass ratio can be written as a density ratio.

$$\frac{\rho_{prism} + \rho'}{\rho_{water}} \tag{2.4}$$

where ρ' is inertia density due to the viscous effect, and ρ is the density

Reduced Damping Parameter, C_n

Reduced damping parameter became one of the parameters for flow-induced vibration of the structure, see e.g. Feng (1968). It is proportionally to structural damping parameter (δ) and the ratio between effective or vibration mass and fluid mass displaced by the structure. It is defined as

$$\frac{2M\delta_{sy}}{\rho_f DH} = 2M \times \delta_{sy} \tag{2.5}$$

where δ_{sy} is logarithm decrement of response amplitude which is taken by hitting the prism at stationary water condition. This term represents the decay rate of dissipation

energy to the fluid which is defined by considering positive peak (P_i) of the waveform of the decay rate. The illustration of the peak decay rate can be represented in the following figure.

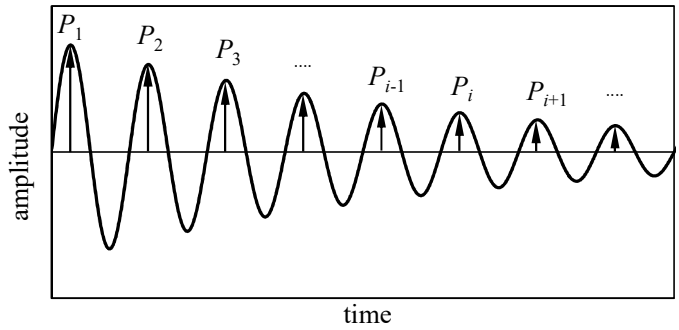

Figure 2.12. Peak decay rate illustration

$$\delta = \frac{\sum \ln \frac{P_i}{P_{i+1}}}{N} \tag{2.6}$$

Non-dimensional Displacement, η

Nondimensional amplitude is the ratio of tip displacement of the prism to cross-section height perpendicular to flow direction.

$$\frac{y_{rms}}{H} = \frac{rms\ value\ of\ tip\ displacement}{cross\ section\ height} \tag{2.5}$$

The Angle of Displacement (θ_{rms})

In the case of cantilevered mounted prisms with the tip, the end is free while another is rigid, velocity displacement on the tip end of the prism is varied along the spanwise prism. In this study, the measurement point of displacement takes place at the tip end as $y_{rms.}$ To deal with different displacement velocity of the prism, the following equation is formulated to calculate the angle of tip displacement as:

$$\frac{y_{rms}}{L+l} \times \frac{180}{\pi} \tag{2.6}$$

where l is spring length (mm).

References

Bearman, P. W. (2011). Circular cylinder wakes and vortex-induced vibrations. *Journal of Fluids and Structures*, *27*(5–6), 648–658. https://doi.org/10.1016/j.jfluidstructs.2011.03.021

Bearman, P. W., Gartshore, I. S., Maull, D. J., & Parkinson, G. V. (1987). Experiments on flow-induced vibration of a square-section cylinder. *Journal of Fluids and Structures*, *1*(1), 19–34. https://doi.org/10.1016/S0889-9746(87)90158-7

Blevins, Robert D. (1974) *Flow induced vibration of bluff structures.* Dissertation (Ph.D.), California Institute of Technology. https://resolver.caltech.edu/CaltechETD:etd-09302005-082356

Corless, R. M., & Parkinson, G. V. (1988). A model of the combined effects of vortex-induced oscillation and galloping. *Journal of Fluids and Structures*, *2*(3), 203–220. https://doi.org/10.1016/S0889-9746(88)80008-2

Donnert, G. D., Kappler, M., & Rodi, W. (2007). Measurement of tracer concentration in the flow around finite-height cylinders. *Journal of Turbulence*, *8*, 1–18. https://doi.org/10.1080/14685240701429792

El Hassan, M., Bourgeois, J., & Martinuzzi, R. (2015). Boundary layer effect on the vortex shedding of wall-mounted rectangular cylinder. *Experiments in Fluids*, *56*(2). https://doi.org/10.1007/s00348-014-1882-6

Feng, C. C. (1968). *The measurement of vortex induced effects in flow past stationary and oscillating circular and D-section cylinders* (T). University of British Columbia. Retrieved from https://open.library.ubc.ca/collections/ubctheses/831/items/1.0104049

Gonçalves, R. T., Franzini, G. R., Rosetti, G. F., Meneghini, J. R., & Fujarra, A. L. C. (2015). Flow around circular cylinders with very low aspect ratio. *Journal of Fluids and Structures*, *54*, 122–141. https://doi.org/10.1016/J.JFLUIDSTRUCTS.2014.11.003

Iwan, W. D., & Blevins, R. D. (1974). A model for vortex induced oscillation of structures. *Journal of Applied Mechanics, Transactions ASME*, *41*(3), 581–586. https://doi.org/10.1115/1.3423352

Kiwata, T., YAMAGUCHI, M., KONO, T., & Ueno, T. (2014). Water tunnel experiments on transverse-galloping of cantilevered rectangular and D-section prisms. *Journal of Fluid Science and Technology*, *9*(3), 1–5. https://doi.org/10.1299/jfst.2014jfst00

KIWATA, T., YAMAGUCHI, M., NAKAJIMA, A., KONO, T., & UENO, T. (2014). PVP2014-28939. In *Flow-Induced Transverse Vibration of A Cantilevered Prism For Energy Harvesting* (pp. 1–10). Proceeding of the ASME Pressure Vessel & Piping Division Confrence.

Knisely, C. W. (1990). Strouhal numbers of rectangular cylinders at incidence: A

review and new data. *Journal of Fluids and Structures*, *4*(4), 371–393. https://doi.org/10.1016/0889-9746(90)90137-T

Laneville, A., & LüZhi Yong. (1983). Mean flow patterns around two-dimensional rectangular cylinders and their interpretation. *Journal of Wind Engineering and Industrial Aerodynamics*, *14*(1–3), 387–398. https://doi.org/10.1016/0167-6105(83)90040-5

Luo, S. C., Chew, Y. T., & Ng, Y. T. (2003). Hysteresis phenomenon in the galloping oscillation of a square cylinder. *Journal of Fluids and Structures*, *18*(1), 103–118. https://doi.org/10.1016/S0889-9746(03)00084-7

Matsumoto, M. (1999). Vortex Shedding of Bluff Bodies: a Review. *Journal of Fluids and Structures*, *13*(7–8), 791–811. https://doi.org/10.1006/jfls.1999.0249

Mannini, C., Marra, A. M., Massai, T., & Bartoli, G. (2016). Interference of vortex-induced vibration and transverse galloping for a rectangular cylinder. *Journal of Fluids and Structures*, *66*, 403–423. https://doi.org/10.1016/j.jfluidstructs.2016.08.002.

NAKAGUCHI, H., HASHIMOTO, K., & MUTO, S. (1968). An Experimental Study on Aerodynamic Drag of Rectangular Cylinders. *The Journal of the Japan Society of Aeronautical Engineering*, *16*(168), 1–5. https://doi.org/10.2322/jjsass1953.16.1

Nakamura, Y., & Hirata, K. (1989). Critical geometry of oscillating bluff bodies. *Journal of Fluid Mechanics*, *208*, 375–393. https://doi.org/10.1017/S0022112089002879

Nakamura, Y., Hirata, K., & Urabe, T. (1991). Galloping of rectangular cylinders inthe presence of a splitter plate. *Journal of Fluids and Structures*, *5*(5), 521–549. https://doi.org/10.1016/S0889-9746(05)80004-0

Nakamura, Y., & Tomonari, Y. (1977). Galloping of rectangular prisms in a smooth and in a turbulent flow. *Journal of Sound and Vibration*, *52*(2), 233–241. https://doi.org/10.1016/0022-460X(77)90642-3

Nakamura, Yasuharu, & Matsukawa, T. (1987). Vortex excitation of rectangular cylinders with a long side normal to the flow. *Journal of Fluid Mechanics*, *180*(1), 171. https://doi.org/10.1017/S0022112087001770

Naudascher, E. Rockwell, D. (2005). *Flow -Induced Vibrations: an Engineering Guide*. Dover Publication Inc.

Naudascher, E., & Wang, Y. (1993). Flow-induced vibrations of prismatic bodies and grids of prisms. *Journal of Fluids and Structures*. https://doi.org/10.1006/jfls.1993.1021

Nourazar, S., & Mirzabeigy, A. (2013). Approximate solution for nonlinear Duffing oscillator with damping effect using the modified differential transform method. *Scientia Iranica*, *20*(2), 364–368. https://doi.org/10.1016/j.scient.2013.02.023

Okajima, A. (1982). Strouhal numbers of rectangular cylinders. *Journal of Fluid Mechanics*, *123*(1), 379. https://doi.org/10.1017/S0022112082003115

OKAJIMA, A., NAGAHISA, T., & ROKUGOH, A. (1990). A Numerical Analysis of Flow around Rectangular Cylinders. *JSME International Journal. Ser. 2, Fluids Engineering, Heat Transfer, Power, Combustion, Thermophysical Properties*, *33*(4), 702–711. https://doi.org/10.1299/jsmeb1988.33.4_702

Okamoto, S., & Sunabashiri, Y. (1992). Vortex Shedding From a Circular Cylinder of Finite Length Placed on a Ground Plane. *Journal of Fluids Engineering*, *114*(4), 512. https://doi.org/10.1115/1.2910062

Park, C.-W., & Lee, S.-J. (2000). Free end effects on the near wake flow structure behind a finite circular cylinder. *Journal of Wind Engineering and Industrial Aerodynamics*, *88*, 231–246. https://doi.org/10.1016/S0167-6105(00)00051-9

Parkinson, G. (1989). Phenomena and modelling of flow-induced vibrations of bluff bodies. *Progress in Aerospace Sciences*, *26*(2), 169–224. https://doi.org/10.1016/0376-0421(89)90008-0

Sakamoto, H., & Oiwake, S. (1984). Fluctuating forces on a rectangular prism and a circular cylinder placed vertically in a turbulent boundary layer. *Journal of Fluids Engineering, Transactions of the ASME*, *106*(2), 160–166. https://doi.org/10.1115/1.3243093

Seiichi TANIGUCHI, Hiroshi SAKAMOTO, M. A. (1981). Flow around Circular Cylinders of Finite Height Placed Vertically in Turbulent Boundary Layers, *24*(187), 37–44. https://doi.org/https://doi.org/10.1299/jsme1958.24.37

Tamura, T., & Itoh, Y. (1999). Unstable aerodynamic phenomena of a rectangular cylinder with critical section. *Journal of Wind Engineering and Industrial Aerodynamics*, *83*(1–3), 121–133. https://doi.org/10.1016/S0167-6105(99)00066-5

Wang, H. F., & Zhou, Y. (2009). The finite-length square cylinder near wake. *Journal of Fluid Mechanics*, *638*, 453–490. https://doi.org/10.1017/S0022112009990693

Wang, Q., Li, M., & Xu, S. (2015). Experimental study on vortex induced vibration (VIV) of a wide-D-section cylinder in a cross flow. *Theoretical and Applied Mechanics Letters*, *5*(1), 39–44. https://doi.org/10.1016/j.taml.2015.01.002

Weaver, D. S., & Veljkovic, I. (2005). Vortex shedding and galloping of open semi-circular and parabolic cylinders in cross-flow. *Journal of Fluids and Structures*, *21*(1 SPEC. ISS.), 65–74. https://doi.org/10.1016/j.jfluidstructs.2005.06.004

Williamson, C. H. K., & Govardhan, R. (2004). VORTEX-INDUCED VIBRATIONS. *Annual Review of Fluid Mechanics*, *36*(1), 413–455. https://doi.org/10.1146/annurev.fluid.36.050802.122128

Yamagata, T., Saito, N., & Fujisawa, N. (2016). Aeolian Tone from a Semi-Circular Cylinder in a Stream. *Journal of Flow Control, Measurement & Visualization*, *4*(4), 30–37. https://doi.org/10.4236/jfcmv.2016.41003

Yang, T., & Mason, M. S. (2019). Aerodynamic characteristics of rectangular cylinders in steady and accelerating wind flow. *Journal of Fluids and Structures*, *90*, 246–262. https://doi.org/10.1016/j.jfluidstructs.2019.07.004

Zdravkovich, M. M. (1982). Modification of Vortex Shedding in the Synchronization

Range. *American Society of Mechanical Engineers (Paper)*, *104*, 513–517.

Zhao, J., Hourigan, K., & Thompson, M. C. (2018). Flow-induced vibration of D-section cylinders: An afterbody is not essential for vortex-induced vibration. *Journal of Fluid Mechanics*, *851*, 317–343. https://doi.org/10.1017/jfm.2018.501

Yu, D., Butler, K., Kareem, A., Glimm, J., & Sun, J. (2013). Simulation of the influence of aspect ratio on the aerodynamics of rectangular prisms. *Journal of Engineering Mechanics*, *139*(4), 429–438. https://doi.org/10.1061/(ASCE)EM.1943-7889.0000494

Chapter 3

Research Method and Procedures

3.1. Experimental Apparatus

All experimental process on flow-induced vibration characteristics was carried out using a water tunnel facility in Fluid Dynamics Laboratory Kanazawa University JAPAN. The general layout of the water tunnel apparatus is shown in figure 3.1 while figure 3.5 shows a schematic diagram of a water tunnel and measurement instruments. The water tunnel equipped with an underground water tank that is circulated by a centrifugal pump completed with the control valves. The rectangular test section of the water tunnel has a height of 400 mm, a width of 167 mm, and a length of 780mm. This water tunnel equipment is also equipped with measurement instruments which connected to the Central Processor Unit (CPU).

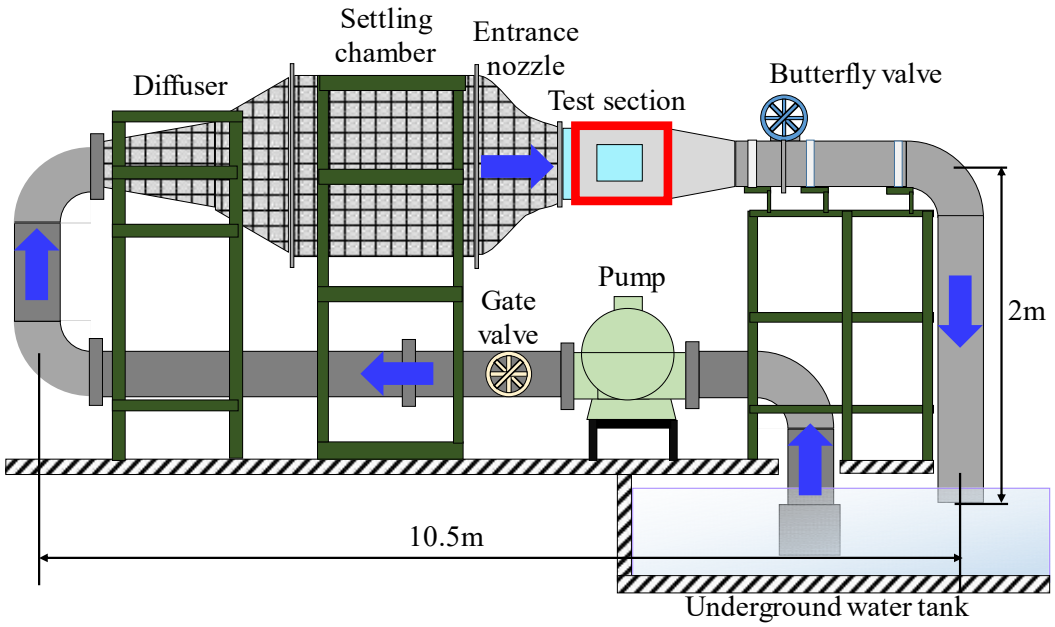

Figure 3.1. The layout of the water tunnel

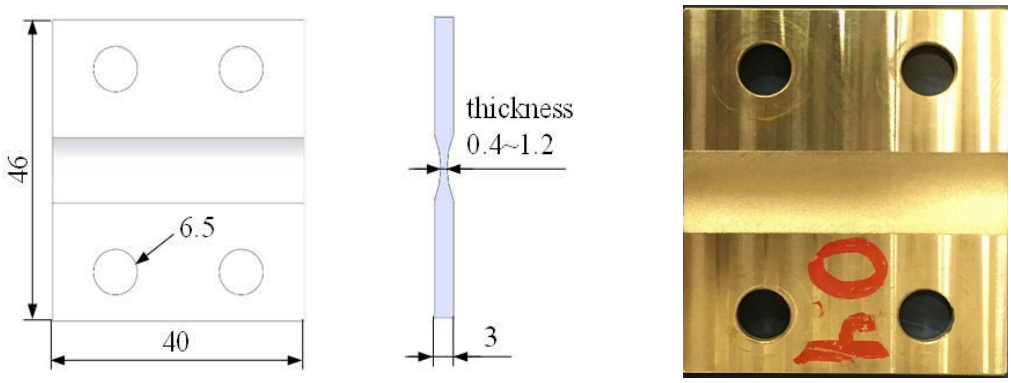

Figure 3.2 Plate spring model

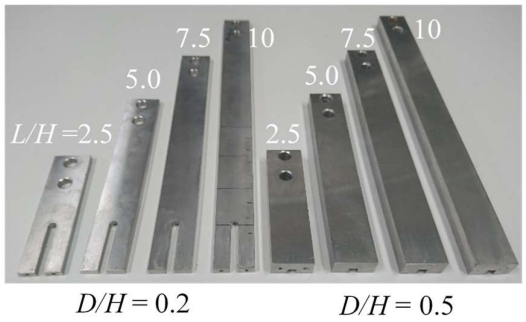

(a) Bluff bodies material - Rectangular

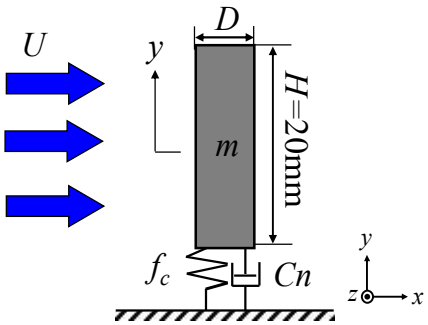

(b) Vibration model with one DoF

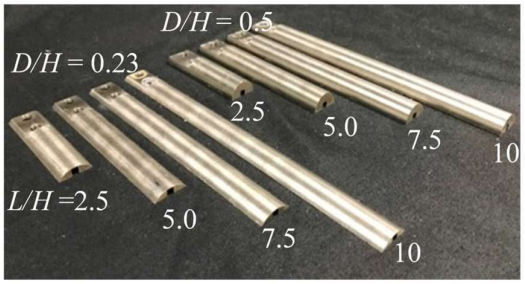

(c) Bluff bodies material: D-section

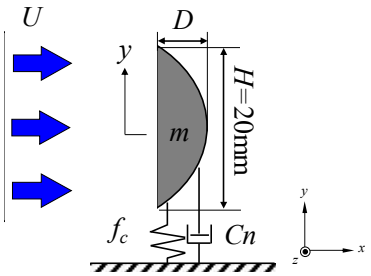

(d) Vibration model with one DoF

Figure 3.3. Cross-section models of bluff bodies and flow-induced vibration models

In the area of the test section, the prism was mounted elastically to a plate spring attached to the ceiling wall of the test section with a jig as a schematic model in figure 3.5a-b (see figure 3.2 for plate spring detail). Figure 3.3 shows two test models of rectangular prisms with different aspect ratios *L/H*. The prisms were made of stainless steel with smooth surfaces and sharp edges with a cross-section height *H* of 20 mm. The side ratios *D/H* (where *D* is the depth of the prism in the flow direction) of the rectangular

prisms were 0.2 and 0.5. The aspect ratios *L/H* (where *L* is span length of a prism) of the prisms were varied from 2.5 to 10 (see figures 3.3a-d).

The dynamic properties of prisms and plat springs were summarized in table 3.1. These flow-induced vibration experimental studies consist of several parts which are plain prism, splitter, attached endplate, and added plate (stepped prisms). Those were carried out in the subsequent experiment process.

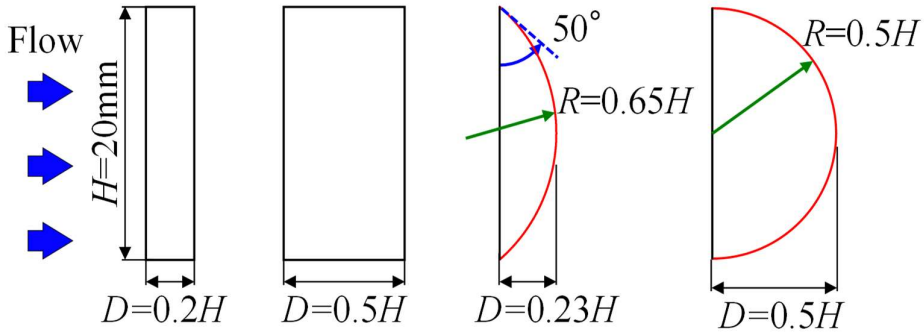

Figure 3.4 The cross-section model of bluff-bodies

3.2. Experimental Method

The transverse flow-induced motion of the prisms which is figured as a schematic diagram in figures 3.4 and the cross-section models are presented in figures 3.5 which are attributed to a single degree of freedom (DOF) representing the fluid-structure interaction. The body motion is compiled as a second derivative linear equation defined equation below.

$$m\ddot{y}(t) + c\dot{y}(t) + ky(t) = F_y(t) \tag{3.1}$$

where m is the total mass of the system (included added mass), c is structural damping parameter of the system, k is plat spring constant, and F_y is a total fluid force acting on the system.

3.2.1. Effect of Aspect Ratios (*L/H*)

Flow-induced vibration characteristics of rectangular and D-section prisms were investigated using a water tunnel in several sequences of the experiment process. The flow velocity U of water flow was varied from 0.7 to 2.8 m/s by controlling pump rotational speed. The uniform flow velocity U was measured using a pitot tube and digital differential pressure gauge (NAGANO KEIKI, GC50). The Reynold number Re (= UH/v, where H and v are the height of prism and kinematic viscosity of water, respectively) range was 1.6×10^4 to 6.6×10^5. The reduced velocity V_r (= U/f_cH,) was calculated from the characteristic frequency of the prism f_c.

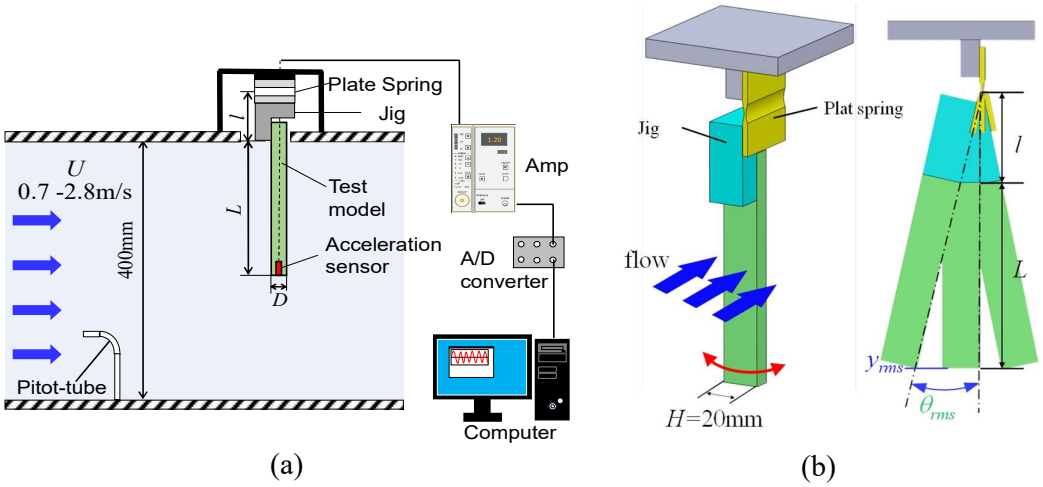

Figure. 3.5 (a) Schematic diagram of the test section and instrument measurement. (b) Illustration of the displacement and angle amplitudes of a prism test

Tip displacement y was measured using an acceleration sensor (SHOWA MEASURING INSTRUMENT, 2302CW) implanted inside the tip of the prism and an integrator (RION UV-12 and UV-05). The signals output of the integrator was converted using 12-bit A/D converter with the sampling frequency of 2 kHz, and 16,834 data points were recorded. The characteristic frequency of the test model's f_c was measured using the FFT analyzer (ONO SOKKI, CF-5201). The characteristic frequency f_c of the prism was

Table 3.1 Specification of the test models for rectangular prisms with different aspect ratios

L/H	ts (mm)	Rectangular						D-section					
		D/H						D/H					
		0.2			0.5			0.23			0.5		
		f_n	δ	C_n	f_n	δ	C_n	f_n	δ	C_n	f_n	δ	C_n
2.5	0.4	34.42	0.111	1.95	43.09	0.016	0.28	41.50	0.022	0.30	29.79	0.024	0.32
	0.6	31.13	0.044	0.77	26.37	0.023	0.40	67.99	0.023	0.32	48.58	0.036	0.49
5	0.4	23.80	0.035	0.61	15.14	0.036	0.63	26.61	0.031	0.36	17.09	0.025	0.32
	0.6	38.70	0.026	0.46	24.78	0.026	0.46	43.58	0.023	0.27	28.08	0.026	0.32
	0.8	-	-	-	33.94	0.017	0.30	60.18	0.030	0.36	38.82	0.016	0.21
7.5	0.6	26.37	0.061	1.08	16.48	0.030	0.52	29.17	0.027	0.30	18.55	0.037	0.45
	0.8	36.38	0.025	0.44	22.71	0.023	0.40	40.41	0.026	0.29	25.63	0.026	0.33
	1.0	46.14	0.023	0.41	28.81	0.017	0.30	50.17	0.022	0.25	32.23	0.021	0.26
10	0.8	26.49	0.026	0.46	16.36	0.031	0.55	29.35	0.029	0.31	19.04	0.011	0.14
	1.0	33.20	0.022	0.39	20.63	0.022	0.39	36.13	0.027	0.29	22.95	0.022	0.27
	1.2	38.94	0.020	0.35	24.29	0.025	0.44	43.21	0.020	0.21	27.34	0.020	0.25

set in a constant value from 16 Hz to 68 Hz using different thicknesses of plate spring (Table 3.1). The root-mean-square (RMS) values of the fluctuation of displacement of a prism tip y_{rms}, the non-dimensional displacement amplitude η_{rms} (= y_{rms}/H), the angle amplitude θ_{rms} [$\approx \tan^{-1}(y_{rms}/(L+l))\cdot 180/\pi$, where l is span length of a jig] were calculated by using a personal computer. The reduced mass damping C_n ($=2m\delta/\rho DH$, where m, δ, and ρ are the mass per unit length of the system, the logarithmic decrement rate of the structural damping parameter of a prism, and the water density, respectively) was measured by considering initial displacement obtained by hitting the prism with a hammer in the stationary water flow.

3.2.2. Effect of Splitter Plate, Endplate, and Added Structures

Prior to observed the effect of splitter plate and end plate on transverse vibration characteristics, the initial state of free vibration test of the prism models had been conducted for which the parameters and other research instruments for both cases were likely identic in state. Comparison of both states of the prisms test section properties such as models, structural damping, and frequency characteristics are detailed in table 3.2.

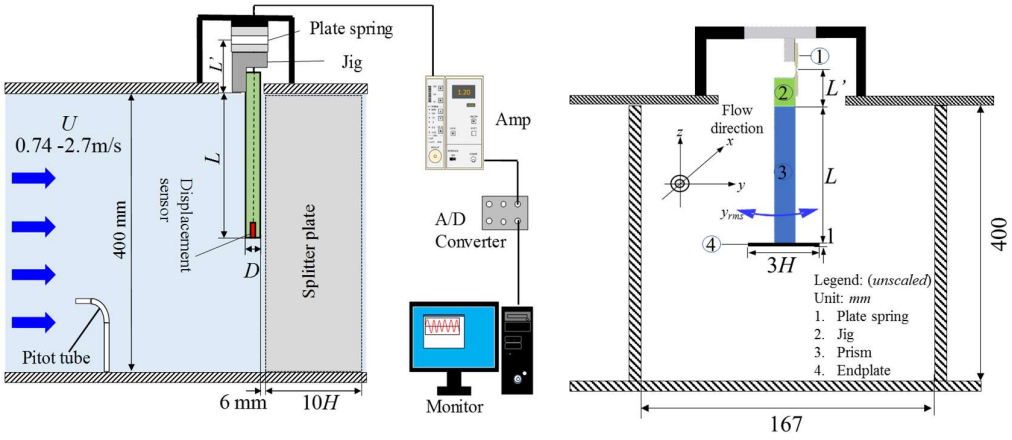

(a) Test section model with splitter plate (b) Test section model with endplate

Figure 3.6 Schematic diagram of test section with splitter plate and endplate

Flow-induced Transverse vibration experiment of cantilevered prisms with splitter plate and attached endplate was also carried out in a water tunnel facility. The detailed model of the test section and research are exhibited in figure 3.6 a-b. A splitter plate with 200 mm and 1.0 mm in length and thickness respectively was centered at the prism trailing edge with a gap around 6 mm from the prism to allow the effect of expanded prism motion during transverse oscillation. Regardless of the prisms expansion, the gap ratio and the length of splitter plate was designed by considering their effect on flow

Table 3.2 Specification of test models for prisms with attached endplate

Cross section	D-section						Rectangular					
	Side ratio(D/H)						Side ratio(D/H)					
	0.23			0.5			0.2			0.5		
L/H	f_c [Hz]	δ	C_n	f_c [Hz]	δ	C_n	f_c [Hz]	δ	C_n	f_c [Hz]	δ	C_n
attached endplate												
2.5	35.5	0.059	1.03	27.34	0.072	1.26	31.9	0.051	0.91	24.1	0.047	0.83
5	34.7	0.113	1.99	25.63	0.079	1.40	32.9	0.072	1.26	22.8	0.062	1.10
7.5							23.0	0.038	0.66	15.5	0.055	0.97
10	33.0	0.046	0.81	17.72	0.070	1.23	24.8	0.044	0.78	16.4	0.026	0.45
free end model												
2.5	41.5	0.022	0.38	29.79	0.013	0.24	38.5	0.022	0.39	26.4	0.023	0.40
5	43.6	0.023	0.41	28.08	0.014	0.25	38.7	0.026	0.46	24.8	0.026	0.46
7.5							26.4	0.050	0.89	16.5	0.030	0.52
10	36.1	0.027	0.48	19.04	0.011	0.20	26.5	0.026	0.46	16.4	0.031	0.55

characteristics as detailed by Nakamura and Tomonari (1977), and Ogurenmi and Sumner (2015). Flow stream velocity ranges and other parameters involved were set up similarly to the study of aspect ratio effects as described previously. In the case of the endplate effect experiment, an aluminum endplate (ρ_{Al} = 2700 kg/m^3) with a diameter of 60 mm and 1.0 mm in thickness was attached at the free end of the prisms in different experiment sequences with splitter effect. However, the mass of endplate was not supposed to influence more on the vibration properties.

Table 3.2 reveals the dynamic properties of prism test model after attaching endplate. The disparity of frequency characteristic (f_c) between prisms with a free end and attached endplate due to endplate mass was negligible. However, damping parameters (C_n) of the attached endplate in still water flow was higher than free end prism resulted in the exponential decay rate of the harmonic motion was large. In this condition,

Table 3.3. Specification of test models with stepped prism

Prism Aspect ratio (L/H)	Added structure-Aspect Ratio (l/h)	Plate spring thickness (mm)	Side Ratio (D/H)											
			0.2 (with added structure)-frontward			0.2 (with added structure)-backward			0.2 (existing data)			0.5(existing data)		
			f_c[Hz]	δ	C_n	f_c[Hz]	δ	C_n	f_c[Hz]	δ	C_n	f_c[Hz]	δ	C_n
L/H =10	2.5	0.8	27.2	0.042	0.74	27.2	0.029	0.50						
		1.0												
		1.2	40.2	0.034	0.60	43.9	0.034	0.60						
	5.0	0.8	26.6	0.039	0.69	26.6	0.035	0.61						
		1.0												
		1.2	39.0	0.044	0.78	37.7	0.040	0.71						
	7.5	0.8	26.0	0.036	0.63	25.6	0.036	0.63						
		1.0												
		1.2	36.8	0.037	0.65	36.87	0.036	0.63						
	0.0	0.8	27.6	0.042	0.74				26.5	0.026	0.46	16.4	0.031	0.55
		1.0							33.2	0.022	0.39	20.6	0.022	0.39
		1.2	40.5	0.030	0.52				38.9	0.020	0.35	24.3	0.025	0.44

more energy is dissipated to the fluid damping system until the oscillation toward zero. Frequency characteristics f_c and the reduced mass damping system C_n (=$2\delta\rho_{st}/\rho_f$, where, ρ_{st}, δ, and ρ_f is the density of prism, the logarithmic decay rate of the structural damping parameter of a prism, and the water density, respectively) of prisms attached endplate

were measured and analysed as similarly to aspect ratios case in term of the experimental process and analysis.

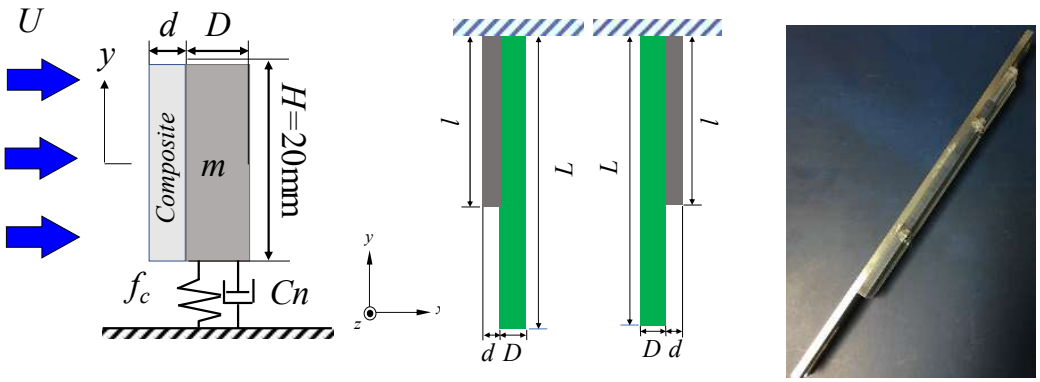

(a) Schematic diagram of the bluff body vibration model (b) Frontward and backward added plate (c) A rectangular prism with additional structure

Figure 3.7. Flow-induced vibration test model with an added plate (stepped prisms)

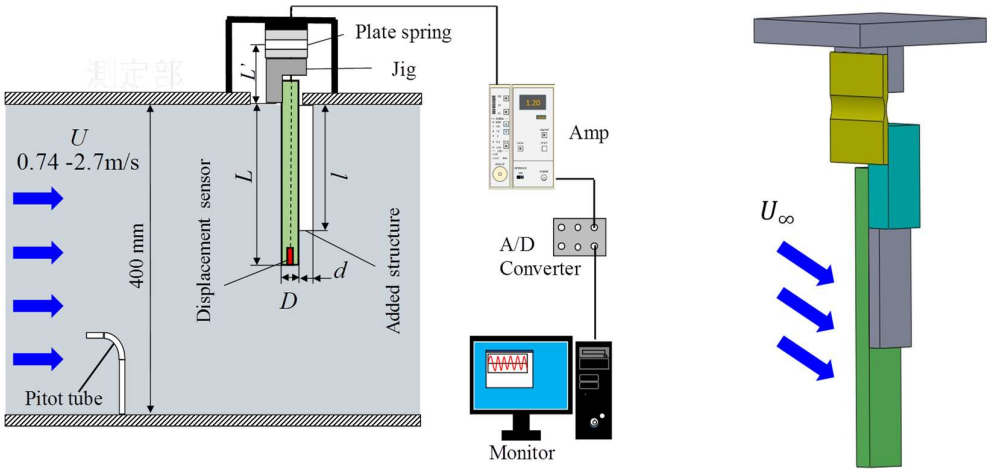

(a) Schematic of experiment design (b) Stepped prisms model

Figure 3.8. Schematic diagram of the test section and measurement devices for experiment with added plat (stepped prism)

Table 3.3 shows the dynamic properties of rectangular prisms with side and aspect ratios of 0.2 and 10 with an added structure of commercial polycarbonate sheet (density ρ = 1.2 gr/cm^3). The structure has a dimension of 20 mm in height normal to flow-stream, similarly to the main rectangular prism, and thickness is 4.0 mm with ranges of length take place 50, 100, and 150 mm (see figures 3.7a-c and 3.8a-b). Those have a respective

aspect ratio (l/h) of 2.5; 5.0; and 7.5. The added structure was set up on the main prism at forward and backward in different sequences of the experiment. This added structure is intended to increase the rigidity of prisms as friction effect by flow stream. The effect of bending stress may absorb energy and reduce the transverse motion of the prism tip. This similar method had also been carried out by Kiwata (2013) using a structure like a fin with different cross-section models located behind the rectangular prism.

Intentionally left blank

Chapter 4
Effect of Aspect Ratios on Flow-Induced Vibration Characteristics of Cantilevered Prisms

4.1. Introduction

Flow behavior around prisms with a sharp edge has outstanding features in the uniform flow that separation flow commonly takes place at leading-edge mainly in high reduced velocity. According to Bearman and Trueman (1972), the model of sharp leading edge normal to the flow stream is responsible for the flow instability incidence. The development of instability behavior of vortices shedding around the prism is subsequently determined by after body shape and Reynold number. Consequently, there is various types of instability as well as vibration model related to after body shape as widely outlined in Naudascher and Rockwell (2005). This phenomenon is potential for a nonlinear case and encouraged many types of research to be analyzed. When the prism is imposed to vibrate, the non-linearity of wake flow instability is more complicated than the fixed condition. An emphasized analysis of vibration characteristic due to the instability of hydrodynamic phenomena on the rectangular prism with a sharp edge is system damping of the structure. The correlation of those remarkable features has been associated to the vibration characteristic of a bluff body in which the essential interdependence of the flow wake fluctuation and the structure resonance is defined succinctly as a reduced resonant velocity ($=U/f_c.H$) (Bearman et al., 1987; Nakamura and Hirata,1991).

In the case of flow-induced motion, some researchers found that galloping takes place typically for all range flow velocity which depends on the system damping, mass, and aerodynamic shape of the structure as mentioned previously. The last feature

mentioned can establish the reattachment type of vortices distribution (some references defined as impinging shear layer) on the side surfaces of a prismatic structure that is related to galloping behaviors. The instability of vortex behavior is a key feature of pressure behavior on the surface of the structure that relates to oscillation motion on the structure mounted elastically. The galloping can be either a single type of galloping or combination. The three remarkable types of flow-induced motion or galloping that commonly take place on the bluff body as described in the preceding chapter, i.e., self-excitation or low-speed galloping, vortex-induced motion, and high-speed galloping. Their features flow wake behavior can be independent each other, depend on reduced resonant velocity and hydrodynamic after body shape or height to width ratio as widely described by many researchers such as Corless and Parkinson, (1988); Okajima and Kitajima (1993); Khalak and Williamson (1999); Tamura and Itoh (1999); Tamura and Dias (2003); Kiwata et al., (2014); and Chauhan et al., (2016).

According to the tests of Scruton (1963) and Okajima et al. (2004) on the flow-induced vibration, the response characteristics of an elastic cantilevered cylinder are different from those of a two-dimensional circular cylinder due to distinctly different in wake flow behavior. In the case of tip end effect, many researchers have investigated the spanwise wake structure interaction behaviors of finite length circular cylinder in various aspect ratios such as Sumner et al. (2004); Rostamy et al., (2014); Palau-Salvador et al., (2010); Wang & Zhou (2009); while Park & Lee (2000) focused on free end effect of the finite cylinder with aspect ratio above critical aspect ratio. Spanwise vortices behavior of cantilevered rectangular prism with the critical aspect ratio is also exhibited in Wang et al. (2017). From those investigations, it can be inferred that the wake structure interaction of the finite cylinder is qualitatively identic for cylinders with aspect ratio above critical

aspect ratios ($L/H \geq 5$). Conversely, different wake structure interaction is found in a cylinder with aspect ratio below the critical aspect ratio.

4.2. Response Amplitude Characteristics

4.2.1. Rectangular Prisms

To control the dynamic response of amplitude-frequency in the specified range with linear behavior, we examined response amplitude with various reduced velocities by using different thickness of plate springs in which their dynamic properties are summarized in table 3.1. The response amplitude for these plate springs is shown in figures 4.1a-b. The effect of the damping parameter can also be found extensively in Vandiver (2012) and Kiwata et al., (2013). Figures 4.1a-b presents an example of mass damping parameter (C_n) variation that is acceptable in the specified range. Hence, vibration onset and non-dimensional response amplitudes over natural frequencies are not distinctly different among them, and the effect of aspect ratio and side ratio on vibration characteristics can be inferred.

When a structure is imposed by fluid force in which the frequency of vortex shedding matches the natural frequency, then the structure starts to resonate. In this case, the frequency of structure oscillation matches the natural frequency of the structure as widely known as vortex-induced vibration. In this study, a bluff body prismatic structure vibrates in the low-speed flow stream, and after body shape does not far enough in length to allow vortices to induce the system to vibrate independently. Hence, this scope of vibration behavior is purely instability of separated shear layer originated from a sharp corner at the leading edge, make those are independent of vortex-induced oscillation. Figure 4.2a-b shows the normalized oscillation frequency of rectangular prism with two different side ratios (D/H) of 0.2 and 0.5 respect to reduced velocity. The oscillating prism

frequency for both the prisms model is unsteady, and their synchronization to frequency characteristic is decreased over time by increasing response amplitude. This deviation is reasonable for denser fluid such water due to viscous effect and added or virtual mass of prism. However, it is also indicated that the dissipation of energy in the water grows linearly with reduced velocity (damping is more negative for this case).

In the case of wake frequency, as outlined numerically by Mizukami (2017), there were not any synchronization between wake frequency and oscillation characteristic frequency over reduced velocity. It implies that strong resonance between two frequencies behavior is not found.

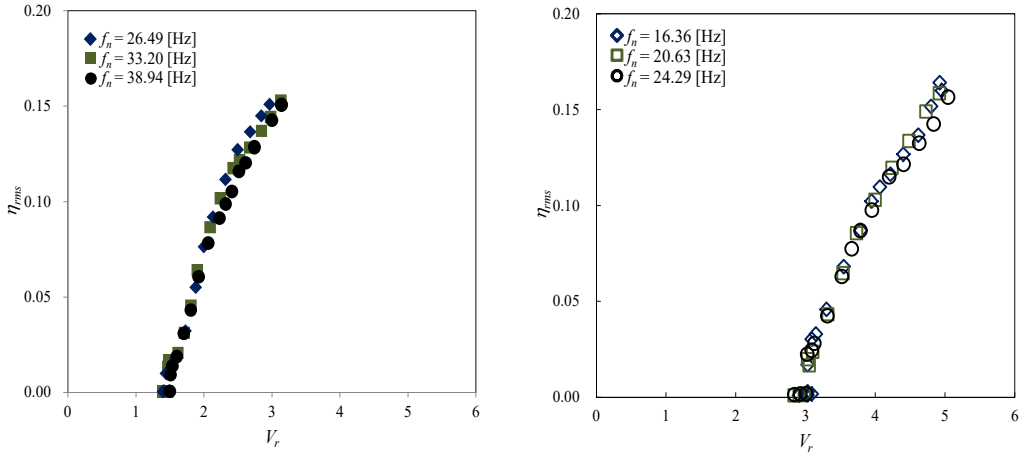

(a) Side ratio $D/H = 0.2$

(b) Side ratio $D/H = 0.5$

Figures 4.1 Non-dimensional response amplitude with various natural frequency of plate spring for prism with aspect ratio $L/H = 10$

Vanishing wake synchronous is reasonable for low-speed galloping case as revealed by experimental data result in Nakamura and Matsukawa, (1987). The synchronous of wake frequency commonly takes place at high-reduced velocity due to the strong resonance of vortex shedding behind the prismatic structure, which is followed by increasing amplitude at a maximum point such as in the prism with critical section (Nakamura &

Hirata, 1991). Similarly, figures 4.2 present the effect of aspect ratio on the root-mean-square value of response amplitude angle θ_{rms} respect to the reduced velocity V_r. The angle of tip displacement is defined in equation 2.6. This term is more reliable due to the cantilevered type case has a different velocity between the tip and certain points along the prism. The remarkable feature on the variation of aspect ratios that an onset vibration of those prisms consist of two group, i.e., prisms with aspect ratio $L/H \geq 5.0$ have onset vibration around $V_r \approx 1.5$ and 3.0 for side ratio of 0.2 and 0.5 respectively while a prism with aspect ratio of 2.5 has onset vibration at reduced velocity V_r around 2.0 for both side ratios pf 0.2 and 0.5. In this case, vibration onset of a rectangular prism is influenced by aspect ratio and side ratio. Both of non-dimensional response amplitude and angle θ_{rms} of response amplitude increase proportionally with reduced velocity V_r. The prisms with aspect ratios $L/H \geq 5.0$ do not differ on the characteristic of the angle of response amplitude. The similarity in response amplitude angle for prisms with large aspect ratio above critical aspect ratios $L/H \geq 5$ can be viewed as there is a similarity on three-dimensional wake structure formation. Their flow patterns are different from two-dimensional wake structure and infinite prismatic bodies mainly at the high reduced velocity (Kawamura, et al., 1984; Sumner, 2013 in his review articles). Moreover, we did not find remarkable feature related to the effect of tip end among these ranges of aspect ratios though there are alteration on the properties of the hydrodynamic forces such drag, lift, and base pressure related to span length variation on prismatic structures as reveled in Taniguchi, et al 1981; Salvador, et al., 2010. These properties mentioned are strongly dependent on the vortices structure from the separated shear layer along spanwise. However, a prism with a small aspect ratio L/H=2.5 had distinctive behavior upon those previously prisms mentioned. It confirmed that flow inclusion of the separated shear layer

from the tip end interacts with the spanwise vortices and suppress regular vortex shedding behind the prism as widely found in experimental and numerical analysis such as Kawamura, 1984; Sakamoto and Oiwake, 1984, Rostamy, et al., 2012; and Goncalves, et al., 2015.

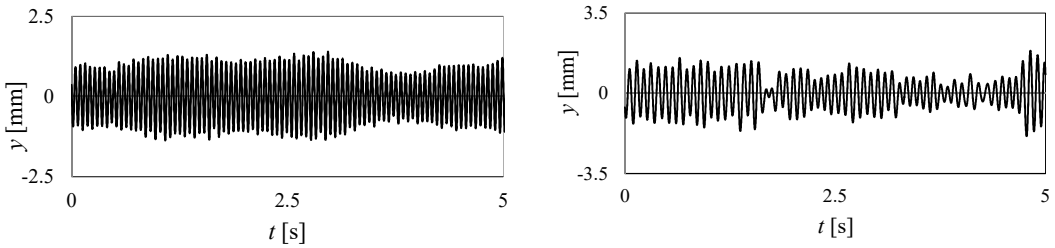

(a) V_r = 3.46 (U = 2.66 m/s), L/H = 2.5, D/H = 0.2 (b) V_r = 5.04 (U = 2.66 m/s), L/H = 2.5, D/H = 0.5

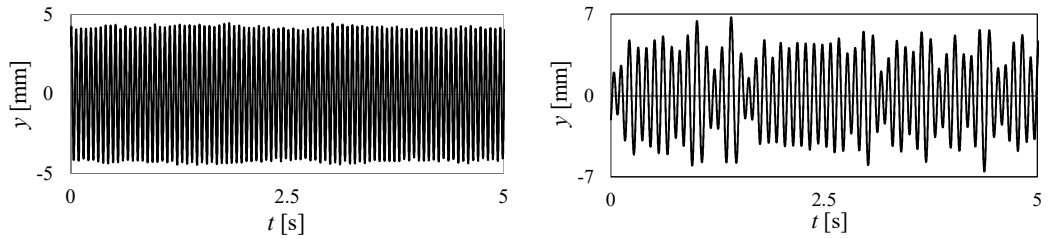

(c) V_r = 3.15 (U = 2.45 m/s), L/H = 10 , D/H = 0.2 (d) V_r = 5.04 (U = 2.45 m/s), L/H = 10, D/H = 0.5

Figure 4.3 Time histories response amplitude of rectangular prism at maximum response amplitude

In case of stability of the peak response amplitude, the FFT method analysis of signal processing was used. Figure 4.3 compares the waveform response amplitude of rectangular prism with different aspect ratios. The discontinuities of the tip displacement fluctuation over time flow for both side ratios of the prisms with small aspect ratios are observed. The effect of these uniformities of peak displacement on response amplitude at maximum response amplitude (maximum reduced velocity) influence *RMS* value of response amplitude.

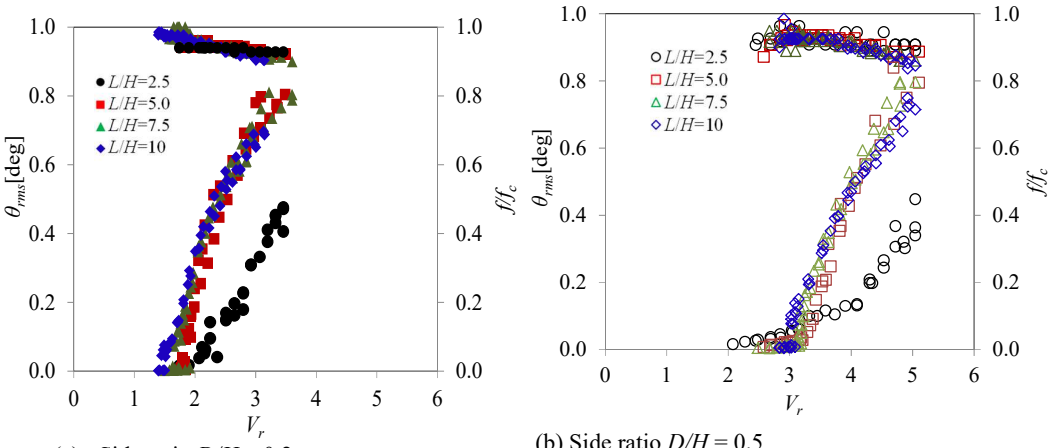

(a) Side ratio $D/H = 0.2$ (b) Side ratio $D/H = 0.5$

Figure 4.2. The angle of response amplitude and normalized frequency of cantilevered rectangular prisms respect to reduced velocity

4.2.2. D-section Prisms

Figure 5.4a-b shows the variation of root mean square of non-dimensional of response amplitude η_{rms} with different aspect ratios L/H for D-section respect to reduced velocity V_r. Reduced velocity of vibration onset is influenced by aspect ratio L/H and side ratio D/H. For aspect ratios, $L/H \geq 5$, vibration onset of D-section prisms with side ratio D/H of 0.23 and 0.5 took place around 1.4 and 2.3 respectively. Reduced velocity of vibration onset for D-section prism with side ratio 0.23 was similar to a rectangular prism (around $V_r = 1.5$). However, for D-section with side ratio D/H of 0.5, it was lower than the rectangular prism ($V_r = 3.0$). According to the previous study such as Nakamura and Hirata (1988), the resonance reduced velocity V_{cr} for D-section with side ratio D/H of 0.5 took place around 7.4.

Feng (1968) demonstrated that the presence of curve surface facing in line downstream brings about a D-section become easy to gallop due to the wake area over which vortex fluctuating effectively expanded is large (see figure 2.11 reproduced from Yamagata, 2016). Hence, cantilevered D-section prisms for the whole aspect ratio L/H

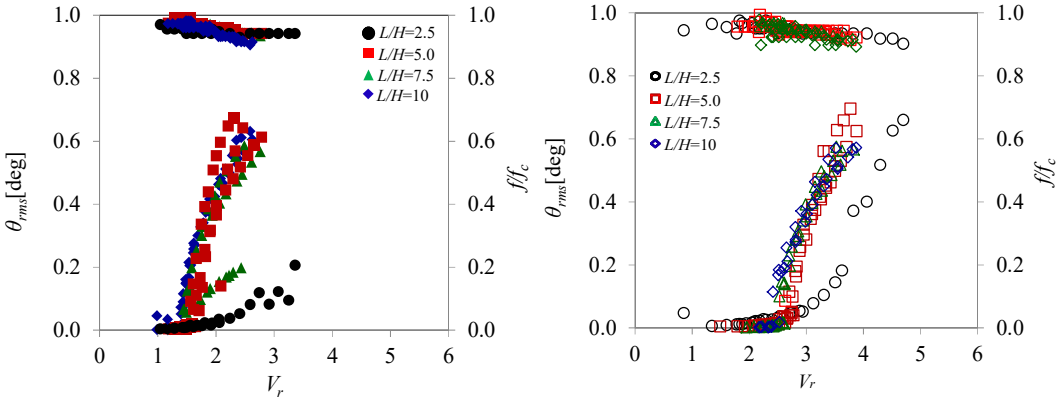

(a) $D/H = 0.23$ (b) D/H=0.5

Figures 4.4. Response angle amplitude of cantilevered D-section prisms

also exhibit low transverse galloping vibration which the prisms oscillate at lower than resonant reduced velocity V_{cr}. After vibration onset, the response amplitude angle increases proportionally with reduced velocity. As the rectangular prisms, D-section prisms with aspect ratios $L/H \geq 5$ also showed similar response amplitude angle both side ratios D/H of 0.23 and 0.5.

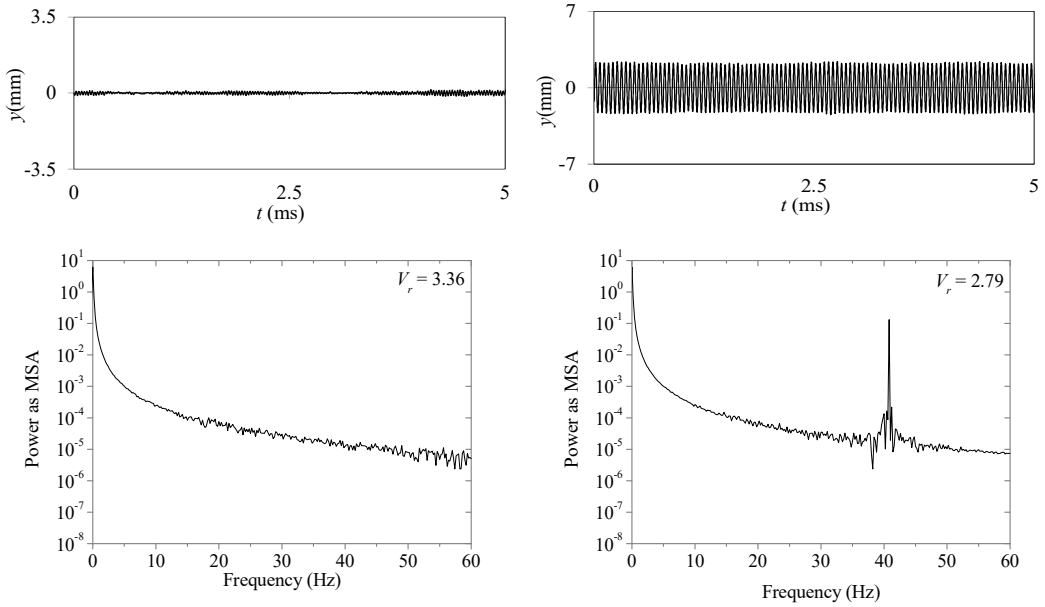

(a) $L/H = 2.5 V_r = 3.36$ ($U = 2.79$ m/s) (b) $L/H = 5 V_r = 2.79$ ($U = 2.43$ m/s)

Figure 4.5 Time histories and power spectrum frequency of tip displacement for D-section with side ratio $D/H = 0.23$

Figures 4.5 and 4.6 show time histories of response amplitude and power spectra frequency of D-section with side ratios 0.23 and 0.5 for aspect ratios of 2.5 and 5.0. In this case, both side ratios, and aspect ratios present a smooth response rather than the rectangular prism mainly in the case of side ratio of 0.5. However, interference of the power spectrum still slightly appears at the D-section prism with a side ratio of 0.5 though it was different from the rectangular prisms in the same side ratio. This is because of the critical depth and reduced resonant velocity are different among them.

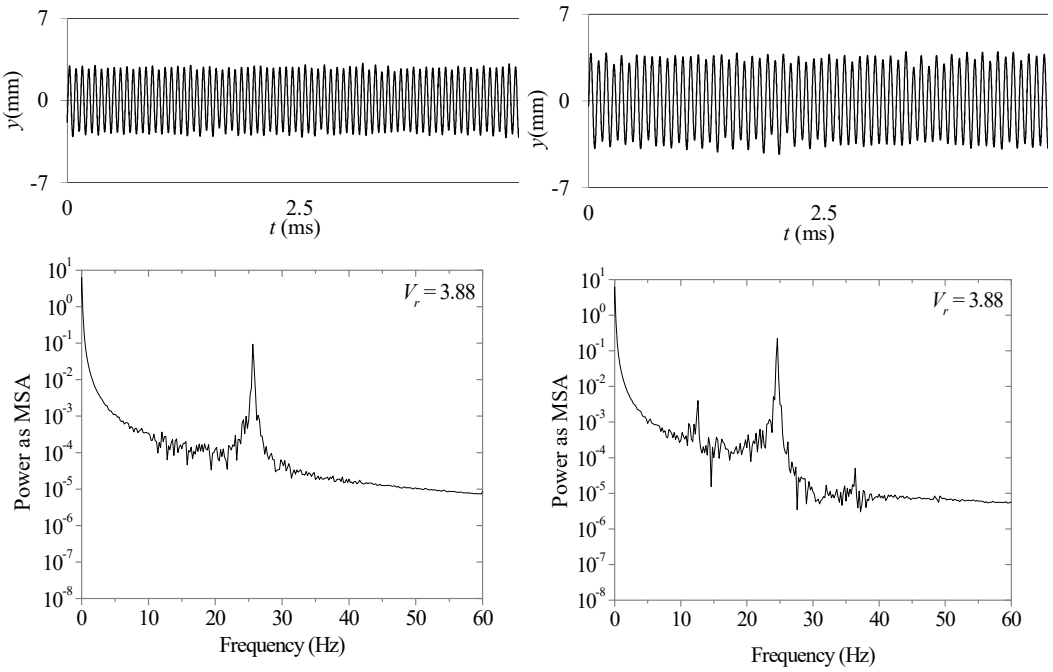

(a) L/H = 5 V_r = 3.88 (U = 2.18 m/s) (b) L/H = 10, V_r = 3.88 (U = 2.12 m/s)

Figure 4.6 Time histories and power spectrum frequency of tip displacement for D-section with side ratio D/H = 0.5

Normalized frequencies f/f_c for D-section prisms both side ratios 0.23 and 0.5 are similar to the rectangular prisms that decreases by pincreasing reduced velocity. However, declining was slightly different from the rectangular prisms because both oscillating and characteristic frequencies of D-section are larger than the rectangular prisms. The

declining of normalized frequency from onset oscillating frequency for both side ratios *D/H* of 0.23 and 0.5 took place around 2 - 9%. Declining oscillating frequency over frequency characteristic was concomitant with increasing reduced velocity which may attribute that more energy is transferred from fluid to the structure.

4.3. Peak Amplitude Stability and Increment Rate of Response Amplitude

Since the waveform of tip displacement is oscillation motion, a fluctuation of peak tip displacement point represents the stability of peak displacement of prisms that can be considered as a standard deviation amplitude peak displacement P_{rms} expressed in the following equation.

$$P_{rms} = \sqrt{\frac{\sum_{i=1}^{N}(|P_i - \bar{P}|)^2}{N}} \tag{5.1}$$

where $|P_i|$, $\bar{P}$, and N are peak displacement of wave form, peak average of $|P_i|$ and the number of peak displacements, respectively.

Figures 4.7 and 4.8 show the variation of the non-dimensional standard deviation of peak displacement of amplitude angle $P\theta_{rms}/\theta_{rms}$ of a prism with various aspect ratios *L/H* respect to reduce velocity V_r for side ratio of 0.2 and 0.5 respectively. In the onset vibration, all prisms showed a large unstable of peak response amplitude. Once response amplitude increased, the standard deviation peak amplitude decrease, and stable peak displacement can be seen in figure 4.5 (b). The stability of response peak amplitude reveals on the prism with aspect ratios $L/H \geq 5$. In contrast, a prism with an aspect ratio of 2.5 both side ratios of 0.2 and 0.5 had relatively unstable on the peak amplitude over reduced velocity. Hence, the response amplitude of the prisms is small as depicted in

figures 4.5 (a) and 4.8(a). Different behaviors on the stability of response amplitude are shown the prism with a side ratio of 0.5 and aspect ratios $L/H \geq 5$ that stability of peak

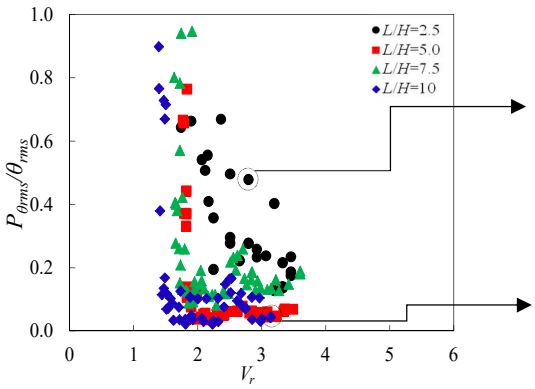

Figure 4.7 Non-dimensional standard deviation of peak displacement $P\theta_{rms}/\theta_{rms}$ for Rectangular prisms D/H = 0.2 with respect reduced velocity V_r.

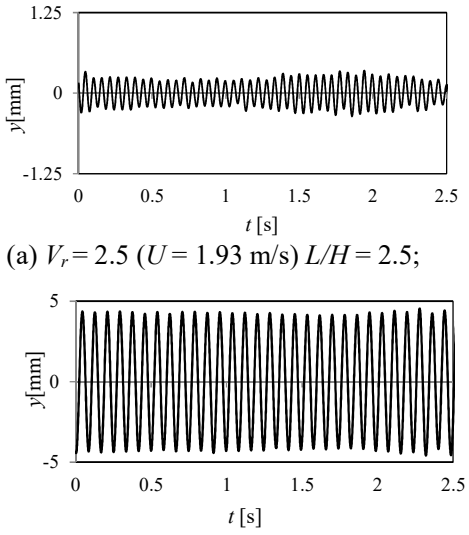

(a) V_r = 2.5 (U = 1.93 m/s) L/H = 2.5;

(b) V_r = 3.1 (U = 1.66 m/s), L/H = 10

Figure 4.8 Time histories tip displacement of the prism with a side ratio of 0.2

of response amplitude relatively tends to increase when reduced velocity uptick. It is reasonable to imply that flow structure behavior is impressed by reduced velocity. Meanwhile, non-uniform and discontinuity of peak amplitude do not predominate during the period of oscillating as shown in figure 4.8(b). It implies that the response amplitude for the small side ratio is more stable rather than its counterpart. On the contrary, the stability response of the side ratio of 0.5 as figures 4.9 and 4.10 showed the discontinuities of amplitude peak along the vibration period. This discontinuity is considered as interferences of vortices behavior upon response amplitude of the tip end that some energy from the vortex fluctuation is absorbed during oscillation. In the same reduced resonant velocity, the stability of peak amplitude increased by increasing the aspect ratio

(see figure 4.10). Ohya (1994) described that the cutoff of peak amplitude on rectangular with a side ratio of 0.5 may attribute to different flow patterns from a slender rectangular prism for which in the range around critical side ratio, abruptly change on flow pattern occur.

In the case of D-section prisms, both side ratios of 0.23 and 0.5, amplitude peak do not exhibit a fluctuation during the oscillating period as presented in the preceding section as figures 4.5 and 4.6. The stability of response amplitude in figure 4.11a showed that at high reduced resonant velocity (V_r), the slender D-section prisms with $L/H \geq 5.0$ showed stability on response amplitude. In figure 4.11b, unstable response amplitude at high resonant reduced velocity exists in $L/H \leq 5.0$ though it did not result in a discontinuity on peak amplitude as the rectangular prisms. Vanishing a discontinuity of waveform signal of the response amplitude may indicate that in the same side ratio with the

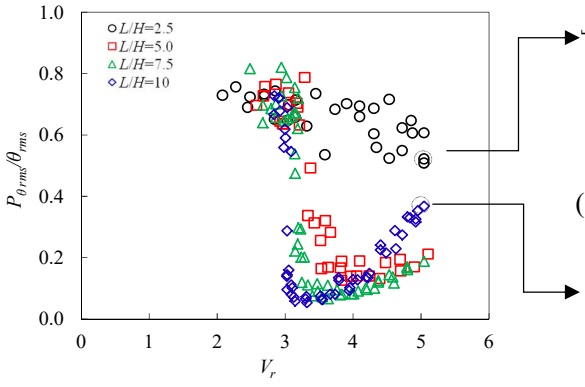

Figure 4.9 Non-dimensional standard deviation of peak displacement $P\theta_{rms}/\theta_{rms}$ for rectangular prisms with D/H = 0.5 respect reduced velocity V_r

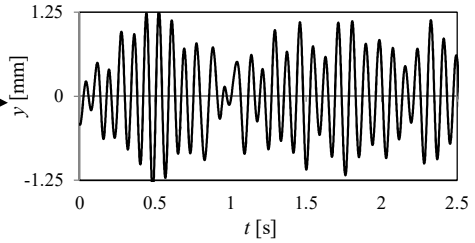

(a) V_r = 5.04 (U = 2.66 m/s) L/H = 2.5;

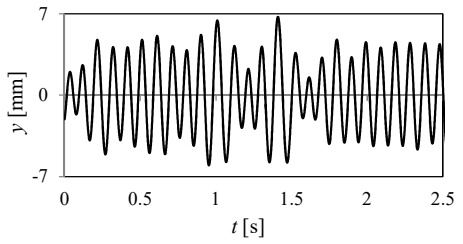

(b) V_r = 5.04 (U = 2.45 m/s) L/H = 10

Figure 4.10 Time histories tip displacement of the prism with a side ratio of 0.5

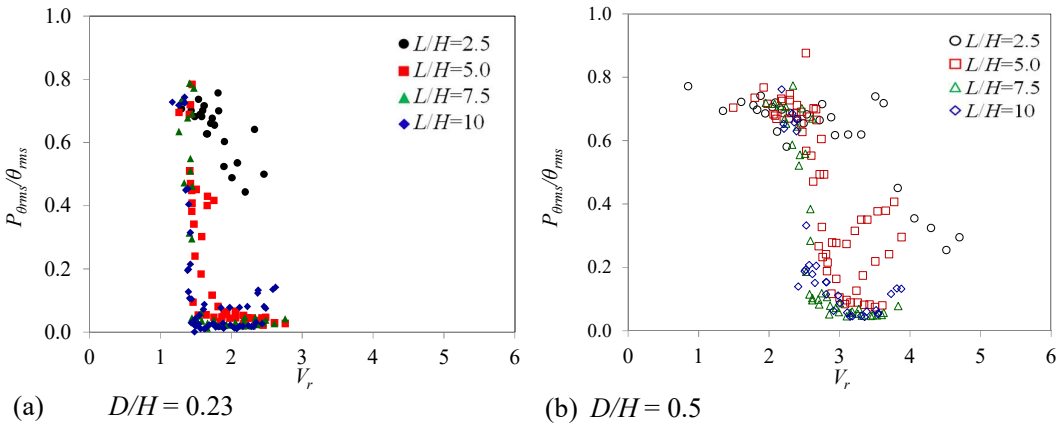

Figure 4.11 Non-dimensional standard deviation of peak displacement *Pθrms*/θ*rms* for D-section prisms with respect reduced velocity V_r

rectangular prism, D-section prism has different in critical range as expressed in the preceding section.

Onset galloping and increment rate of response amplitude for both prism models are shown in figures 4.12 and 4.13. Onset galloping of the D-section prisms was lower than the rectangular prisms, meanwhile, it was also influenced by aspect ratios and side ratios. For small side ratio, onset galloping takes place at low reduced velocity rather than its counterpart while for aspect ratio effect, onset galloping was not influenced by aspect ratio for aspect ratio above critical aspect ratios $L/H \geq 5.0$. However, prisms with aspect ratio below the critical aspect ratio $L/H = 2.5$ had a relatively high in onset galloping.

In the case of increment rate of response amplitude, the D-section prisms with $L/H \geq 5.0$ have a high increment rate of response amplitude over other the rectangular prisms. For the small aspect ratio of 2.5, both prism models are not distinctly different in an increment rate instead of the side ratio effect. Increment rate of the response amplitude increase by increasing aspect ratio and it is constant after reaching an aspect ratio of 10 except D-section with small side ratio. It seems that D-section prism has different with a rectangular prism in the case of *D/H* effect on response amplitude which may also

indicate distinguishable flow pattern in the wake result in different critical cross-section range (see Nakamura and Hirata, 1989). Afterall, D-section with small side ratio and large aspect ratio L/H = 10 has a high increment rate of the response amplitude.

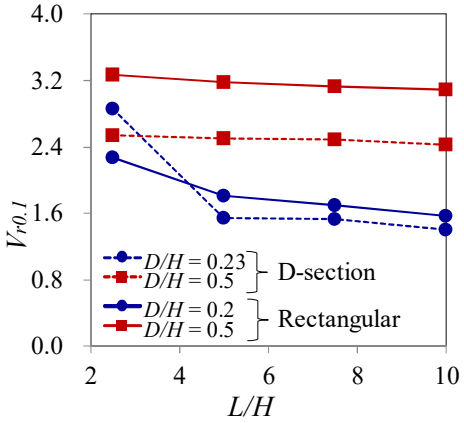

Figure 4.12. Reduced velocity at 10% of response amplitude

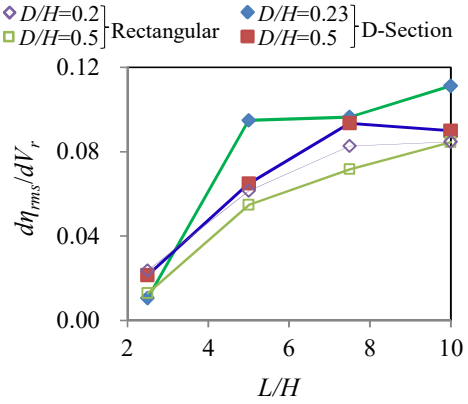

Figure 4.13. Non-dimensional increment rate of response amplitude angle $d\eta_{rms}/dV_r$ of prisms

4.4. Conclusions

Vibration characteristic of rectangular prisms with different aspect ratios of L/H = 2.5, 5.0, 7.5, and 10 has been investigated experimentally in the water tunnel. The main conclusions of this study are as follow

1. Based on the experiment result that vibration characteristic can be viewed into two groups i.e. the prisms with aspect ratio L/H of ≥ 5.0 have similar response amplitude and the prisms with aspect ratio below the critical aspect L/H = 2.5.
2. The prisms with aspect ratios below critical aspect ratio show non-uniform amplitude peak displacement, unstable response amplitude, and low increment rate of response amplitude. The discontinuity of oscillation waveform is also introduced on the prism with critical side ratio D/H = 0.5 which is inverse with rectangular prism with a side ratio of 0.2.
3. In the case of normalized frequency, it is acceptable that the frequency of response amplitude of flow-induced vibration is smaller than the frequency characteristic of the prism model due to mass inertia of fluid and viscous effect.

Intentionally left blank

References

Chauhan, M. K., Dutta, S., Gandhi, B. K., & More, B. S. (2016). Experimental Investigation of Flow Over a Transversely Oscillating Square Cylinder at Intermediate Reynolds Number This. *Journal of Fluids Engineering*, *138*(5), 051105. https://doi.org/10.1115/1.4031878

Corless, R. M., & Parkinson, G. V. (1988). A model of the combined effects of vortex-induced oscillation and galloping. *Journal of Fluids and Structures*, *2*(3), 203–220. https://doi.org/10.1016/S0889-9746(88)80008-2

Gonçalves, R. T., Franzini, G. R., Rosetti, G. F., Meneghini, J. R., & Fujarra, A. L. C. (2015). Flow around circular cylinders with very low aspect ratio. *Journal of Fluids and Structures*, *54*, 122–141. https://doi.org/10.1016/J.JFLUIDSTRUCTS.2014.11.003

KAWAMURA, T., HIWADA, M., HIBINO, T., MABUCHI, I., & KUMADA, M. (1984). Flow around a Finite Circular Cylinder on a Flat Plate : Cylinder height greater than turbulent boundary layer thickness. *Bulletin of JSME*, *27*(232), 2142–2151. https://doi.org/10.1299/jsme1958.27.2142

Khalak, A., & Williamson, C. H. . (1999). Motions, Forces and Mode Transitions in Vortex-Induced Vibrations At Low Mass-Damping. *Journal of Fluids and Structures*, *13*(7–8), 813–851. https://doi.org/10.1006/jfls.1999.0236

KIWATA, T., YAMAGUCHI, M., NAKAJIMA, A., KONO, T., & UENO, T. (2014). PVP2014-28939. In *Flow-Induced Transverse Vibration of A Cantilevered Prism For Energy Harvesting* (pp. 1–10). Proceeding of the ASME Pressure Vessel & Piping Division Confrence.

Mizukami, S. (2017). *Study on the flow around the elastic supported prism and the vibration dynamics of the flow (in Japanese)*. Master Thesis. Kanazawa University.

Nakamura, Y., & Hirata, K. (1991). Pressure fluctuations on oscillating rectangular cylinders with the long side normal to the flow. *Journal of Fluids and Structures*, *5*(2), 165–183. https://doi.org/10.1016/0889-9746(91)90460-7

Nakamura, Yasuharu, & Matsukawa, T. (1987). Vortex excitation of rectangular cylinders with a long side normal to the flow. *Journal of Fluid Mechanics*, *180*(1), 171. https://doi.org/10.1017/S0022112087001770

Naudascher, E. Rockwell, D. (2005). *Flow -Induced Vibrations: an Engineering Guide*. Dover Publication Inc.

Okajima, A., & Kitajima, K. (1993). Numerical study on aeroelastic instability of cylinders with a circular and rectangular cross-section. *Journal of Wind Engineering and Industrial Aerodynamics*, *46–47*, 541–550. https://doi.org/10.1016/0167-6105(93)90321-E

Palau-Salvador, G., Stoesser, T., Fröhlich, J., Kappler, M., & Rodi, W. (2010). *Large eddy simulations and experiments of flow around finite-height cylinders*. *Flow, Turbulence and Combustion* (Vol. 84). https://doi.org/10.1007/s10494-009-9232-0

Park, C.-W., & Lee, S.-J. (2000). Free end effects on the near wake flow structure behind a finite circular cylinder. *Journal of Wind Engineering and Industrial Aerodynamics*, *88*, 231–246. https://doi.org/10.1016/S0167-6105(00)00051-9

Rostamy, N., Sumner, D., Bergstrom, D. J., & Bugg, J. D. (2014). Flow above the free end of a surface-mounted finite-height cylinder. In *Lecture Notes in Mechanical Engineering* (Vol. 8, pp. 167–172). https://doi.org/10.1007/978-3-642-40371-2_24

Rostamy, Noorallah, Sumner, D., Bergstrom, D. J., & Bugg, J. D. (2012). An Experimental Study of the Flow Above the Free Ends of Surface-Mounted Bluff Bodies. In *Volume 1: Symposia, Parts A and B* (p. 981). ASME. https://doi.org/10.1115/FEDSM2012-72028

Sakamoto, H., & Oiwake, S. (1984). Fluctuating forces on a rectangular prism and a circular cylinder placed vertically in a turbulent boundary layer. *Journal of Fluids Engineering, Transactions of the ASME*, *106*(2), 160–166. https://doi.org/10.1115/1.3243093

Seiichi TANIGUCHI, Hiroshi SAKAMOTO, M. A. (1981). Flow around Circular Cylinders of Finite Height Placed Vertically in Turbulent Boundary Layers, *24*(187), 37–44. https://doi.org/https://doi.org/10.1299/jsme1958.24.37

Sumner, D. (2013). Flow above the free end of a surface-mounted finite-height circular cylinder: A review. *Journal of Fluids and Structures*, *43*, 41–63. https://doi.org/10.1016/j.jfluidstructs.2013.08.007

Sumner, D., Heseltine, J. L., & Dansereau, O. J. P. (2004). Wake structure of a finite circular cylinder of small aspect ratio. *Experiments in Fluids*, *37*(5), 720–730. https://doi.org/10.1007/s00348-004-0862-7

Tamura, T., & Dias, P. P. N. . (2003). Unstable aerodynamic phenomena around the resonant velocity of a rectangular cylinder with small side ratio. *Journal of Wind Engineering and Industrial Aerodynamics*, *91*(1–2), 127–138. https://doi.org/10.1016/S0167-6105(02)00340-9

Tamura, Tetsuro, & Itoh, Y. (1999). Unstable aerodynamic phenomena of a rectangular cylinder with critical section. *Journal of Wind Engineering and Industrial Aerodynamics*, *83*(1–3), 121–133. https://doi.org/10.1016/S0167-6105(99)00066-5

Vandiver, J. K. (2012). Damping Parameters for flow-induced vibration. *Journal of Fluids and Structures*, *35*, 105–119. https://doi.org/10.1016/j.jfluidstructs.2012.07.002

Wang, H. F., & Zhou, Y. (2009). The finite-length square cylinder near wake. *Journal of Fluid Mechanics*, *638*, 453–490. https://doi.org/10.1017/S0022112009990693

Wang, H., Zhao, X., He, X., & Zhou, Y. (2017). Effects of oncoming flow conditions on the aerodynamic forces on a cantilevered square cylinder. *Journal of Fluids and Structures*, *75*, 140–157. https://doi.org/10.1016/J.JFLUIDSTRUCTS.2017.09.004

Chapter 5
Effect of a Splitter Plate, and an Endplate on Vibration Characteristics of Cantilevered Prisms

5.1. Introduction

An outstanding feature of bluff bodies with a sharp edge in uniform flow with high Reynold number that separation flow takes place immediately on the leading edge which is followed bubble forming on the side surfaces and Karman vortex behind the prism. Consecutive flow behaviors and their effects on the flow structure as well as dynamic response both fluid and prism motion are dependent on some parameters such as the system damping and after body hydrodynamic shape. Interdependency of those parameters extends to the types of flow-induced vibration bluff bodies in the case of elastically mounted bluff bodies such as revealed in Nakamura and Hirata (1991). Meanwhile, flow characteristics due to reattachment point on the side surface have dramatically changed fluid forces and vortex shedding fluctuation behavior as described in Okajima (1982), Nakamura and Matsukawa (1987).

In the case of finite rectangular prisms mounted elastically in the water tunnel, Kiwata (2014) investigated the effect of side ratio on response amplitude characteristic in the range of below resonant reduced velocity. Shifting on onset galloping and uniformity of dynamic response amplitude is the key features for the foregoing article. Meanwhile, it is different from a circular cylinder in which dynamic response amplitude can be dominated by alternating vortices shedding and the excitation may suppress in high reduced velocity (Okajima and Kiwata, 2019). It is not surprising that a circular cylinder has distinctive features on flow characteristics as well as dynamic response amplitude with a rectangular prism. Considering flow wake characteristics related to low-speed galloping features, we consider that galloping for low aspect ratio ($L/H \leq 5.0$) is

considerably influenced by three-dimensional vortices and alternating vortex shedding behind the bluff bodies as detailed and visualized by Sumner (2013) in the case of stationary mode. Nakamura et al. (1991) had been successful to reduce the effect of interaction alternating vortex shedding behind the prism by mounting a splitter plate in the case of the oscillating bluff body. In this case, the length of splitter plate relative to the prism and gap between the prism should take into account on galloping effect.

Oregunmi and Sumner (2015) also viewed the flow field around fixed rectangular prism in the presence of a splitter plate with various length and no gap over the finite rectangular prisms with different aspect ratios. Suppression of vortex shedding is a function of splitter length with a reduction in aerodynamic force over the prisms with a small aspect ratio. These also are in line with the investigation in Nakamura and Tomonari (1977) which considered the instability of prism as a function of splitter length and gap ratio.

In preventing a three-dimensional vortex effect, Morse et.al (2008) with a *finite* circular cylinder, Fox and West (1990), with infinite circular cylinder, attached endplate at the end of the bluff body to avoid swirling vortex effect and the boundary layer interference on wake structure. Galloping properties were also examined both attached and unattached endplate conditions by Morse et al (2008). The latter condition is situated to investigate galloping behavior due to the boundary layer from the shear wall.

In the recent study, the scope of transverse galloping with low-speed galloping mode of the cantilever mounted rectangular and semi-circular with different aspect ratios in the water tunnel had been studied. In the case of splitter plate effect, this study is focused on *finite* oscillating prisms to describes the finding related to transverse galloping improvement by setting-up a splitter plate and investigate the effect of the attached

endplate at the free-end of bluff bodies. Our intentional objectives are improving response amplitude characteristics, the stability of dynamic response, and onset galloping. The primary concerns are improving response amplitude characteristics of the prism with the critical aspect ratio. Finally, this optimization attempt is supposed to support the study harvesting energy research from transverse vibration in low-speed flow mode as well as provide physical insight related to low-speed galloping phenomena.

5.2. Effect of a Splitter Plate on Dynamic Response

This part of the study focuses on the effect of splitter plate on transverse vibration characteristics of cantilevered rectangular and D-section with different aspect ratios as shown in figure 3.4. The previous chapter showed that an aspect ratio influences dynamic response characteristics both rectangular and *D*-section. The main consideration is focused on the prisms whose physical properties around critical point such aspect ratio (span length to width ratio, *L/H*) and side ratio, depth to width ratio, *D/H*) i.e. $L/H \leq 5.0$ and $D/H = 0.5$

5.2.1. Rectangular Prisms

Response amplitude of rectangular prism with different aspect ratios is shown in figure 5.1(a - b) in which clustering amplitude characteristics can be seen at the prisms with aspect ratio $L/H \geq 5.0$. However, both prisms with splitter plate and without mounting splitter plate that there is not any difference in onset galloping and response amplitude within a range of 0.26 of designed maximum amplitude, ~ 3.00 mm (dashed line) or within a range around $V_r = 2.0$. Increasing reduced velocity over this range has shown remarkable improvement in response amplitude over the prisms below critical aspect ratio $L/H \geq 5.0$. Unevenly, small aspect ratio $L/H = 2.5$ shows a surprising

improvement in response amplitude in the presence of a splitter plate (figure 5.1b). The feature of sharp edge of the prism, make the excitation mechanism of the prism below critical side ratio is solely induced by the instability of shear layer due to separation flow at the leading edge and this type of galloping is independent to vortex-induced excitation. The splitter plate has successfully promoted the instability by reducing the effect of alternating vortices behind the prisms by avoiding direct interaction of symmetrical vortices on the prism with a critical side ratio of 0.5.

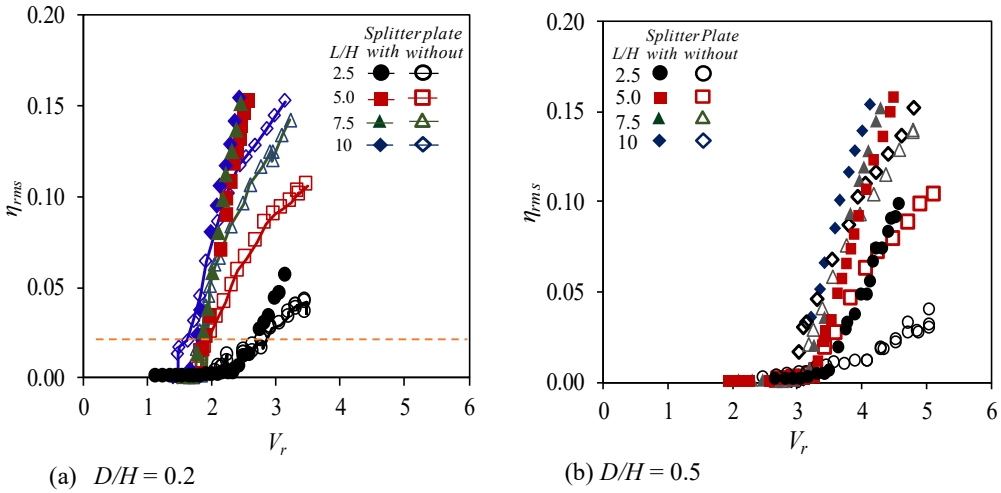

(a) $D/H = 0.2$ (b) $D/H = 0.5$

Figure 5.1. Effect of splitter plate on transverse vibration characteristics for rectangular prisms

Mounting splitter plate behind the prism with a critical side ratio of 0.5 had prolonged instability behavior over the critical aspect ratio for an oscillating prism as indicated by vanishing discontinuity of waveform of tip displacement in figure 5.2. Hence, the length of the splitter plate and gap relative to the side length of prism is sufficient to encounter alternating vortices behind the prisms as depicted in Chauhan, Dutta, More, & Gandhi (2018) and all aspect ratios for both side ratios model experience improved response amplitude. In the case of small side ratio $D/H = 0.2$, which is known as pure instability and not controlled by vortex-induced oscillation, a splitter plate also

fiercely increased instability which is concomitant with the study of reference (Y. Nakamura & Tomonari, 1977).

For short prism (L/H=2.5) with critical side ratio (D/H=0.5), free end effect and base vortices are dominated resulted in absence of vortex shedding and shedding frequency may be generated by end effect (Gonçalves, Franzini, Rosetti, Meneghini, & Fujarra, 2015). Hence, we cannot find a meaningful improvement in response amplitude by setting up a fixed splitter plate. In contrast, for short prism with pure instability (D/H=0.2) splitter plate must improve response amplitude (Figure 5.1a)

Furthermore, we analyze FFT spectra of dynamic response at the maximum amplitude of bluff bodies which represents energy transfer during vibration motion as shown in figure 5.2. Figure 5.2(a), (b)-left present overshoots due to the fluctuation of alternating vortices interference at the trailing edge of during oscillation which implies that the fluid absorbs energy from the oscillating bluff body. Therefore, there are small disturbances adjacent to the sharp peak of FFT spectra in left figure 5.2(a) and two dominant sharp peaks on FFT spectra in left figure 5.2(b) which the highest sharp peak represents amplitude-frequency and another one is wake fluctuation. By mounting a splitter plate, those intermittent of the waveform vanished for all aspect ratio yielding only one sharp peak on the FFT spectra. Vanishing of the intermittent of a second peak adjacent to the sharp peak represents increasing of the instability of galloping and alters the critical point of this bluff bodies as mentioned in Yasuharu Nakamura & Hirata (1989). Figure 5.2 represents the effect of inserting the splitter plate on the vibration characteristic from two aspect ratios for comparison.

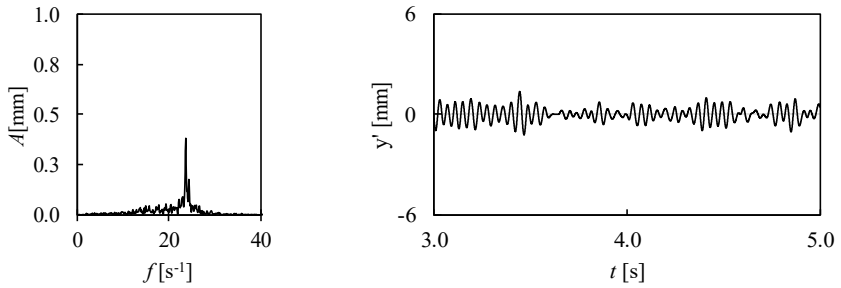

i. FFT Spectrum ii. time lapses of the waveform

a. Plain rectangular prism, L/H= 2.5, V_r = 5.04

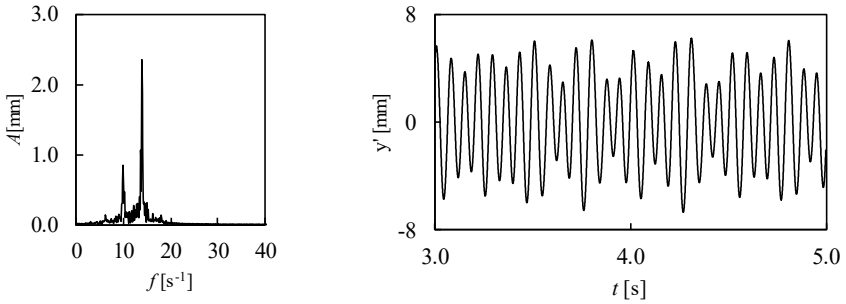

i. FFT Spectrum ii. time-lapses of the waveform

b. Plain rectangular prism, L/H= 10, V_r = 4.95

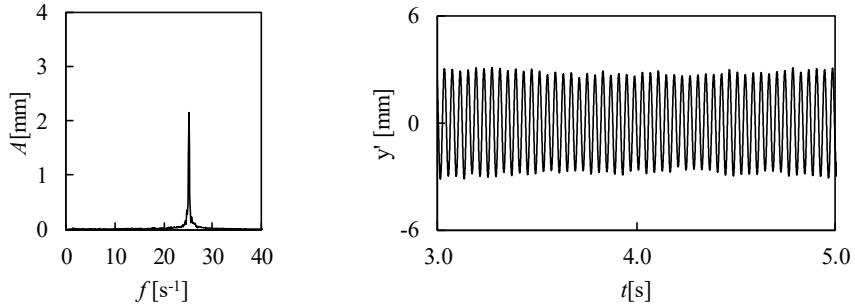

i. FFT Spectrum ii. time lapses of the waveform

c. Rectangular prism, L/H= 2.5, V_r = 4.57 (with splitter plate)

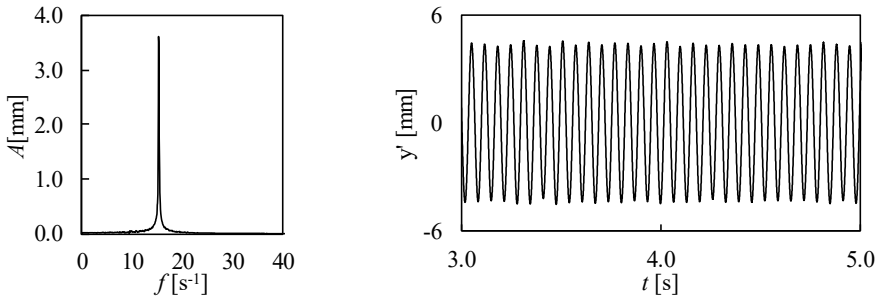

i. FFT Spectrum ii. time lapses of the waveform

d. Rectangular prism, L/H = 10, V_r = 4.13 (with splitter plate)

Figure 5.2. The FFT Spectra and time-lapses of response amplitude for the rectangular prism D/H = 0.5 with splitter plate.

5.2.2. *D*-section Prisms

In this study, noticeable characteristics of D-section on response amplitude over rectangular prisms were an onset galloping, the evolution of response amplitude as well as their response on a fixed splitter mounting in trailing edge of the bluff body. Our current study on D-section without mounting splitter plate that D-section exhibits stable in response amplitude, large amplitude, and galloping take place quickly rather than a rectangular prism. The distinction of after body length in the down-stream has made this prism distinctly different from the rectangular prism. Nakamura and Hirata (1989) had categorized the critical side ratio of D-section of 0.7 with V_r = 5.5 by observing base suction behavior acting on the prism. Hence, in the case of the critical side ratio, it is not surprising that *D*-section is different from a rectangular prism in response amplitude characteristics. However, Nakamura and Tomonari (1981) found critical side ratio and onset galloping behavior which was attributable to the base suction behavior which was similar to the rectangular prism.

Figure 5.3 compares FFT spectra and time histories of waveform response amplitude of short D-section prism (L/H = 2.5) which is considered as below critical aspect ratio in terms of response amplitude behavior. The discontinuity on waveform during the oscillation period is not found in short prism even though the response amplitude and onset galloping slightly different from other aspect ratios. As mentioned previously that low-speed galloping is solely due to the presence of unstable behavior of separated shear layer in the leading edge which induces negative damping of the fluid system and affects dynamic response properties. In this case, we prove that interferences of alternating afterbody vortices were not found in D-section with a side ratio of 0.5. It

was different from a critical point of oscillating rectangular prisms of 0.4 mentioned in Ohya (1994) for the rectangular prism.

Therefore, the galloping behavior of D-section with a side ratio of 0.5 is still pure instability type of galloping and free from alternating vortex interferences at the after body. For this, only one sharp peak comes out to the FFT spectrum for all aspect ratios.

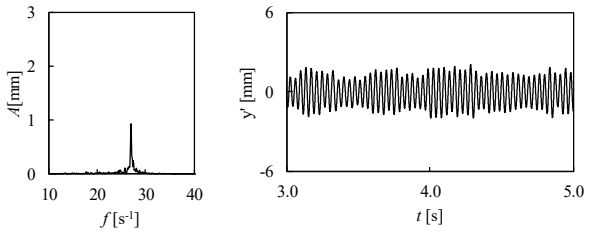

(a) Plain prism, V_r = 4.7, U= 2.8 m/s

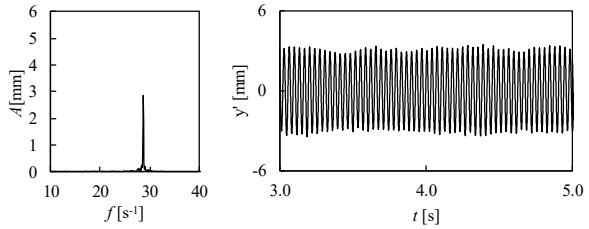

(b) with splitter plate V_r = 3.34 U = 2.4 m/s

Figure 5.3. FFT spectra and time histories of the waveform for short D-section L/H = 2.5 with side ratio D/H=0.5 at maximum response amplitude

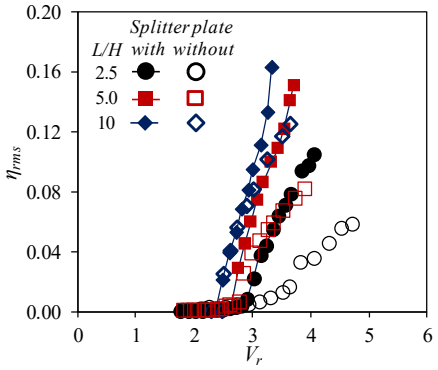

Figure 5.4. Effect of splitter plate on transverse vibration characteristics for D-section with critical side ratio D/H=0.5

Mounting splitter plate at the trailing edge of D-section enhanced instability of separated shear layer originated from a sharp corner of leading-edge and brought about high response amplitude on the prism with aspect ratio below critical aspect ratio $L/H \leq 5.0$ as shown in figure 5.4. Splitter plate length considered to allow vortex formation in the downstream to re-attach, enhancing pressure difference between two side surfaces which transfers more energy for the fluid system to the prisms (Assi and Bearman, 2015).

Therefore, in the same flow stream velocity in figure 5.3, a fixed splitter plate at the trailing edge has built up a top response amplitude.

5.2.3. Stability of Peak Amplitude

Figures 5.5a-b and 5.6 show the deviation of peak amplitude for the prism with a splitter plate. As mentioned in the preceding section that a mounted splitter plate promotes response amplitude. A noticeable change is shown for the prism below the critical points that is, L/H = 2.5 and D/H = 0.5 which is different from those without a splitter plate (figure 4.9). Moreover, for a slender prism, an improvement of peak amplitude stability at high reduced velocity is also found by mounting a fixed splitter plate (see figure 4.7 for comparison).

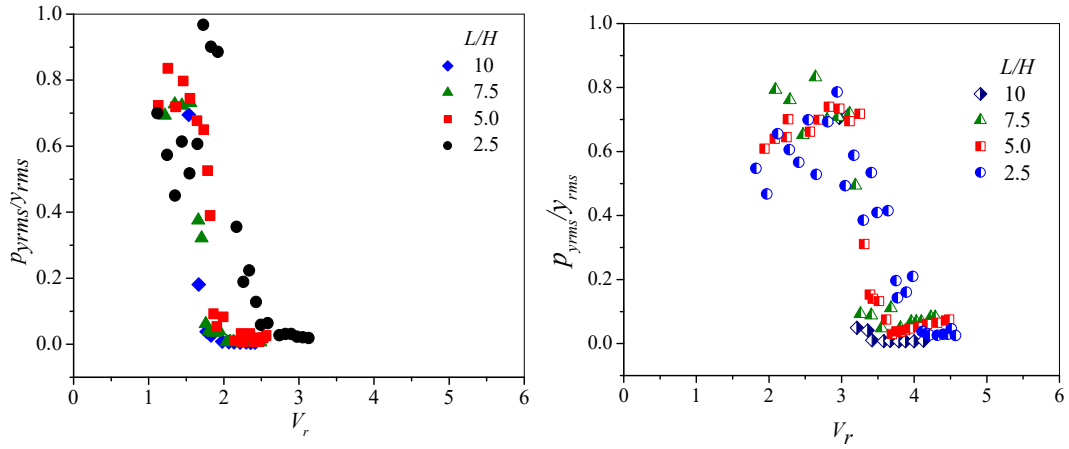

a. D/H = 0.2 b. D/H = 0.5

Figure 5.5 stability of amplitude peak of the rectangular prism with splitter plate

In the case of a rectangular prism with critical points, figure 5.5b shows an effect of the mounted splitter plate. All of the aspect ratios exhibited a stable peak at high reduced velocity though at the low reduced velocity peak deviation was still high like a plain prism (see figure 4.11b). The effect of this peak stability on response amplitude can be found in figure 5.1b over which all prisms show improved response amplitude by eliminating a discontinuity of peak deviation of response amplitude as in figure 5.2

In the case of D-section prisms mounted a fixed splitter plate, figure 5.6 shows the peak deviation of response amplitude for a selected aspect ratio and side ratio of 0.5. In the previous section that D-section with a side ratio of 0.5 for all aspect ratios does not exhibit a notable peak fluctuation as in rectangular prisms. Hence, in the same reduced velocity, D-section prisms exhibited stable peak amplitude rather than the rectangular prism. D-section prism with aspect ratio below critical point showed a notable improvement in the stability of peak amplitude as figure 5.6 (see also figure 5.11b for comparison).

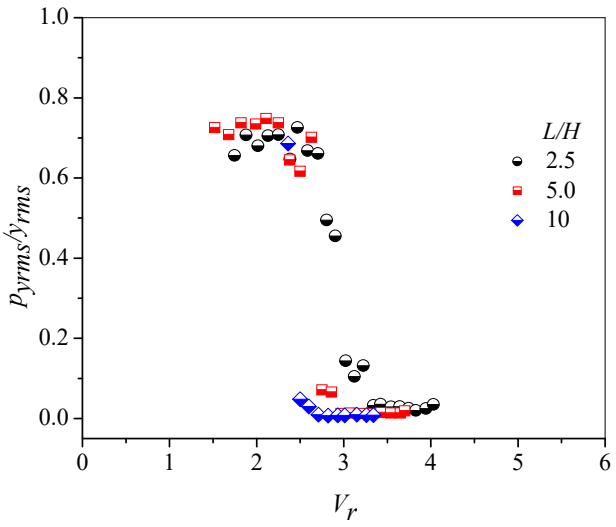

Figure 5.6. Stability of amplitude peak of D-section prism D/H = 0.5 with mounted splitter plate

5.3. Effect of an Endplate

As outlined in the preceding section in this chapter the attached endplate at the tip end of the bluff bodies is intended to diminish the free end effect and keep two-dimensional flow-pattern. Stansby 1974 in Fox and West 1990, suggested the minimum critical side ratio between the endplate and the bluff body was 7 for *infinite* bluff bodies. This investigation also presented that base suction decreases when endplate approaching

the wall. While Okajima (2004) studied the effect of attached endplate at the tip end of a *finite* circular cylinder with the ratio of *3Diameter.* Two excitation modes were found in response amplitude which approaches two-dimensional cylinder (*infinite*) though the transition to the second excitation region was not similar to a two-dimensional one. Morse et al (2008) used the ratio of attached endplate with 4*D* that response amplitude of the cylinder with an attached end plate was slightly similar to the previous investigation. However, the slop of amplitude increment was nearly flat over the range of reduced velocity till approaching the characteristics of amplitude of the cylinder without an endplate.

Table 3.2 shows the initial condition of the attached endplate both rectangular and D-section prisms in stationary water flow. Frequency characteristics (f_c) on the prism with the attached endplate are slightly different from plain prism due to the presence of endplate mass. This disparity is larger on the prisms with small sides and aspect ratios. However, the effect of viscous and inertia mass has increased the damping system (C_n) which increases damping. This can be seen that attached endplate at the tip end of prisms both rectangular and D-section are expected to diminish three-dimensional flow pattern due to flow tip effect. In this study, the effect of endplate mass on response amplitude characteristic has been distinct from the frequency characteristic between the attached endplate and its counterpart about 2 Hz.

5.3.1. Rectangular Prisms

The responses amplitude of two cross-sections of rectangular prisms with the attached endplate for different aspect ratios is presented in figure 5.5a-b. The performance of the attached endplate on response amplitude is out of the initial premises particularly the prisms below critical aspect ratios $L/H \leq 5$. In figure 5.5a, the attached

endplate suppressed effectively the transverse vibration for the prisms with aspect ratios of 2.5 and 5.0 while it was no meaningful effect of response amplitude on the prisms with a side ratio of 0.5 (figure 5.7b). However, this study is a distinct treatment on the attached endplate with the experiment studied by Morse et al. (2008), that is the investigation model was free from the shear layer wall effect at all. However, the main inference on the attached endplate treatment on response amplitude behavior was generally similar.

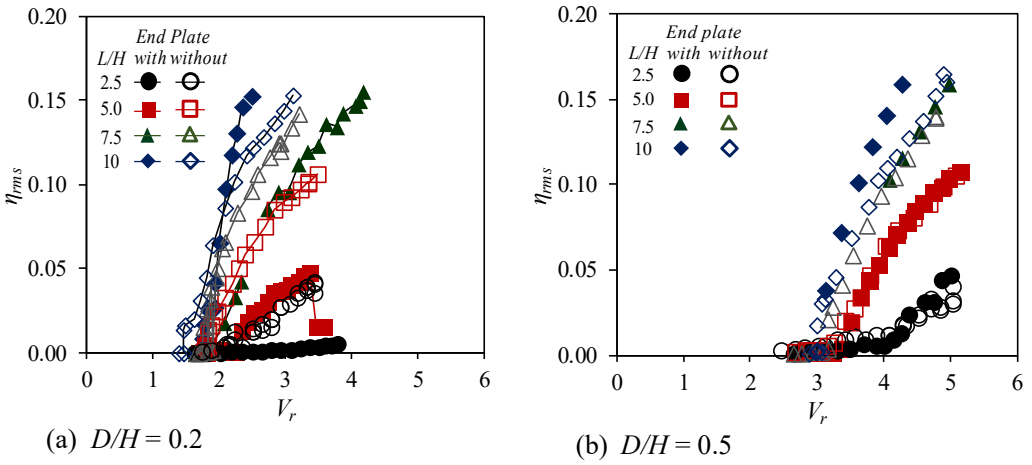

(a) $D/H = 0.2$ (b) $D/H = 0.5$

Figure. 5.7. Effect of endplate on transverse vibration characteristics for Rectangular

In the short prism (L/H=2.5) the discontinuity waveform of peak amplitude was clearly shown in the time histories and FFT spectra of rectangular prism for side ratio of 0.2 as figure 5.2a. It implies that the attached endplate reduces galloping instability of response amplitude though wake interference due to Karman vortex behind the prisms was not observed. It can be confirmed by the FFT spectrum that only one dominant sharp peak with a small disturbance adjacent to the peak.

In the case of prisms with the critical side ratio, figure 5.7 shows the attached endplate effect on the response amplitude is out of the initial premise that preventing tip end swirling vortex does not affect response amplitude. FFT spectral analysis in figure 5.9 was identic with a plain prism that is interferences in the FFT spectrum still exists.

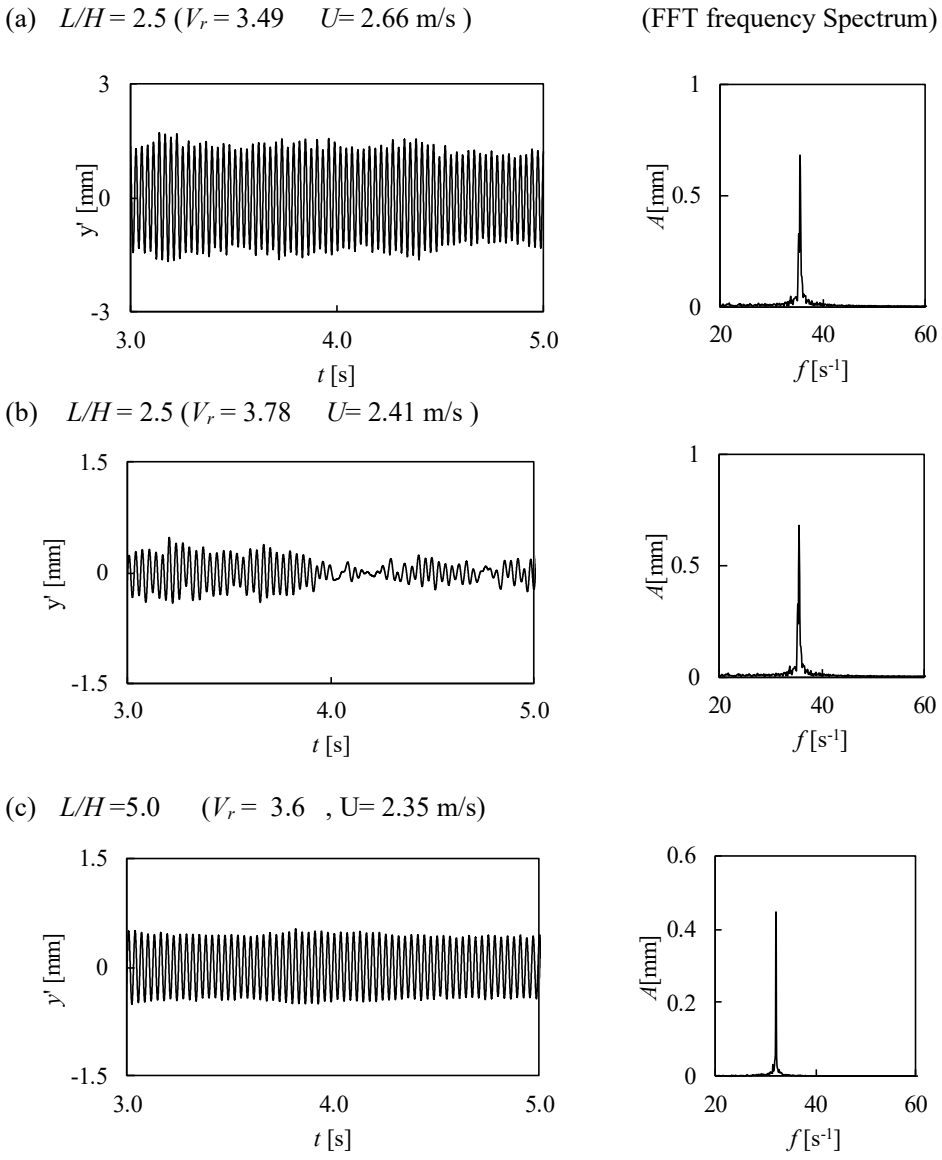

Figure 5.8. Time histories of the tip displacement and power spectra for rectangular prism with D/H = 0.2. (a) L/H = 2.5 plain prism (b) L/H = 2.5 plain prism with attached (b) L/H = 5.0 with attached endplate

Suppressing response amplitude was also presented in time histories of fluctuation wave of amplitude as shown in figure 5.8. Figure 5.8(b) shows discontinuities of the waveform proved that response amplitude was suppressed which was not found in plain prisms. Meanwhile, in figure 5.8(b) the evolution of fluctuation amplitude is not found in D-section that is discussed in the next section. Furthermore, we confirmed the FFT

spectrum of amplitude in figure 5.9c for the prism with critical side ratio that is the interference of wake fluctuation on amplitude persists throughout the prisms for which spanwise wake interference was clearly shown at long prism (*L/H*=10).

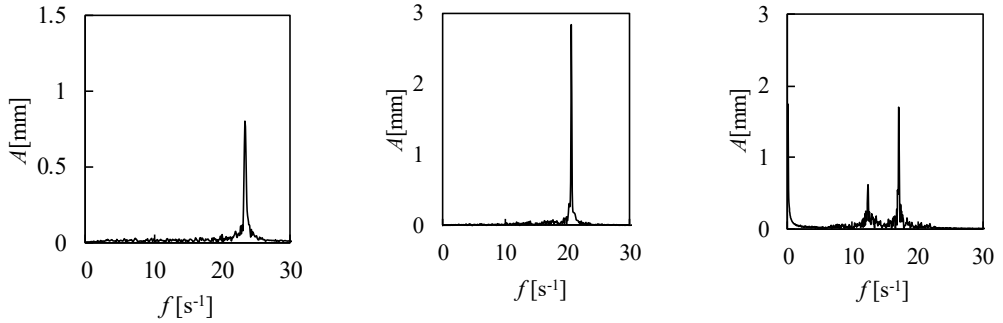

(a) L/H = 2.5 D/H = 0.5, V_r = 5.01, U = 2.14 m/s

(b) L/H = 5.0 D/H = 0.5, V_r = 5.14 ,U = 2.35 m/s

(c) L/H = 10 D/H = 0.5, V_r = 4.56, U = 1.80 m/s

Figure 5.9. FFT Spectra of transverse vibration characteristics for rectangular with endplate at maximum response amplitude.

5.3.2. D-Section Prisms

Figure 5.10 shows the response amplitudes of D-section prisms with side ratios of D/H = 0.5, and aspect ratios of L/H = 2.5, 5.0 and 10. The non-dimensional response amplitude η_{rms} of the prism with endplate increases slightly at the large value of reduced velocity than that without an endplate. Figure 5.11 shows D-section prism with D/H = 0.23 and with attached endplate that response amplitude hardly suppressed at aspect ratio $L/H \leq 5.0$ which was similar to rectangular prism D/H = 0.2. It implies that attached endplate reduced instability of the separated shear layer and Karman vortex behind the prism along the span length of the prism. Sumner et al (2013) in his article review on finite height cylinder present that tip end of the prism promotes wake instability and it descends by reducing aspect ratio. In the case of prism $L/H \leq 2.5$ von Karman vortex was predominated by the interaction of tip vortex and base vortex yielding vortex street and

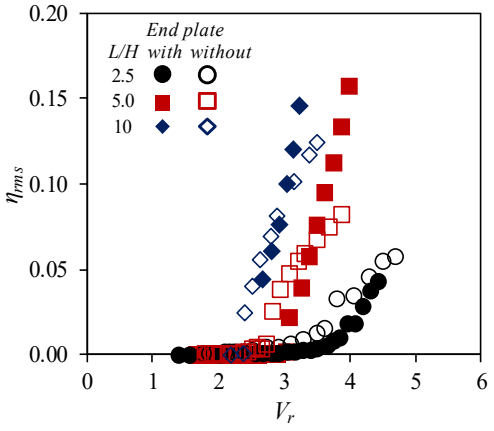

Figure 5.10 Effect of attached endplate on transverse vibration characteristics for D-section with side ratio D/H = 0.5.

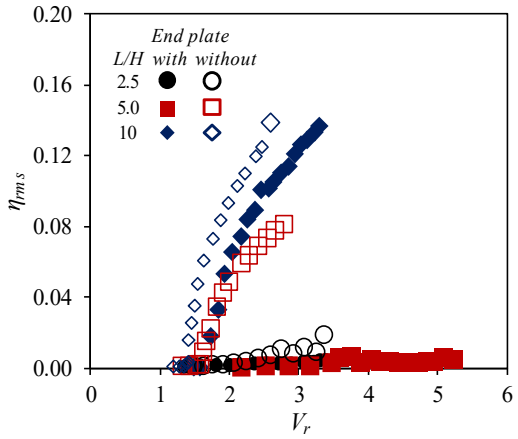

Figure 5.11 Effect of attached endplate on transverse vibration characteristics for D-section with side ratio D/H=0.23. C_n for L/H = 5.0 is 1.99

transverse fluctuation force from separated shear layer (Palau and Salvador, 2010; Goncalves et al, 2015).

Figure 5.12 shows a non-linearity of response amplitude in the case of a prism with aspect ratio at critical point L/H=5.0. In the plain prisms, the variation of reduced damping parameter is not notable differences among them for all aspect ratios are used in this study. In the case of the attached endplate, those only slightly differ on onset galloping for all attached endplate cases. For the case of the aspect ratio of 5.0, when using plate spring thickness of 0.6 with the attached endplate, *Cn* rises from 0.41 to 1.99, it hardly suppressed the response amplitude and remarkable difference in response amplitude with a plain prism was observed (figure 5.12). Figure 5.13(a) shows the FFT spectrum for this case in which a discontinuity of amplitude waveform was found across time lapses.

At the C_n = 1.09, response amplitude initiates to increase at V_r > 3.0 till suddenly jump in response amplitude when reaching V_r > 3.8. in this case linearity of Hook's law for plate spring deformation is not applicable. Some studies about non-linear dynamic

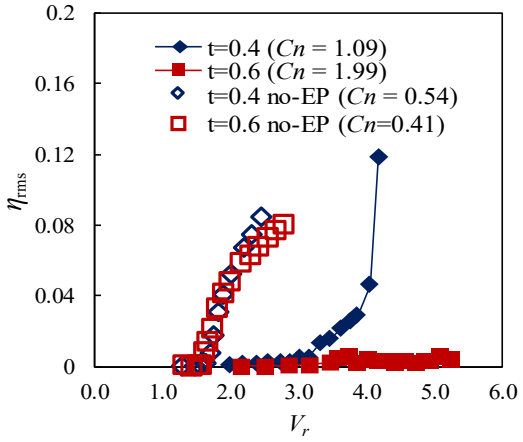

Figure 5.12. Response amplitude of D-section $D/H = 0.23$ and $L/H = 5.0$ with attached endplate

response have presented that the Duffing oscillator is a model to describe the non-linearity phenomenon such as in Poore et al. 1986; Luo et al. 2003, Nourazar and Mirzabeigy (2013). Iwan and Blevins (1974) and Blevins (1974) developed a model to describe such a jumping phenomenon in the elastically mounted prism over which it is

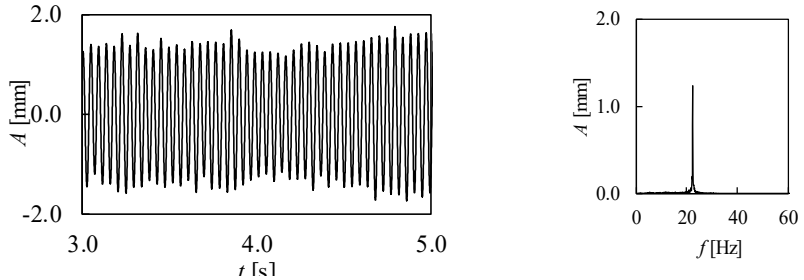

(a) V_r = 4.05; U = 1.82 m/s, t = 0.4 mm

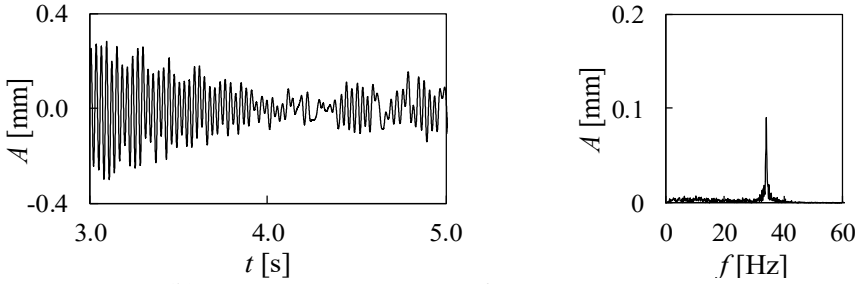

(b) V_r = 5.08; U = 2.28 m/s t = 0.6 mm

Figure 5.13. Time lapses of amplitude waveform and spectrum frequency at maximum amplitude for $L/H = 5.0$ attached endplate

related to reduced damping parameters that affect peak resonance amplitude and limits cycle of oscillation and frequency flow entrainment.

In the case of small aspect ratio L/H = 2.5 figure 5.14 presents the FFT spectra frequency and time-lapses of the waveform amplitude for both side ratios. A chaotic waveform of amplitude along vibration time was observed followed by chaotic in the FFT spectrum. This is in contrast with the plain D-section. Hence, amplitude becomes hardly suppressed as shown in figure 5.11.

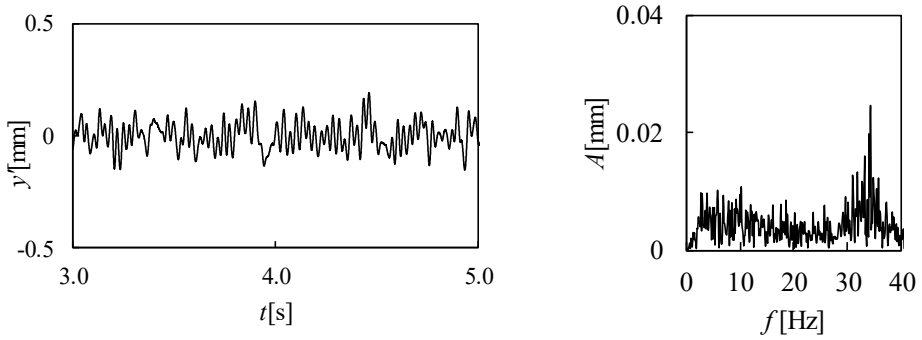

(a) D/H=0.23 (V_r = 3.4; U = 2.41 m/s

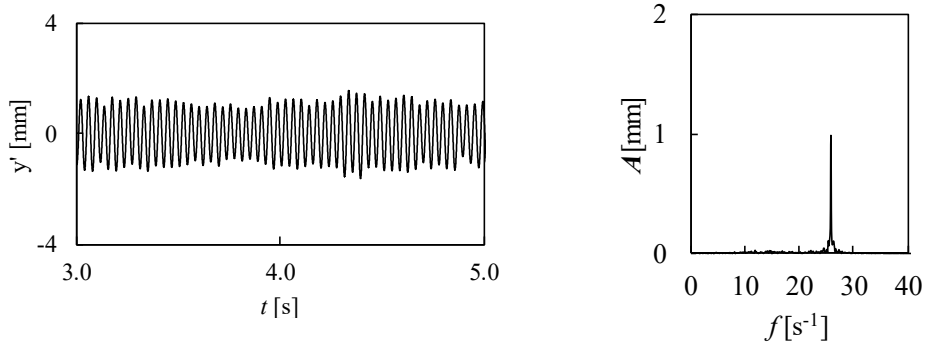

(a) D/H=0.5 (V_r = 3.6; U = 2.05 m/s)

Figure 5.14. Time lapses of amplitude waveform and spectrum frequency at maximum amplitude for L/H = 2.5

5.3.3. Stability of Peak Amplitude

The deviation of peak amplitude for both rectangular and D-section with the attached endplate is shown consecutively in figures 5.15 and 5.16. Peak stability of

dynamic response had a relationship to the magnitude of amplitude. Attached endplate at the tip of a prism with a side ratio of 0.5 did not affect noticeably peak amplitude as shown in figures 5.15 b and 5.16b for both prism models. However, at slender rectangular and D-section prisms, attached endplate enhanced instability of peak amplitude at the aspect ratio of 2.5. The deviation of peak amplitude remains high along the period of motion for aspect ratio of 2.5 (figure 5.15a) yielding the dynamic response is suppressed. The stability of peak amplitude was achieved for the prism above critical aspect ratio $L/H \geq 5.0$ though it was not contributed in enhancing dynamic response. In figure 5.16a, the peak amplitude of $L/H = 5.0$ seemed stable at some ranges of reduced velocity which similar to a plain prism. However, the dynamic response was smaller than a plain prism. The deviation of peak amplitude for rectangular prism increased with uptick an aspect ratio and remained stable at high reduced velocity except for aspect ratio of 2.5.

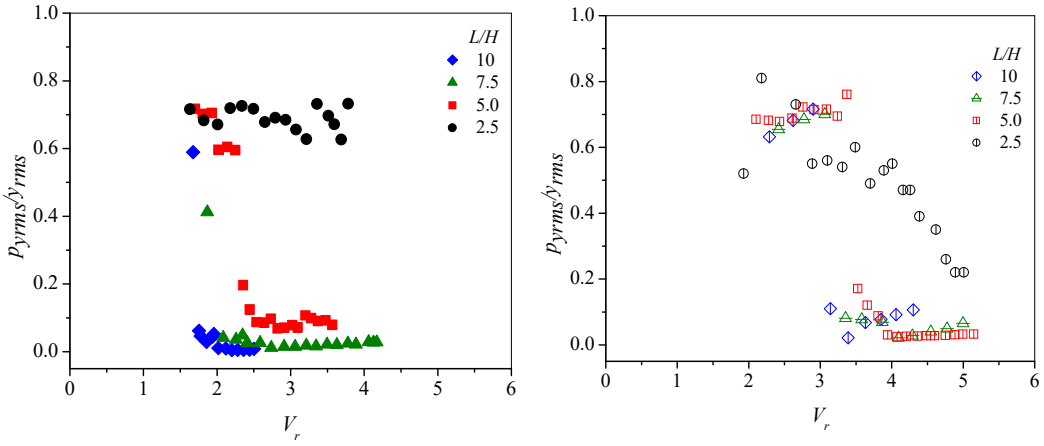

(a) $D/H = 0.2$ (b) $D/H = 0.5$

Figure 5.15. Stability of the peak amplitude for the rectangular prisms with attached endplate

In the case of D-section prism with endplate, in which it was recognized as pure instability galloping, peak deviation was relatively similar to plain prism for $D/H = 0.5$. Meanwhile, for small side ratio of 0.23, peak deviation for aspect ratio $L/H > 5.0$ remained unchanged but for aspect ratios at critical and below critical aspect ratio $L/H \leq 5.0$,

attached endplate promoted peak deviation of response amplitude along reduced velocity points (figure 5.16a). This phenomenon is in contrast to the rectangular prisms. Consequently, the response amplitudes were suppressed as figure 5.12. It is implied that the wake flow structure of D-section is distinctly different from its counterparts because of differences in the afterbody shape, even if the presence of endplate at the tip end needs to be investigated further.

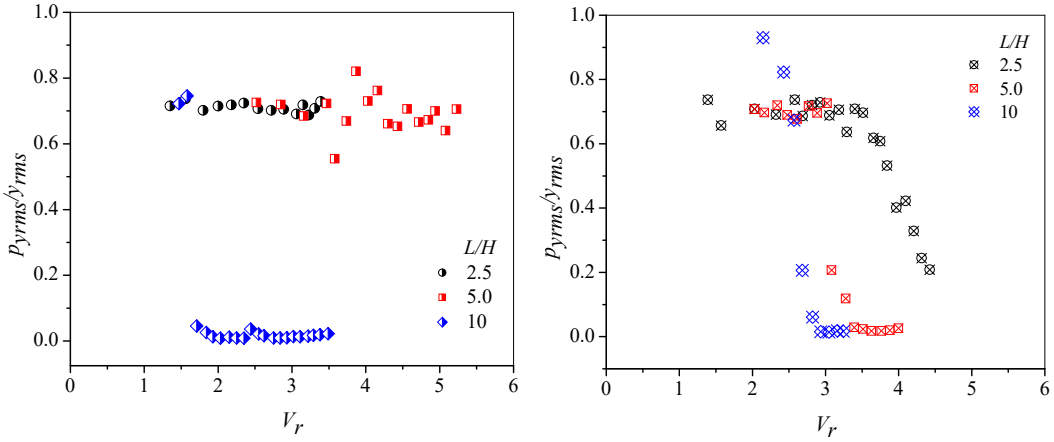

(a) $D/H = 0.23$ (b) $D/H = 0.5$

Figure 5.16. Stability of the peak amplitude for the D-section prisms with attached endplate

5.4. Conclusions

This result of the experiment has proved our initial premises regarding the controlling wake behavior to improve response amplitude of bluff bodies of two different cross-section models i.e. rectangular and D-section with different aspect ratios. Hence from those result, it may be concluded that

1. Mounting a splitter plate at prisms trailing edge has improved response amplitude for both cross-section models by modifying the vortex dynamic behind the prisms instead of allowing them to interact directly; hence which prevents wake interference on the response amplitude.
2. The fluctuation of amplitude peak is uniform with only one sharp peak is found on the FFT spectra analysis. For rectangular prism below critical aspect ratio $L/H \leq 5.0$ and side ratio of 0.2 in which the galloping relies on instability, mounting splitter plate does not affect response amplitude. In contrast, mounting splitter plate on the prism with $D/H = 0.5$ diminish interference of peak amplitude yielding response amplitude increase successfully.
3. Mounting splitter plate promotes stable peak amplitude for the prism with critical side ratio and aspect ratio while attaching endplate uptick the deviation of amplitude peak mainly at side ratio of 0.2/0.23 and aspect ratio below critical point $L/H \leq 5.0$ both rectangular and D-section.
4. Attaching endplate at the end of prisms does not influence the uniformity of waveform amplitude for both prisms model with D/H of 0.5. Hence, there is not any meaningful improvement amplitude.
5. Attaching endplate at the prism with small depth section $D/H = 0.2$ (rectangular) and 0.23 (D-section) is a meaningless way related to amplitude improvement for

aspect ratio $L/H \geq 5.0$. For the prism with $L/H \leq 5.0$, attaching endplate has suppressed response amplitude. Hardly suppressing on response amplitude was found in the prisms below critical aspect ratio, $L/H = 2.5$ and D-section with $L/H = 5.0$ and C_n property is 1.99.

6. A non-linear response amplitude over reduced velocity was found at D-section prism with $L/H = 5.0$ and $Cn = 1.09$ which is indicated by suddenly jump of response amplitude.

References

Assi, G. R. S., & Bearman, P. W. (2015). Transverse galloping of circular cylinders fitted with solid and slotted splitter plates. *Journal of Fluids and Structures*, *54*, 263–280. https://doi.org/10.1016/J.JFLUIDSTRUCTS.2014.11.005

Blevins, Robert D. (1974) *Flow induced vibration of bluff structures.* Dissertation (Ph.D.), California Institute of Technology. https://resolver.caltech.edu/CaltechETD:etd-09302005-082356

Chauhan, M. K., Dutta, S., More, B. S., & Gandhi, B. K. (2018). Experimental investigation of flow over a square cylinder with an attached splitter plate at intermediate reynolds number. *Journal of Fluids and Structures*, *76*, 319–335. https://doi.org/10.1016/j.jfluidstructs.2017.10.012

Fox, T. A., & West, G. S. (1990). On the use of end plates with circular cylinders. *Experiments in Fluids*, *9*(4), 237–239. https://doi.org/10.1007/BF00190426

Iwan, W. D., & Blevins, R. D. (1974). A model for vortex induced oscillation of structures. *Journal of Applied Mechanics, Transactions ASME*, *41*(3), 581–586. https://doi.org/10.1115/1.3423352

Kiwata, T., Yamaguchi, M., Kono, T., & Ueno, T. (2013). Flow-Induced Transverse Vibration of a Cantilevered Prism and Vibration-Generated Power Using Magnetostrictive Material. In *Volume 4: Fluid-Structure Interaction* (p. V004T04A034). ASME. https://doi.org/10.1115/PVP2013-97277

Kiwata, T., YAMAGUCHI, M., KONO, T., & Ueno, T. (2014). Water tunnel experiments on transverse-galloping of cantilevered rectangular and D-section prisms. *Journal of Fluid Science and Technology*, *9*(3), 1–5. https://doi.org/10.1299/jfst.2014jfst00

Luo, S. C., Chew, Y. T., & Ng, Y. T. (2003). Hysteresis phenomenon in the galloping oscillation of a square cylinder. *Journal of Fluids and Structures*, *18*(1), 103–118. https://doi.org/10.1016/S0889-9746(03)00084-7

Morse, T. L., Govardhan, R. N., & Williamson, C. H. K. (2008). The effect of end conditions on the vortex-induced vibration of cylinders. *Journal of Fluids and Structures*, *24*(8), 1227–1239. https://doi.org/10.1016/j.jfluidstructs.2008.06.004

Nakamura, Y., & Hirata, K. (1989). Critical geometry of oscillating bluff bodies. *Journal of Fluid Mechanics*, *208*, 375–393. https://doi.org/10.1017/S0022112089002879

Nakamura, Y., & Hirata, K. (1991). Pressure fluctuations on oscillating rectangular cylinders with the long side normal to the flow. *Journal of Fluids and Structures*, *5*(2), 165–183. https://doi.org/10.1016/0889-9746(91)90460-7

Nakamura, Y., Hirata, K., & Urabe, T. (1991). Galloping of rectangular cylinders in the presence of a splitter plate. *Journal of Fluids and Structures*, *5*(5), 521–549. https://doi.org/10.1016/S0889-9746(05)80004-0

Nakamura, Yasuharu, & Matsukawa, T. (1987). Vortex excitation of rectangular

cylinders with a long side normal to the flow. *Journal of Fluid Mechanics*, *180*(1), 171. https://doi.org/10.1017/S0022112087001770

Naudascher, E. Rockwell, D. (2005). *Flow -Induced Vibrations: an Engineering Guide*. Dover Publication Inc.

Nakamura, Y., & Tomonari, Y. (1977). Galloping of rectangular prisms in a smooth and in a turbulent flow. *Journal of Sound and Vibration*, *52*(2), 233–241. https://doi.org/10.1016/0022-460X(77)90642-3

Nourazar, S., & Mirzabeigy, A. (2013). Approximate solution for nonlinear Duffing oscillator with damping effect using the modified differential transform method. *Scientia Iranica*, *20*(2), 364–368. https://doi.org/10.1016/j.scient.2013.02.023

Ogunremi, A. R., & Sumner, D. (2015). The effect of a splitter plate on the flow around a finite prism. *Journal of Fluids and Structures*, *59*, 1–21. https://doi.org/10.1016/j.jfluidstructs.2015.09.001

Ohya, Y. (1994). Note on a discontinuous change in wake pattern for a rectangular cylinder. Journal of fluids and structures.pdf.

Okajima, A. (1982). Strouhal numbers of rectangular cylinders. *Journal of Fluid Mechanics*, *123*(1), 379. https://doi.org/10.1017/S0022112082003115

Okajima, A., & Kiwata, T. (2019). Flow-Induced Stream-Wise Vibration of Circular Cylinders. *Journal of Flow Control, Measurement & Visualization*, *07*(03), 133–151. https://doi.org/10.4236/jfcmv.2019.73011

Okajima, A., Nakamura, A., Kosugi, T., Uchida, H., & Tamaki, R. (2004). Flow-induced in-line oscillation of a circular cylinder. *European Journal of Mechanics - B/Fluids*, *23*(1), 115–125. https://doi.org/10.1016/j.euromechflu.2003.09.009

Poore, A. B., Doedel, E. J., & Cermak, J. E. (1986). Dynamics of the Iwan-Blevins wake oscillator model. *International Journal of Non-Linear Mechanics*, *21*(4), 291–302. https://doi.org/10.1016/0020-7462(86)90036-3

Slaouti, A., & Gerrard, J. H. (1981). An experimental investigation of the end effects on the wake of a circular cylinder towed through water at low Reynolds numbers. *Journal of Fluid Mechanics*, *112*(1), 297–314. https://doi.org/10.1017/S0022112081000414

Sumner, D. (2013). Flow above the free end of a surface-mounted finite-height circular cylinder: A review. *Journal of Fluids and Structures*, *43*, 41–63. https://doi.org/10.1016/j.jfluidstructs.2013.08.007

Chapter 6
The Effect of Added Structure on Vibration Characteristics

6.1. Introduction

The wake flow behind a stepped circular cylinder, which consists of two circular cylinders with different diameters, was investigated by Ko, et al. 1982 and Wu, et al. 2007 to obtain the flow interaction in the wakes of two cylinders. According to this study, the Strouhal number is not noticeably different between two co-axials cylinders near the connecting point. At his point, the wake interaction among them is dispensable. Meanwhile, it was different among large and small diameters of the co-axials cylinder which is similar to the plain cylinder. Moreover, the vortex-induced vibration of a tapered circular cylinder was studied by several researchers such as Zeinoddini et al., (2013), Balasubramanian (2001), and Seyed-Aghazadeh et al., (2015). Seyed-Aghazadeh et al., (2015) investigated the influence of the tapered ratio on the vortex-induced vibration of circular cylinders free to oscillate in the transverse direction. They found that the lock-in range of a circular cylinder with a small tapered ratio was sustained through largely reduced velocities. Kiwata et al., 2013 on their experiment installed the fin behind the rectangular to prevent axial vibration due to fluid friction. The result showed that the flexural rigidity influenced response amplitude by shifting the onset galloping.

In case of the dynamics of an oscillating stepped rectangular prism, it is receiving less attention. Through this section, the stepped rectangular prism facing upstream and downstream was investigated. The additional plate is supposed to absorb friction-induced bending; hence improved response amplitude might be achieved over which the alteration of wake interaction along spanwise due to stepped surface was dispensable.

6.2. Response Amplitude of Stepped Prism

The response amplitude of stepped rectangular prism is shown in figures 6.1a-b with different added plate configuration. The effect of axial force on the vibration characteristic influences bending stress behavior acting on the span length of the rectangular prism. In this case, bending or deflection stress is considered to affect the free vibration characteristic. Hence, the initial premise that increasing the rigidity by putting a light structure behind the prism is supposed to improve response amplitude. However, the effect of the added structure at the frontward or backward position on the prisms was not successful to increase response amplitude instead of shifting onset vibration. The evolution of onset galloping was linear with increasing the length ratio of added structure and response amplitude grow with a similar characteristic.

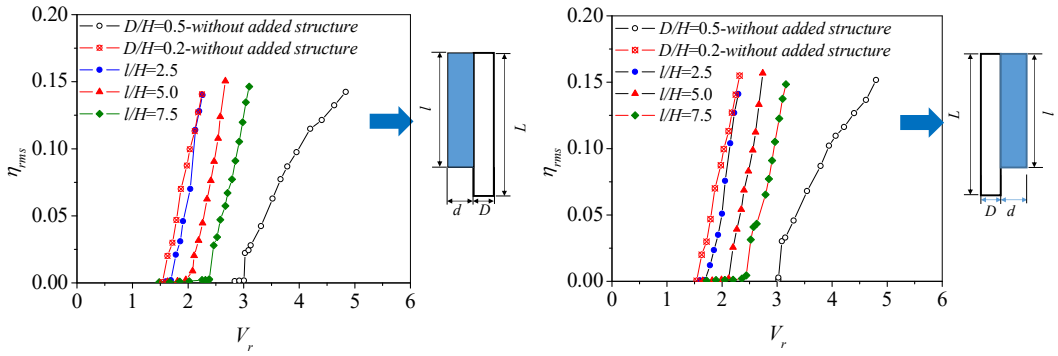

(a) The added plate is located at the front of the prism

(b) The added plate is located at the back of the prism

Figure 6.1. Transverse vibration characteristic of a rectangular prism with a side ratio of 0.2 with added structure

Figure 6.1a-b also shows a comparison of the response amplitude of stepped prism with the plain prisms. There is not any significant difference in free vibration behavior upon the position of additional structure perpendicular to flow direction as presented in figure 6.1a-b. In this figure, increasing stepped ratio *l/h* delay galloping growth in small amplitude range. Increased stepped length (*l/H*) till 0.8 was still prolong galloping range

into small amplitude before suddenly jump when reaching $V_r \approx 2.4$ (for $l/h = 7.5$). However, maximum stepped prisms (l/h=7.5) with side ratio D/d of 0.8 did not reach onset galloping of a plain prism with side ratio D/H=0.5.

Figure 6.2 shows time lapses of waveform amplitude for the prism with added structure facing upstream (stepped prism). The fluctuating of waveform was slightly similar with a plain rectangular prism with a side ratio of 0.2 as presented in figure 4.2 in the preceding chapter even if the added side ratio was 0.45, near 0.5 for plain prism.

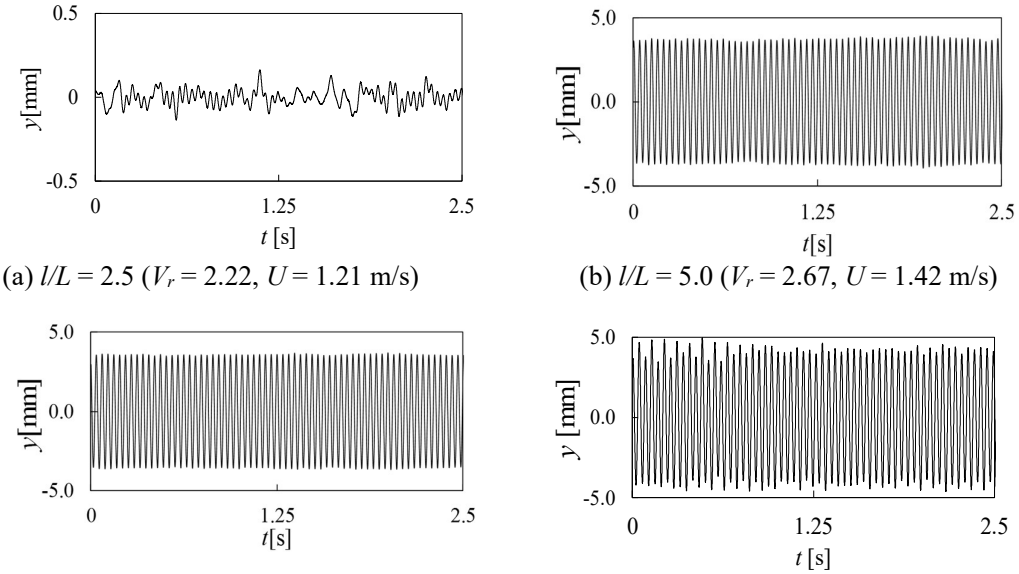

(a) l/L = 2.5 (V_r = 2.22, U = 1.21 m/s) (b) l/L = 5.0 (V_r = 2.67, U = 1.42 m/s)

(c) l/L = 7.5 (V_r = 2.38, U = 1.24 m/s) (d) l/L = 7.5 (V_r = 3.16, U = 1.62 m/s)

Figure 6.2. Time histories tip displacement for a rectangular prism of D/H = 0.2 with an added plate facing upstream.

In the previous study such as Kiwata et al., (2013), that put a light structure like a fin behind the prism also showed a similar phenomenon as the present study even if the configuration added structure was slightly different. The evolution of onset galloping and response amplitude with various sizes of the fitted fin can be found in figure 6.3 below.

Figure 6.4 shows the evolution of the second-moment area for a rectangular prism with a fin to represent the investigation model on the flexural rigidity of the structure.

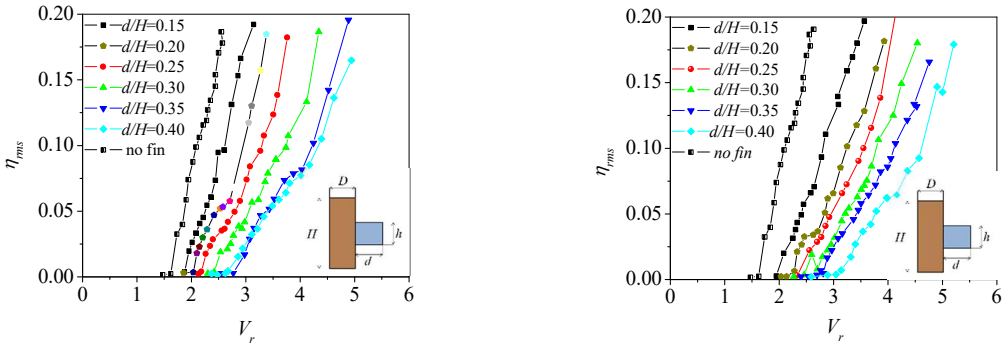

(a) depth ratio $h/H = 0.25$ (b) depth ratio $h/H = 0.50$

Figure 6.3. Transverse vibration characteristic of a rectangular prism with a side ratio of 0.2 with a fin behind the prisms

The flexural rigidity is intended to reduce or prevent axial vibration due to axial friction as mentioned previously. This figure is also reproduced from Kiwata, Yamaguchi, Kono, & Ueno, 2013 that the stiffness of various side ratios of the rectangular prism was examined by fitting a structure like a fin on the backward of the models.

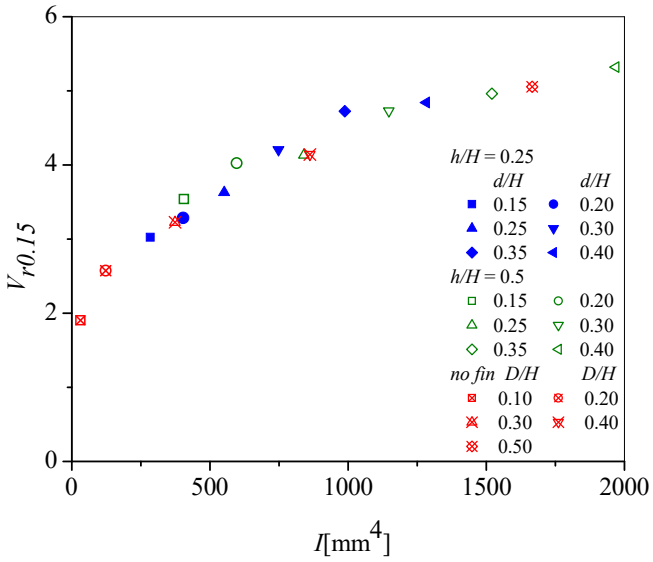

Figure 6.4. Second-moment area of a rectangular prism with a fitted fin on the backward (reproduced form Kiwata et al, 2013)

In this figure, the stiffness of a rectangular prism grows up exponentially with side ratio and depth per width ratio of finned prisms for which flexural rigidity of the prism is represented by the second-moment area. This second-moment area of the rectangular

prism is defined in equation 3 below. In this case, only two terms that influence the rigidity, are depth and width ratio (cross-section models). Both depth and width ratio, their flexural rigidity evolution are good agreement with side ratio effect (*D/H*) without a fin (plain prism). According to figure 6.4, the fitted fin on the backward of the prism has increased rigidity of the prism. The thicker of the fitted fin, the more rigidity of the prism is achieved. Consequently, the initial response amplitude goes up concomitant with the thickness or depth ratio of the fitted fin.

$$I = \frac{HD^3 + hd^3}{3} + hdD(D + d) - \left\{ \frac{hd\left(D + \frac{d}{2}\right) + \frac{HD^2}{2}}{hd + HD} \right\}^2 (Hd + hd) \qquad (3)^*$$

*reproduced from Kiwata et al 2013

Both stepped prism and fitted fin, it is considered that the added plate has modified after body flow structure behavior. We also note that the prisms with a fitted plate provide a smooth increment on response amplitude and shifting onset galloping to be higher than those of prism without an additional structure. It is not only preventing a bluff body from axial bending due to drag force but also bring the structure to become harder to oscillate in low reduced velocity as indicated in figures 6.1 and 6.3.

Subsequent work is to modify the flexural rigidity of the prism model to be 810 mm^4 by putting stepped plate length with side ratio *D/d* of 0.8. It is assumed that the second-moment area is only a function of the cross-section model perpendicular to the flow stream instead of a span-length variation of the stepped prism. Considering the second-moment area stipulated in figure 6.4, the rigidity of stepped prism is similar to the plain prism with *D/H* = 0.4 and finned prism with depth ratio *d/H* = 0.25, *h/H*= 0.5.

6.3. Stability of Peak Amplitude

In the case of stability of peak amplitude, figure 6.5 presents the peak deviation of amplitude for finned prisms reproduced from Kiwata et al (2013). The deviation peak amplitude for finned prism is proportional to depth ratio (*D/h*) which is similar to the shifting onset galloping phenomenon. Meanwhile, the effect of the width ratio (*h/H*) affects the peak deviation amplitude slightly. The fitted fin at backward of the prisms with small side ratio has extended the deviation of amplitude peak as well as the range of onset galloping.

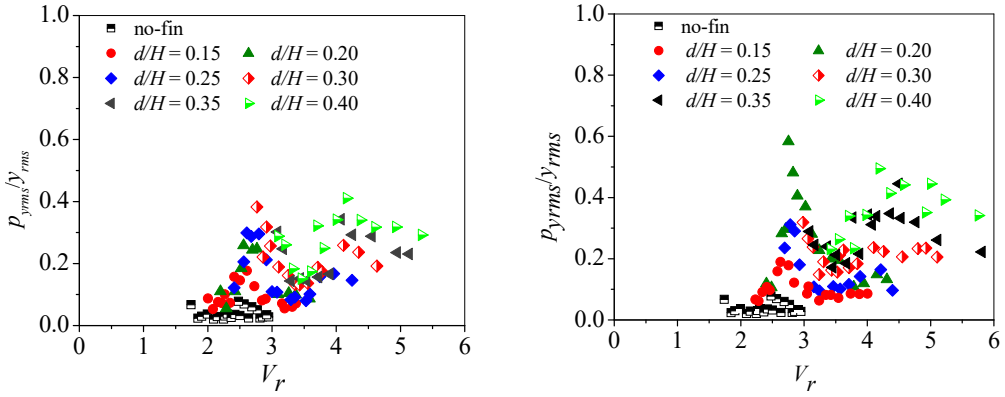

(a) Rectangular prisms with fitted fin, depth ratio $h/H = 0.25$

(b) Rectangular prisms with fitted fin, depth ratio $h/H = 0.5$

Figure 6.5. The standard deviation of the peak amplitude for rectangular prism with a fitted fin on the backward.

In the case of peak amplitude stability for stepped prisms, figures 6.6a-b present the effect of added structure on the peak amplitude deviation respect to reduced velocity. The stability of peak amplitude for prism with a small added plate is similar to the plain prism with a small side ratio ($D/H = 0.2$). Naturally, at low reduced velocity, the deviation of peak amplitude is high and tends to diminish at a high reduced velocity range. This phenomenon is the same for all stepped ratio (*l/H*). However, adding additional plate maintained peak amplitude stability at high reduced velocity even if the combined side ratio (*D/H* + *d/h*) approached the side ratio of plain prism for which peak amplitude

deviation tend to uptick at high reduced velocity range for the prism with critical side ratio ($D/H = 0.5$). As response amplitude evolution, there was not any distinction on peak amplitude deviation related to the position of stepped prism either facing upstream or downstream.

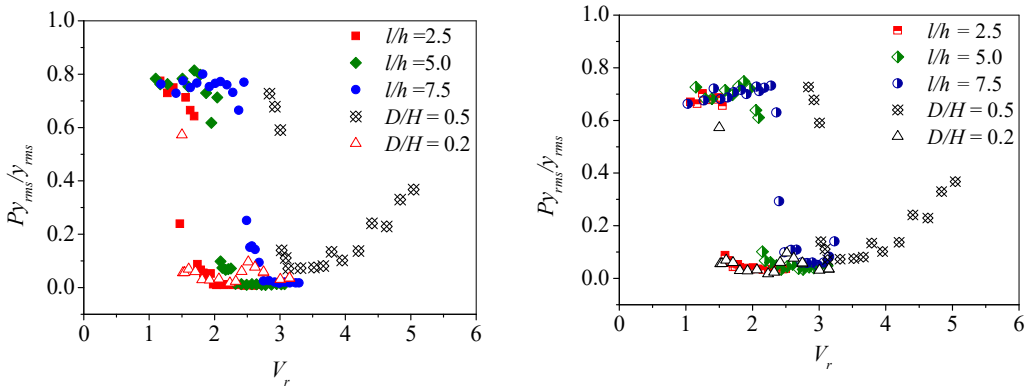

(a) Plate put on the front surface (b) Plate put on the back surface

Figure 6.6. The non-dimensional standard deviation of peak displacement for a rectangular prism of $D/H = 0.2$ with an added plate

Intentionally left blank

6.4. Conclusions

The study on the effect of added structure on the response amplitude characteristics has been performed with the following conclusion that may be inferred, those are :

1. Finned and stepped prism increase rigidity of the prism which is indicated by the stability of response peak displacement.
2. Fined and stepped shift onset galloping regularly with increasing depth ratio, however, stepped prisms prolong galloping range with a small amplitude that changes the onset galloping.
3. Stepped prism preserves peak amplitude stability remains stable even if the depth ratio approached to 0.45.

Intentionally left blank

References

Kiwata, T., Yamaguchi, M., Kono, T., & Ueno, T. (2013). Flow-Induced Transverse Vibration of a Cantilevered Prism and Vibration-Generated Power Using Magnetostrictive Material. In *Volume 4: Fluid-Structure Interaction* (p. V004T04A034). ASME. https://doi.org/10.1115/PVP2013-97277

Balasubramanian, S., Haan, F. L., Szewczyk, A. A., & Skop, R. A. (2001). An experimental investigation of the vortex-excited vibrations of pivoted tapered circular cylinders in uniform and shear flow. *Journal of Wind Engineering and Industrial Aerodynamics*, *89*(9), 757–784. https://doi.org/10.1016/S0167-6105(00)00093-3

Seyed-Aghazadeh, B., Carlson, D. W., & Modarres-Sadeghi, Y. (2015). The influence of taper ratio on vortex-induced vibration of tapered cylinders in the crossflow direction. *Journal of Fluids and Structures*, *53*, 84–95. https://doi.org/10.1016/j.jfluidstructs.2014.07.014

Zeinoddini, M., Tamimi, V., & Saeed Seif, M. (2013). Stream-wise and cross-flow vortex induced vibrations of single tapered circular cylinders: An experimental study. *Applied Ocean Research*, *42*, 124–135. https://doi.org/10.1016/j.apor.2013.05.005

Wu, P., Hanu, H. and Miyakoshi, K. (2007). Generation Different of New Frequencies by Nonlinear Interaction between Vortex Shedding Frequencies in Span Wise Direction of a Stepped Circular Cylinder. *Transactions of the Japan Society of Mechanical Engineers.*, *B37*, 103–111. https://doi.org/https://www.jstage.jst.go.jp/article/kikaib1979/73/725/73_725_103/_pdf/-char/ja

Intentionally left blank

Chapter 7
Concluding Remarks

Based on the experiment result that vibration characteristic can be viewed into two groups based on the identical response amplitude characteristics, those are the prisms with aspect ratios L/H of ≥ 5.0, and aspect ratio below the critical aspect ratio $L/H = 2.5$. The prism with aspect ratios below the critical aspect ratio showed non-uniform amplitude peak displacement, unstable response amplitude, and low increment rate of response amplitude. The discontinuity of oscillation waveform was also introduced on the prisms with critical side ratio $D/H = 0.5$ which is in contrast to the rectangular prism with a side ratio of 0.2.

By mounting a splitter plate at the prisms trailing edge, it improved response amplitude for both cross-section models (rectangular and D-section prisms) by modifying the vortex dynamic behavior behind the prisms instead of allowing them to interact naturally; as the result, it prevented wake interference on the response amplitude signal. Moreover, fluctuation of the amplitude peak was uniform with only one sharp peak that was found on the FFT spectra analysis. For rectangular prism below critical aspect ratio $L/H < 5.0$ with small side ratio (0.2/0.23) where the galloping relies on the instability of separated shear layer, mounting splitter plate does not affect response amplitude. It seems that the effect of swirling vortex generated by tip end reduced the unstable separated shear layer in the wake. In case of attaching endplate at the end of prisms to diminish the effect of swirling vortex, it did not influence the uniformity of waveform amplitude for both prisms model with side ratio D/H of 0.5. Hence, there is not any meaningful improvement in response amplitude characteristics. However, attaching endplate at the prism with small depth section $D/H = 0.2$ (rectangular) and 0.23 (D-section) was a meaningless way

related to amplitude improvement for aspect ratio $L/H \geq 5.0$. For the prism with $L/H \leq 5.0$, attaching endplate suppressed response amplitude. Hardly suppressing on response amplitude was found in the prisms below critical aspect ratio, $L/H = 2.5$ at the D-section prism with $L/H = 5.0$ and C_n property was 1.99. However, a non-linear response amplitude over reduced velocity was found at D-section prism with $L/H = 5.0$ and $Cn = 1.09$ which was indicated by suddenly jump of response amplitude.

Furthermore, the investigation of axial bending intrusion effect on transverse vibration, the rectangular prism with small side ratio $D/H = 0.2$ and $L/H = 10$ was fitted by a fin, and a plate to increase prism rigidity. In the case of response amplitude, fined prism and stepped prism shifted onset galloping regularly in line with increasing total depth ratio, however, stepped prism prolonged galloping range with a small amplitude that changed the onset galloping. In case of peak amplitude stability, a prism with fitted fin promoted unstable peak amplitude in line with the depth ratio (d/H) and height ratio (h/H) of a fitted fin. Meanwhile, the stepped prism preserved peak amplitude stability even if the total depth ratio ($(D + d)/H$) approached to 0.45.

Understanding flow structure characteristics in the wake either numerical or advanced experimental is a curious work for the future to get a comprehensive insight related to their effect on response amplitude characteristics of those bluff bodies. Moreover, modifying the structural part of the bluff bodies or vortex behavior in the wake is supposed to improve response amplitude in terms of supporting the research of harvesting energy from flow-induced vibration.